

LIBRARY
Michigan State
University

This is to certify that the

thesis entitled

COLLOIDAL PROCESSING OF TITANIUM

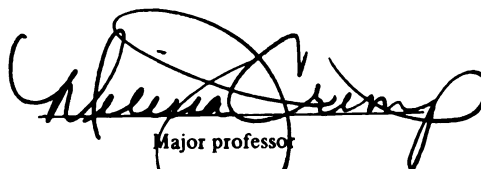
DIBORIDE/ALUMINA ($\text{TiB}_2/\text{Al}_2\text{O}_3$)

presented by

Lisa Prokurat Franks

has been accepted towards fulfillment
of the requirements for

Master's degree in Materials Science
and Engineering


Major professor

Date August 22, 2001

PLACE IN RETURN BOX to remove this checkout from your record.
TO AVOID FINES return on or before date due.
MAY BE RECALLED with earlier due date if requested.

DATE DUE	DATE DUE	DATE DUE

COLLOIDAL PROCESSING OF TITANIUM DIBORIDE/ALUMINA ($\text{TiB}_2/\text{Al}_2\text{O}_3$)

By

Lisa Prokurat Franks

A THESIS

**Submitted to
Michigan State University
in partial fulfillment of the requirements
for the degree of**

MASTER OF SCIENCE AND ENGINEERING

Department of Materials Science and Mechanics

2001

ABSTRACT

COLLOIDAL PROCESSING OF TITANIUM DIBORIDE/ALUMINA ($\text{TiB}_2/\text{Al}_2\text{O}_3$)

By

Lisa Prokurat Franks

$\text{TiB}_2/\text{Al}_2\text{O}_3$ powders produced using self-propagating high-temperature synthesis (SHS) have been densified using hot pressing and dynamic consolidation techniques, but the microstructure and phase distribution have been inconsistent. Since the SHS powders are available commercially, it's possible to also improve green body formation by controlling interparticle potentials during processing. The interactions between TiB_2 and Al_2O_3 have been analyzed with respect to their colloidal properties, as measured by their respective zeta potentials, density, volume fraction, and particle size. The colloidal properties and the resulting microstructure of sintered SHS $\{\text{TiB}_2/\text{Al}_2\text{O}_3\}$, with SHS TiB_2 in two different aluminas, have been compared. The coagulation behavior of SHS $\{\text{TiB}_2/\text{Al}_2\text{O}_3\}$ powders was insensitive to colloidal processing, and no matter the processing condition, the microstructure associated with resistance to ballistic penetration was present. The coagulation behavior of the SHS TiB_2 in two different aluminas was sensitive to colloidal processing, and the SHS TiB_2 in the Alcoa SG Al_2O_3 processed at pH 7 showed potential to produce the microstructure associated with resistance to ballistic penetration.

DEDICATION

This work is dedicated to my parents, Mary Pesta Prokurat and Michael A. Prokurat, whose love, encouragement and support I have always known. Thankfully, they are of that generation Tom Brokaw has called *The Greatest Generation*, who know and teach the value of work, especially that which comes from the labor of one's own hands. Any graduate work, especially one that includes laboratory bench work, requires an integrity, humility, perseverance and patience that I had to have seen and lived with all these years, to be able to apply to my own work. I will always be grateful for the sacrifices that gave me, my brother, Rev. Dr. Michael D. Prokurat and my sister, Dr. Elaine M. Carroll, M.D., opportunities many children only dream about. But my parents' lasting gift is that basically, they always were, still are, and will always be, just crazy in love with us.

ACKNOWLEDGMENTS

This study was made possible through the cooperation and support of the Defense Advanced Research Projects Agency (DARPA), U.S. Army Tank-Automotive Research Development and Engineering Center (TARDEC) and Michigan State University under the Clinton Administration's Technology Reinvestment Project (TRP).

When one pursues a graduate degree, it is never done alone. When one pursues an advanced degree as a late vocation while employed full-time, married and a parent, guidance and support are voluminous and difficult to list completely, however I'd like to mention specifically:

For inspiring me to climb the mountain: Dr. Gordon Filbey, Dr. William Carson, Dr. William Gillich, Dr. Andy Niiler and Dr. William Bruchey.

For initiating this program, and opening the doors I needed to get started: Dr. Ken Oscar, Ms. Pame Watts, Mr. Michael Zapf, Dr. Richard McClelland, Dr. Douglas Templeton, Dr. Douglas Rose, Dr. Jayaraman, Dr. Larry Drzal and my advisor Dr. Melissa Crimp.

For getting me past bumps in the road and over the mountain: Dr. Kathryn Logan, Dr. Douglas Templeton, Dr. Jim Thompson, Dr. Ernest Chin, Mr. Gary Gilde, Dr. Jim McCauley, Dr. Eldon Case, Dr. Melissa Crimp, Mr. Jeff Swab, Mr. Jack Mullins, Mr. Patrick Sneary, Mr. Brett Wilson, Mr. Dean Opperman, Mr. Scott Hodges, Mr. Michael Parham, Ms. Mary Prokurat, Ms. Juliana Franks, Dr. Renate Snider, Dr. Susan Masten, Mr. Hiroyuki Fukushima, Mr. Yu Liu, Dr. James E. (Ned) Jackson, Ms. Julide Celik, Ms. Lili Duan, Ms. Xiangshu Jin, Ms. Tara Stabryla, Dr. James Lucas, and Dr. Andre Lee.

For their friendship, inspiration and support during this journey: Ms. Sarah Newton, Dr. Elaine M. Carroll, Mr. Robert El Henicky, Ms. Elizabeth Davison, Dr. Roxanne Freedman-Petros, Ms. Kathleen (Kitty) Derbin, Ms. Lee Reimann, J.D., Ms. Juanita Pipkin, Ms. Beverly K. Sobolewski, Rev. Michael Matsko, and members of the Great Lakes Chapter of Federally Employed Women (FEW).

Without the love and support of my dear husband David and my sweet daughter Juliana, I could not have completed this important work, thank you.

TABLE OF CONTENTS

LIST OF TABLES.....	viii
LIST OF FIGURES	x
INTRODUCTION	1
 1 LITERATURE REVIEW	 7
1.1 Titanium Diboride (TiB ₂) – Alumina (Al ₂ O ₃) Composites	7
1.2 Colloidal Processing	9
1.2.1 Colloidal Systems	9
1.2.2 Particle Description.....	11
1.3 Derjaguin-Landau-Verwey-Overbeek (DLVO) Theory	17
1.4 Hogg, Healy and Fuerstenau (HHF) Theory.....	18
1.4.1 Development of HHF Theory	18
1.4.2 Modeling HHF Theory	21
 2 EXPERIMENTAL PROCEDURE	 23
2.1 Starting Powders	23
2.1.1 Self-propagating-high-temperature-synthesis (SHS) TiB ₂	23
2.1.2 Alumina (Al ₂ O ₃) Powders.....	24
2.1.3 SHS Composite TiB ₂ /Al ₂ O ₃	26
2.2 Electrokinetic Sonic Amplitude (ESA) Measurement.....	27
2.3 Stability Predictions.....	28
2.3.1 Hamaker Constant Calculation	28
2.3.2 Computer Model	28
2.4 Slip Preparation and Casting.....	29
2.4.1 Electrolyte	29
2.4.2 Slip Suspensions	29
2.4.3 Ultrasonication.....	29
2.4.4 Plaster Mold Preparation.....	30
2.4.5 Casting	30
2.5 Traditional Binder	31
2.6 Cold Isostatic Pressing (CIPing).....	32
2.7 Green Bodies.....	32
2.7.1 Density Measurement	32
2.7.2 Binder Burnout and Thermogravimetric Analysis (TGA).....	32
2.7.3 Conductivity Measurement.....	33
2.8 Pressureless Sintering	33
2.9 Sintered Samples.....	34
2.9.1 Density Measurement	34
2.9.2 Conductivity Measurement.....	35
2.9.3 Mounting and Polishing.....	35

2.10	Scanning Electron Microscopy (SEM) Observations	36
2.10.1	Powders.....	36
2.10.2	Polished Specimens	36
2.11	Microhardness Measurement	36
3	RESULTS AND DISCUSSIONS.....	37
3.1	Properties of $\text{TiB}_2/\text{Al}_2\text{O}_3$ Suspensions	38
3.1.1	Electrokinetic Sonic Amplitude (ESA) Measurement	38
3.1.2	Stability Ratio (W)	43
3.2	Effect of pH on Green Body Density	46
3.2.1	Material Loss and Sample Attrition	46
3.2.2	Green Body Density Measurements	49
3.2.3	Green Density vs. Cold Isostatic Pressure	51
3.2.4	Green Body Conductivity	51
3.3	Sintered Density	52
3.3.1	Binder Burnout and Thermogravimetric Analysis (TGA).....	52
3.3.2	Material Loss and Sample Attrition.....	54
3.3.3	Sintered Density Measurements	54
3.3.4	Consistency of Sintered Microstructure with <i>Suspension Stability</i> [®] Predictions.....	55
3.3.5	Sintered Sample Conductivity	65
3.4	Microstructure.....	65
3.4.1	SHS Composites	65
3.4.2	SHS $\text{TiB}_2 / \text{Al}_2\text{O}_3$ Composites	65
3.5	Microhardness Measurement	66
4	CONCLUSIONS.....	67
5	FUTURE WORK.....	70
	REFERENCES	71
	APPENDICES	78
A.	Equations for Evaluating Armor Efficiencies.....	79
B.	Electrokinetic Sonic Amplitude (ESA) Measurements	82
C.	Green Body Density Measurements	94
D.	Sintered Density Measurements	100
E.	Conductivity Measurements	102
F.	Microhardness Measurements	104
G.	Porosity Measurements from Backscatter SEM Micrographs.....	106

LIST OF TABLES

Table 1: Physical properties reported by the manufacturer for SHS powders, TiB ₂ and Composite {TiB ₂ /Al ₂ O ₃ }.....	24
Table 2: The chemical and impurity analysis and physical properties for AKP-50 Al ₂ O ₃ reported by the manufacturer.....	25
Table 3: The chemical and impurity analysis and physical properties for Alcoa-SG Al ₂ O ₃ reported by the manufacturer.....	26
Table 4: Ceramic properties for Alcoa-SG Al ₂ O ₃ reported by the manufacturer.....	26
Table 5: The calculation of the Hamaker constant (A_i) in a vacuum [Bleier, 1983] where $A_i(kT) \sim 113.7\{(e_i-1)^2/[(e_i+1)^{3/2}(e_i+2)^{1/2}]\}$	28
Table 6: Binder burnout schedules for PEG processed samples.....	33
Table 7: Pressureless sintering schedules for all samples.....	34
Table 8: Hand polishing papers for sample preparation in the order used.....	35
Table 9: Relative stability between SHS TiB ₂ and AKP50 Al ₂ O ₃ predicted by <i>Suspension Stability</i> [©]	44
Table 10: Relative stability between SHS TiB ₂ and Alcoa-SG Al ₂ O ₃ predicted by <i>Suspension Stability</i> [©]	45
Table 11: Summary of processing conditions chosen for the three composite systems investigated.....	45
Table 12: Material loss during green body forming for each composite recipe and processing pH.....	46
Table 13: Sample attrition during green body forming for each composite recipe and processing pH.....	48
Table 14: Evaluation of sintered microstructure for consistency with processing behaviors.....	56
Table 95: Potentiometric Titration (POTN729.esa), 0.5 vol. % TiB ₂ , 1x10 ⁻⁴ M KNO ₃ ...	83
Table 16: Potentiometric Titration (POTN733.esa), 0.5 vol. % TiB ₂ , 1x10 ⁻³ M KNO ₃ ...	84
Table 17: Potentiometric Titration (POTN731.esa), 0.5 vol. % TiB ₂ , 1x10 ⁻² M KNO ₃ ...	85

Table 18: Potentiometric Titration (POTN717.esa), 0.5 vol. % AKP-50 Al ₂ O ₃ , 1x10 ⁻⁴ M KNO ₃	85
Table 19: Potentiometric Titration (POTN719.esa), 0.5 vol. % AKP-50 Al ₂ O ₃ , 1x10 ⁻³ M KNO ₃	87
Table 20: Potentiometric Titration (POTN723.esa), 0.5 vol. % AKP-50 Al ₂ O ₃ , 1x10 ⁻² M KNO ₃	88
Table 21: Potentiometric Titration (POTN710.esa), 0.5 vol. % Alcoa SG A-1000 Al ₂ O ₃ , 1x10 ⁻⁴ M KNO ₃	89
Table 22: Potentiometric Titration (POTN713.esa), 0.5 vol. % Alcoa SG A-1000 Al ₂ O ₃ , 1x10 ⁻³ M KNO ₃	90
Table 23: Potentiometric Titration (POTN725.esa), 0.5 vol. % Alcoa SG A-1000 Al ₂ O ₃ , 1x10 ⁻² M KNO ₃	91
Table 24: Potentiometric Titration (POTN702.esa), 0.5 vol. % SHS Composite {TiB ₂ /Al ₂ O ₃ }, 1x10 ⁻³ M KNO ₃	92
Table 25: Potentiometric Titration (POTN705.esa), 0.5 vol. % SHS Composite {TiB ₂ /Al ₂ O ₃ }, 1x10 ⁻³ M KNO ₃	93
Table 26: Green Body Density Data and Calculations for SHS TiB ₂ /AKP 50 Al ₂ O ₃ Ceramic Composites.....	95
Table 27: Green Body Density Data and Calculations for SHS TiB ₂ /Alcoa SG A-1000 Al ₂ O ₃ Ceramic Composites.....	96
Table 28: Green Body Density Data and Calculations for SHS TiB ₂ /Al ₂ O ₃ Ceramic Composites.....	98
Table 29: Sintered Density Measurements for the Three Composite Systems Investigated.....	101
Table 30: Conductivity Measurements.....	103
Table 31: Microhardness Measurements (Vickers (HV)).....	105
Table 32: Porosity Measurements from Backscatter SEM Micrographs.....	108
Table 33: Summary of Lineal Analysis Data for Porosity Measurements from Backscatter SEM Micrographs.....	112

LIST OF FIGURES

Figure 1: The microstructure termed “continuous” and more penetration resistant, taken from Logan [1997]. Light areas are TiB_2 and dark areas are Al_2O_3	8
Figure 2: The microstructure termed “discontinuous” and less penetration resistant, taken from Logan [1997]. Light areas are TiB_2 and dark areas are Al_2O_3	9
Figure 3: Surface charge influence on the distribution of nearby ions in the polar medium, after Shaw [1992, p. 178].....	12
Figure 4: Potential energy of the diffuse electrical double layer, after Shaw [1992, p. 178].....	13
Figure 5: Representation of the electrical double layer according to Stern's theory, after Shaw [1992, p. 183] and Heimenz [1997, p. 541].....	14
Figure 6: Potential of the electrical double layer according to Stern's theory, after Shaw [1992, p. 183] and Heimenz [1997, p. 541].....	14
Figure 7: Total potential energy of interaction (V_T) between two particles as function of their separation, after Hogg et al. [1966].....	18
Figure 8: Geometrical representation of the interaction between two dissimilar spherical particles of radii a_1 and a_2 as two infinitesimally small, flat plates where $h \ll a_1$ and $h \ll a_2$, after Hogg et al [1966].....	19
Figure 9: Zeta potentials determined from ESA data collected using the Matec ESA 8000 for AKP-50 Al_2O_3 suspended in three different concentrations of electrolyte.....	38
Figure 10: Zeta potentials determined from ESA data collected using the Matec ESA 8000 for Alcoa SG A-1000 Al_2O_3 suspended in three different concentrations of electrolyte.....	39
Figure 11: Zeta potentials determined from ESA data collected using the Matec ESA 8000 for SHS TiB_2 suspended in three different concentrations of electrolyte.....	39
Figure 12: Zeta potentials for each starting powder suspended in 1×10^{-3} M electrolyte from ESA data collected using the Matec ESA 8000.....	40
Figure 13: Stability ratio data prepared from the computer program, <i>Suspension Stability</i> ^o , for SHS TiB_2 and AKP 50 Al_2O_3	43
Figure 14: Stability ratio data prepared from the computer program, <i>Suspension Stability</i> ^o , for SHS TiB_2 and Alcoa-SG A-1000 Al_2O_3	44

Figure 15: Green density vs. processing pH for each composite recipe.....	50
Figure 16: Green density vs. pressure applied to composite samples during cold isostatic pressing.....	51
Figure 17: Thermogravimetric analysis (TGA) for the SHS TiB_2 – AKP 50 Al_2O_3 composite green samples prepared with a traditional binder; the 2 wt% polyethylene glycol (PEG) binder was removed by binder burnout before sintering.....	52
Figure 18: Thermogravimetric analysis (TGA) for the SHS TiB_2 – Alcoa SG Al_2O_3 composite green samples prepared with a traditional binder; the 2 wt% polyethylene glycol (PEG) binder was removed by binder burnout before sintering.....	53
Figure 19: Thermogravimetric analysis (TGA) for the SHS $\{\text{TiB}_2/\text{Al}_2\text{O}_3\}$ composite green samples prepared with a traditional binder; the 6 wt% polyethylene glycol (PEG) binder was removed by binder burnout before sintering.....	53
Figure 20(a): Sintered density (g/cc) vs. processing condition for each composite recipe.....	54
Figure 20(b): Sintered density (% Theoretical) vs. processing condition for each composite recipe.....	55
Figure 21: Backscatter scanning electron micrographs (20.0 kV) of the microstructures of each of the three composite systems at the four processing conditions; markers are 100 μm in every micrograph; white areas are the TiB_2 , gray areas are the Al_2O_3 , and black areas are pores.....	57
Figure 21(a): Backscatter scanning electron micrograph (20 kV) of SHS composite $\{\text{TiB}_2/\text{Al}_2\text{O}_3\}$ processed with PEG20M binder; marker (white line at bottom of micrograph) is 100 μm ; white areas are the TiB_2 , gray areas are the Al_2O_3 , and black areas are pores.....	58
Figure 21(b): Backscatter scanning electron micrograph (20 kV) of SHS composite $\{\text{TiB}_2/\text{Al}_2\text{O}_3\}$ processed at pH 4; white areas are the TiB_2 , gray areas are the Al_2O_3 , and black areas are pores.....	58
Figure 21(c): Backscatter scanning electron micrograph (20 kV) of SHS composite $\{\text{TiB}_2/\text{Al}_2\text{O}_3\}$ processed at pH 7; marker (white line at bottom of micrograph) is 100 μm ; white areas are the TiB_2 , gray areas are the Al_2O_3 , and black areas are pores.....	59
Figure 21(d): Backscatter scanning electron micrograph (20 kV) of SHS composite $\{\text{TiB}_2/\text{Al}_2\text{O}_3\}$ processed at pH 9; marker (white line at bottom of micrograph) is 100 μm ; white areas are the TiB_2 , gray areas are the Al_2O_3 , and black areas are pores.....	59

Figure 21(e): Backscatter scanning electron micrograph (20 kV) of SHS TiB_2 /AKP 50 Al_2O_3 processed with PEG20M binder; white areas are the TiB_2 , gray areas are the Al_2O_3 , and black areas are pores.....	60
Figure 21(f): Backscatter scanning electron micrograph (20 kV) of SHS TiB_2 /AKP 50 Al_2O_3 processed pH 4; white areas are the TiB_2 , gray areas are the Al_2O_3 , and black areas are pores.....	60
Figure 21(g): Backscatter scanning electron micrograph (20 kV) of SHS TiB_2 /AKP 50 Al_2O_3 processed pH 7.5; white areas are the TiB_2 , gray areas are the Al_2O_3 , and black areas are pores.....	61
Figure 21(h): Backscatter scanning electron micrograph (20 kV) of SHS TiB_2 /AKP 50 Al_2O_3 processed pH 8; white areas are the TiB_2 , gray areas are the Al_2O_3 , and black areas are pores.....	61
Figure 21(i): Backscatter scanning electron micrograph (20 kV) of SHS TiB_2 /Alcoa SG Al_2O_3 processed with PEG20M binder; marker (white line at bottom of micrograph) is 100 μm ; white areas are the TiB_2 , gray areas are the Al_2O_3 , and black areas are pores...	62
Figure 21(j): Backscatter scanning electron micrograph (20 kV) of SHS TiB_2 /Alcoa SG Al_2O_3 processed at pH 4; marker (white line at bottom of micrograph) is 100 μm ; white areas are the TiB_2 , gray areas are the Al_2O_3 , and black areas are pores.....	62
Figure 21(k): Backscatter scanning electron micrograph (20 kV) of SHS TiB_2 /Alcoa SG Al_2O_3 processed at pH 7; marker (white line at bottom of micrograph) is 100 μm ; white areas are the TiB_2 , gray areas are the Al_2O_3 , and black areas are pores.....	63
Figure 21(l): Backscatter scanning electron micrograph (20 kV) of SHS TiB_2 /Alcoa SG Al_2O_3 processed at pH 8; marker (white line at bottom of micrograph) is 100 μm ; white areas are the TiB_2 , gray areas are the Al_2O_3 , and black areas are pores.....	63
Figure 22: Scanning Electron Microscope (SEM) image of SHS $\{\text{TiB}_2/\text{Al}_2\text{O}_3\}$ composite powder dusted onto carbon tape; the large charging particles were thought to be the non-conducting Al_2O_3 and the small particles were thought to be the conducting TiB_2 ; recent investigations [Wilson, 2001] indicate most particles are a mixture of both the TiB_2 and the Al_2O_3	64
Figure 23: Backscatter SEM micrograph with lineal analysis, after EMSE [1986, p. 3832]	107

Introduction

The skin, structure, or add-on module that protects military vehicles against bullets, shells or other projectiles, is armor. In the past, the most capable armor was heavy and developed for main battle tanks weighing 50 tons or more. The increasingly changing state of global politics requires rapid deployment of a military force anywhere in the world. Rapid deployment dictates that the best armor be available for lightweight military vehicles.

Since the material used in fabricating the first armors was steel, the effectiveness of other armor material is compared to the first rolled homogeneous steel armor referred to as RHA. The protective ability of armor is characterized by its ballistic performance, which is quantified by its mass efficiency, a dimensionless factor that compares the areal density (mass/area) of an alternate armor material or system to RHA. For example, the typical specification of the material used to construct a lightweight military vehicle to provide protection against 7.62 mm armor piercing bullets at point blank range, is steel having an areal density of about 114 kg/m² [Ogorkiewicz, 1995]; the mass efficiency at this specification would therefore be 1.0 [Woolsey et al., 1989; see also Appendix A].

Hardening steel increases its effectiveness by enabling it to break the bullet or projectile more efficiently, but hardening also increases residual stresses making the hardened steel more prone to cracking. Dual hardness armor consists of two different steels roll-bonded together and heat treated to give the outer layer high hardness while the inner layer remains softer but tougher; dual hardness armor can have a mass effectiveness of as much as 1.78 [Ogorkiewicz, 1995]. Although the combination of a hard outer layer

with a softer inner one obviously improves ballistic performance, the weight of steel has a negative impact on the speed and transportability of a military vehicle.

Aluminum (Al) is used successfully as a structural material for military vehicles [Haworth, 1999, pp. 28, 95] as it has less weight and the ability to absorb the kinetic energy of projectiles. An Al inner structure with a high hardness steel outer plate is widely employed as ballistic protection for light armored vehicles; this dual hardness armor has a mass effectiveness of between 1.2 and 1.3 against 7.62 mm armor piercing bullets [Ogorkiewicz, 1995]. However, when weight is considered as a factor, even harder, non-metallic materials, namely ceramics, afford the best protection [Callister, 2000, p. 441]. The most common metal-non-metallic armor system is Al faced with tiles of aluminum oxide (Al_2O_3) [Ogorkiewicz, 1995]. This dual metal-ceramic system has a mass effectiveness ranging from 2.2 to 2.7 against 7.62 mm armor piercing bullets [Ogorkiewicz, 1995] and can have a weight saving of 60% [Hetherington, 1995] when compared with RHA. Other ceramics such as boron carbide (B_4C), silicon carbide (SiC) and titanium diboride (TiB_2) are even more effective [Hohler et al., 1995], but also more costly.

An Al_2O_3 based armor system is advantageous. Al_2O_3 is a sintered, rather than hot-pressed, component of armor, and because of its large demand by the Al industry [EMH Vol. 4, 1991, p. 50], is inexpensive as compared to B_4C , SiC and TiB_2 . Al_2O_3 , no matter the type, resists penetration linearly as tile thickness increases (0 to 30 mm) [Strassburger et al., 1995]. Its mechanical properties can be improved by the addition of a second phase of small, dispersed, non-equiaxed TiB_2 particles [Liu and Ownby, 1991].

The high cost of TiB_2 powders stems from its energy intensive processing via carbothermal reduction [EMH Vol. 4, 1991, p.48]. Fuel costs are high to reach the temperatures required for TiB_2 production. An alternate synthesis route is via a particular form of combustion termed self-propagating-high-temperature-synthesis (SHS) [Merzhanov, 1990, pp. 1-3]. SHS is an instantaneous event rather than a long-term, high-temperature reaction as is carbothermic reduction. SHS thereby eliminates high fuel costs, and also incidentally increases the purity of the resulting powders. Logan [Ph.D. Thesis, 1992] is able to produce not only TiB_2 powders by SHS, but also the composite titanium diboride/alumina ($\text{TiB}_2/\text{Al}_2\text{O}_3$) powder.

$\text{TiB}_2/\text{Al}_2\text{O}_3$ powders produced by SHS have been hot pressed into armor tiles that exhibit superior resistance to penetration as compared to TiB_2 , SiC, B_4C or Al_2O_3 [Logan Ph.D. Thesis, 1992]. As with other advanced ceramics, however, difficulties in processing $\text{TiB}_2/\text{Al}_2\text{O}_3$ arise from the inability to reproduce specimens with consistent microstructure and properties [Lange, 1989]. Commercial availability of SHS TiB_2 and SHS $\{\text{TiB}_2/\text{Al}_2\text{O}_3\}$ powders makes it possible to investigate alternative processing methods that may reduce the range and variation of properties of $\text{TiB}_2/\text{Al}_2\text{O}_3$ armor tiles. An additional consideration is that any alternative processing method should be low cost.

The unique feature of SHS-produced starting powders is that the combination reaction is self-sustaining [Hoke and Meyers, 1995]. Upon lowering the free energy of the starting materials, the energy released to the products typically raises the temperature of the products. Many contaminants (oxygen, nitrogen, etc.) that may exist on the starting powders volatilize and leave behind escape paths in the freshly synthesized material. These escape paths, combined with a typical volume decrease during reaction

and the initial porosity of the reacting mixture, produce a material with 40-50% residual porosity. Hoke and Meyers [1995] suggest that densification can best be achieved by “forced consolidation” techniques that occur over small time scales immediately following combustion synthesis. In contrast to conventional consolidation of ceramic powders such as hot pressing or hot isostatic pressing, which are time-consuming and slow, forced consolidation is a rapid technique.

Kecskes and others [1996] applied forced consolidation, termed dynamic consolidation (DC) techniques, to $\text{TiB}_2/\text{Al}_2\text{O}_3$ powders immediately after their synthesis by SHS. In DC, a powdered amatol explosive (80/20 $\text{NH}_4\text{NO}_3/\text{TNT}$) drives two high-hardness steel compression plates (Brinell Hardness of 480-530) containing the SHS reacted product to effect consolidation. However, the large differences between the melting point of the TiB_2 and Al_2O_3 phases, and the susceptibility of densified samples to contamination (from the surrounding insulating media and sand) have limited the success of DC [Kecskes et al., 1996].

Ultimately, the advantages of combining SHS and DC techniques will be to eliminate the demands of conventional green body formation, that is mixing, shaping, drying and firing, all of which are labor-time-cost-intensive steps in ceramic processing. With the commercial availability of inexpensive SHS products such as TiB_2 and $\text{TiB}_2/\text{Al}_2\text{O}_3$ powders, and the current lack of large-scale success with DC, other conventional processing techniques should be considered. Particularly, processing steps that control green body formation as well as densification should be investigated. One of the potentially most viable alternatives is colloidal processing [Lange, 1989; Wilson and Crimp, 1993].

After the commercial powders have been synthesized, they are mechanically mixed (e.g. by ball milling) to optimize particle size and the range of particle-size distribution in the SHS powders. However, only chemical mixing (colloidal processing) can improve processing reliability and therefore provides more consistent ceramics [Lange et al., 1990]. Wilson and Crimp [1993] have modeled the colloidal processing of ceramic composites based on the approximations developed by Hogg, Healy and Fuerstenau (HHF). The model, *Suspension Stability*®, uses measurable material data to create information to predict the coagulation state of two component colloidal suspensions.

The colloidal processing of $\text{TiB}_2/\text{Al}_2\text{O}_3$ composites, both the SHS produced composite and composites mixed from other readily available commercial aluminas with the SHS produced TiB_2 , will be investigated.

The objectives of this investigation were to:

- show that the model, *Suspension Stability*® [Wilson and Crimp, 1993], developed to predict coagulation behavior based on the $\text{Si}_3\text{N}_4/\text{SiC}$ composite system, will predict the coagulation behavior of the $\text{TiB}_2/\text{Al}_2\text{O}_3$ composite system.
- show that colloidal processing will reproduce the microstructure obtained by Logan [1997] in $\text{TiB}_2/\text{Al}_2\text{O}_3$ composites associated with penetration resistance in ceramic armor.
- measure the zeta potential (ζ) for SHS TiB_2 , Sumitomo AKP50 Al_2O_3 , Alcoa Superground A-1000 Al_2O_3 and Composite SHS $\{\text{TiB}_2/\text{Al}_2\text{O}_3\}$.
- predict the coagulation behavior of the $\text{TiB}_2 - \text{Al}_2\text{O}_3$ ceramic composite system in suspension using the model *Suspension Stability*® [Wilson and Crimp, 1993].

- slip cast 30/70 wt. % $\text{TiB}_2/\text{Al}_2\text{O}_3$ suspensions at conditions for coagulation, heterocoagulation and dispersion behavior based on these predictions.
- free-sinter the slip cast $\text{TiB}_2/\text{Al}_2\text{O}_3$ samples to maximum densification.
- measure the density of the slip cast $\text{TiB}_2/\text{Al}_2\text{O}_3$ samples in the green and sintered states.
- measure the microhardness of the sintered $\text{TiB}_2/\text{Al}_2\text{O}_3$ samples.
- examine the microstructure of the $\text{TiB}_2/\text{Al}_2\text{O}_3$ samples and compare to the
 - predictions for coagulation, heterocoagulation and dispersion behavior of the TiB_2 and Al_2O_3 , and
 - microstructures of samples prepared by Logan [1997] associated with penetration resistance in ceramic armor.

1 Literature Review

The recent and relevant literature for ceramic armor performance, colloidal systems with emphasis on particle interactions, and theories of colloidal stability was reviewed to understand:

- the desired microstructure for titanium diboride-alumina ceramic composites for penetration resistance, and
- the predictive basis of the computer model used to establish conditions for colloidal processing of the titanium diboride-alumina powders.

1.1 *Titanium Diboride (TiB₂) – Alumina (Al₂O₃) Composites*

Titanium diboride (TiB₂), silicon carbide (SiC), boron carbide (B₄C), and alumina (Al₂O₃) perform well as armor materials, but TiB₂/Al₂O₃ composites have superior resistance to penetration [Logan Ph.D. Thesis, 1992]. Composite TiB₂/Al₂O₃ powders made by self-propagating high temperature synthesis (SHS) and then immediately hot pressed into armor tiles demonstrate a superior resistance to the high strain rate penetration required for armor [Abfalter et al., 1992]. Analysis of TiB₂/Al₂O₃ targets indicate a bias in the microstructure of the penetration resistant targets [Logan, 1997]. Superior performance is associated with a “continuous” microstructure where the TiB₂ forms an interconnecting network at the Al₂O₃ grain boundaries. Targets where the TiB₂ is distributed in the Al₂O₃ grains, termed “discontinuous,” lack the same penetration resistant performance [Logan, 1997]. According to Logan [1997], the term continuous describes TiB₂ surrounding the Al₂O₃ grains, forming an unbroken, interconnected,

electrically conductive TiB_2 network in the target (Fig. 1), and discontinuous describes TiB_2 dispersed in Al_2O_3 grains forming a more homogenous though electrically non-conductive target (Fig. 2). Although much work has been done to refine the process for synthesizing the composite $\text{TiB}_2/\text{Al}_2\text{O}_3$ powders and define the properties of the hot pressed, ceramic composites, there has been no alternative processing of the powders to improve the reproducibility of $\text{TiB}_2/\text{Al}_2\text{O}_3$ armor tiles. One of the potentially most viable alternatives is colloidal processing [Lange, 1989; Wilson and Crimp, 1993].

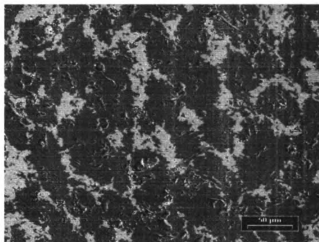


Figure 1: The microstructure termed “continuous” and more penetration resistant, taken from Logan [1997]. Light areas are TiB_2 and dark areas are Al_2O_3 .

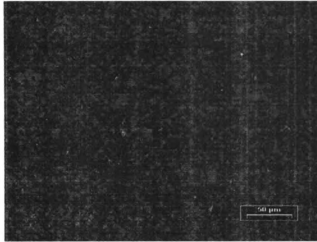


Figure 2: The microstructure termed “discontinuous” and less penetration resistant, taken from Logan [1997]. Light areas are TiB_2 and dark areas are Al_2O_3 .

1.2 Colloidal Processing

1.2.1 Colloidal Systems

1.2.1.1 Colloidal Suspensions

Colloidal suspensions form when an insoluble substance is broken down into very small particles (disperse phase) and distributed more or less uniformly through another substance (dispersion medium), regardless of the state of the matter [Hunter, 1993, p.2]. A sol is the specific name for the particular suspension of a solid disperse phase in a liquid dispersion medium [Takeo 1999, p. 5]. Another designation for a sol is lyophobic, or *solvent-hating*, colloid [Becher, 1990, p. 95]. Sols are distinguished from true solutions by the size of the particles: one nanometer or less for solute and solvent in a solution, and one nanometer to one micron (or more) for the dispersed phase of a sol [Hunter, 1993, p. 2]. In a typical sol, the dispersed phase is much larger than the molecules of the liquid medium.

1.2.1.2 Coagulation

The challenge in forming colloidal suspensions is controlling aggregation, which is also termed coagulation or agglomeration [Hunter, 1993, p. 7]. The colloid suspension forms through distribution of the disperse phase in the dispersion medium while maintaining a discrete nature for the particles of the disperse phase [Hunter, 1993, p. 2]. A colloidal system, consisting of the particles, the liquid and any electrolytes present in the liquid, has the important feature of a large ratio of surface area to volume of the dispersed solid [Takeo, 1999, p. 1] such that the area of contact between the dispersed particles and the dispersion medium is relatively large. The energy associated with creating and maintaining that interface can be significant and depends on its fundamental chemistry. The total free energy of a colloidal system can always be lowered by a reduction in the interfacial area, i.e., coagulation or agglomeration, which is controlled by the electrostatic character of the particle-liquid interface. Attractive and repulsive electrostatic forces dictate the rate of coagulation [Hunter, 1993, p. 98].

1.2.1.3 Colloidal Forces

Particles in a colloidal suspension come together because of attractive van der Waals forces. For covalently bonded ceramic materials, “London forces” explain almost all of the van der Waals attraction [Shaw, 1992, p. 216]. London [1930, as cited in Shaw, 1992, p. 215] explained that attraction between molecules is due to the polarization of one molecule by fluctuations in the charge distribution in a second molecule, and vice versa. This attractive energy is very short-range and additive; it varies inversely with the sixth power of the interparticle distance, and can be computed by summing the attractions between all interparticle pairs [Shaw, 1992, p. 216]. Hamaker [1937, as cited in Shaw,

1992, p. 216] derived an expression for the London interaction energy (V_A) for the case of two spherical particles of radii a_1 and a_2 separated in a vacuum by a shortest distance H , where $x = H / (a_1 + a_2)$ and $y = a_1 / a_2$:

$$V_A = -\frac{A}{12} \left[\frac{y}{x^2 + xy + x} + \frac{y}{x^2 + xy + y} + 2 \ln \frac{x^2 + xy + x}{x^2 + xy + x + y} \right] \quad (1)$$

A is the Hamaker constant. Bleier (1983) calculated the Hamaker constant in a vacuum using a simplified Lifshitz method:

$$A_i(kT) \cong 113.7 \frac{(e-1)^2}{(e_i+1)^{3/2}(e_i+2)^{1/2}} \quad (2)$$

Particles in a liquid, rather than a vacuum or air, have a considerably lower London - van der Waals interaction energy [Shaw, 1992, p. 217]. For two different particles in a liquid medium, an effective Hamaker constant is used [Shaw, 1992, p. 218]:

$$A_{\text{eff}} = (A_i^{1/2} - A_m^{1/2})(A_j^{1/2} - A_m^{1/2}) \quad (3)$$

To consider other forces in a colloidal suspension, a detailed description of the particles themselves is needed.

1.2.2 Particle Description

1.2.2.1 Surface Charge of Particles

Generally, particles develop a surface charge when in contact with a polar, liquid medium. The origin of this surface charge may be ionization, ion adsorption or ion dissolution [Shaw, 1992, p. 174]. The surface charge affects the distribution of ions in the immediate vicinity of the particle (Fig. 3).

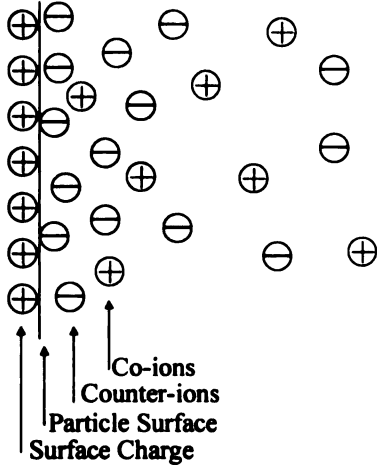


Figure 3: Surface charge influence on the distribution of nearby ions in the polar medium, after Shaw [1992, p. 178].

If the charged particle surface is considered a plane carrying a uniformly distributed charge, then, applying *Boltzmann's distribution law*, the electrical potential (ψ) decreases exponentially with distance from the surface:

$$\psi = \psi^0 \exp(-\kappa z) \quad [\text{Everett, 1988, p. 42}] \quad (4)$$

where ψ^0 is the electric potential at the surface and z is a measure of distance. At a distance $1/\kappa$ the potential drops by a factor of $1/e$ (Fig. 4). The influence of charge from the particle surface and the mixing tendency of thermal motion lead to the formation of an electrical double layer [Shaw, 1992, p. 174]. The parameter $1/\kappa$ is also a measure of the thickness of the electrical double layer [Everett, 1988, p. 42] taken from:

$$\kappa^2 = \frac{8\pi v^2 e^2 N_A C}{1000 \epsilon k T} (cm^{-2}) \quad (5)$$

where v is the counter-ion valence, e is the electronic charge, k is Boltzmann's constant, T is temperature, C is electrolyte concentration, N_A is Avagadro's number, and ϵ is the dielectric constant [Texter, 2000]. Figure 4 denotes the simple case of a particle in a

medium with no adsorbed surface-active ions or polyvalent counter ions present so that as the distance from the charged particle surface increases, the potential energy decreases, and $1/\kappa$ defines the ionic atmosphere [Everett, 1988, p. 42].

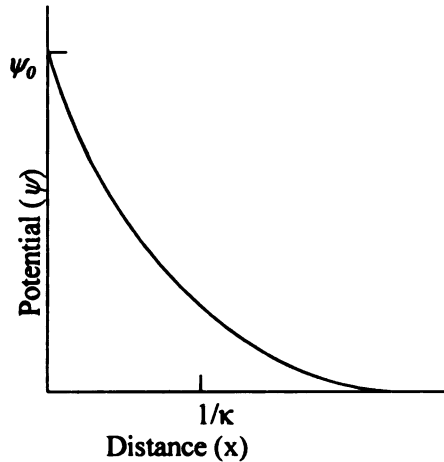


Figure 4: Potential energy of the diffuse electrical double layer, after Shaw [1992, p. 178].

1.2.2.2 Electrical Double Layer

The electric double layer is the charged particle surface and the neutralizing excess of counter-ions over co-ions diffused in the liquid polar medium [Shaw, 1992, p. 174]. The variation in ion density near the particle interface with the liquid polar medium may be further subdivided into two phases that carry equal and opposite charge [Hiemenz, 1997, p.499]. Stern [1924, as cited in Shaw, 1992, p. 182, or Hiemenz, 1997, p.527] proposed that these two phases (inner and outer parts of the double layer) are separated by a plane (surface) referred to as the Stern plane or surface (Fig. 5).

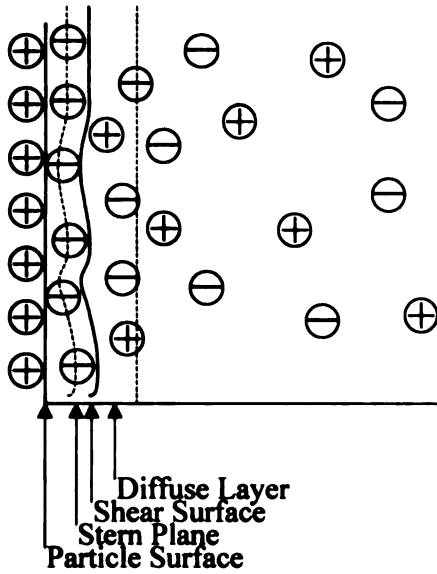


Figure 5: Representation of the electrical double layer according to Stern's theory, after Shaw [1992, p. 183] and Heimenz [1997, p. 541].

The Stern surface lies at a distance δ from the particle surface. Outside the Stern surface, the surface potential decreases exponentially (Fig. 6).

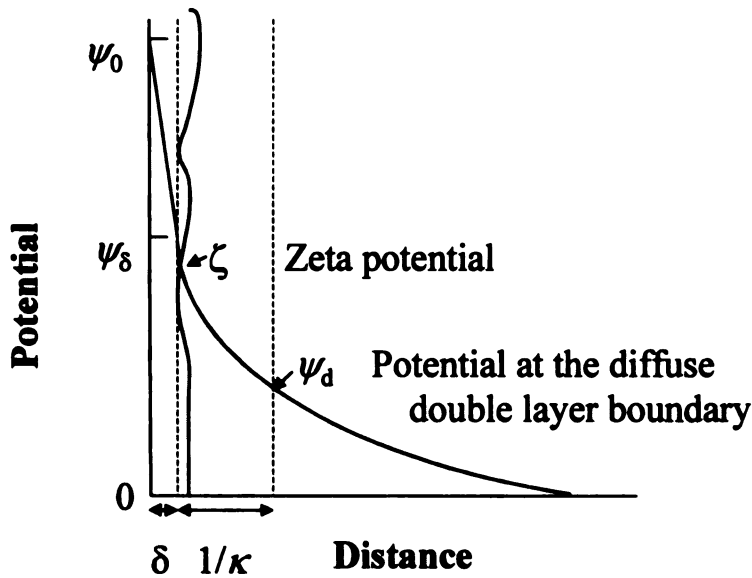


Figure 6: Potential of the electrical double layer according to Stern's theory, after Shaw [1992, p. 183] and Heimenz [1997, p. 541].

When adsorbed surface-active ions or polyvalent counter-ions are present, the Stern surface potential may change sign or intensity. Applying Stern theory quantitatively to determine potential is problematic because parameters such as ψ_δ cannot be assessed experimentally [Heimenz, 1997, p. 529]. However, the potential in the diffuse double layer can be measured near the inner limit (ψ_0), which is either the actual surface or the Stern surface, and is called the zeta potential (ζ) [Heimenz, 1997, p. 529; Everett, 1988, p. 90].

1.2.2.3 Zeta (ζ) Potential

The “boundary” between the Stern layer and the diffuse layer is a surface where movement between the particle with its adsorbed ions and the liquid medium occurs. This boundary is referred to as a hydrodynamic slip plane or plane of shear; the zeta (ζ) potential is defined at this boundary [Heimenz, p. 541; Everett, p. 90]. Electrokinetic phenomena, that is, electrophoresis, electroosmosis and streaming potential, can be measured experimentally to determine the potential in the double layer near the charged surface [Heimenz, 1997, p. 534]. Electrophoresis has the greatest practical applicability of these electrokinetic phenomena [Shaw, 1992, p. 190]. Interpreting these measurements yields the zeta potential (ζ). Although electrophoresis has long had the greatest practical applicability of these electrokinetic phenomena [Shaw, 1992, p.190], electrokinetic sonic amplitude (ESA) is one of the most practical and repeatable tools for obtaining zeta potential (ζ) data [Hunter, 1993, p. 382; Wilson and Crimp, 1993].

1.2.2.4 Electrokinetic Sonic Amplitude (ESA)

ESA is a patented method to measure electrokinetic properties without the limitations and restrictions of traditional microelectrophoresis technique [Matec, 2001]. Specifically, ESA is an electroacoustic method whereby a high frequency electric field is applied to the colloidal suspension. When the particles move (electrophoretically) in the applied field, if there is a difference in density between the particles and the liquid, the motion of the particles produce an alternating acoustic wave called the electrokinetic sonic amplitude (ESA). The measure of ESA is in pressure amplitude per unit of applied electric field ($ESA(\omega)$), and is used to determine the ESA dynamic mobility ($\mu_d(\omega)$) by the following equation [O'Brien, 1986 & 1990, as cited in Wilson and Crimp, 1993]:

$$\mu_d(\omega) = \frac{ESA(\omega)}{\phi \Delta \rho c} \quad (6)$$

where ϕ is the volume fraction of solids, $\Delta \rho$ is the density difference of the particles and the liquid, and c is the velocity of sound in the suspension. The ESA dynamic mobility is used to determine the zeta potential (ζ) by the equation [O'Brien, 1986 & 1990, as cited in Wilson and Crimp, 1993]:

$$\zeta = \left(\frac{\mu_d \eta}{\epsilon_0 \epsilon_r} \right) G(\alpha)^{-1} \quad (7)$$

where η is the viscosity of the suspension, $\epsilon_0 \epsilon_r$ is the applied electric field, and $G(\alpha)^{-1}$ is the correction for the inertia of the particle in an alternating field. Using a Matec ESA-8000 system to collect ESA data, the pH, conductivity and temperature can also be measured concurrently [Matec, 2001] to employ zeta potential (ζ) in the application of

theories of colloidal stability to ceramic composite suspensions [Wilson and Crimp, 1993].

1.3 Derjaguin-Landau-Verwey-Overbeek (DLVO) Theory

The forces that arise between similar particles in aqueous media are described by the classical DLVO theory of the stability of lyophobic colloids [Colic et al., 1997]. According to DLVO theory, the total interaction energy between two particles (V_T) is obtained by summing the interaction energies due to the van der Waals attraction (V_A) and the electrostatic double layer repulsion (V_R):

$$V_T = V_A + V_R \quad (8)$$

When two particles are forced together, their respective diffuse layers overlap, increasing the concentration of counterions between them and giving rise to an osmotic pressure, and thus a repulsive force [Colic et al., 1997]. However, most ceramic composite systems are made up of dissimilar rather than similar particles, and the theoretical analysis of the interaction of dissimilar double layers using DLVO theory requires tedious graphical or numerical integrations [Derjaguin (1954) and Devereux and de Bruyn (1963), as cited in Hogg et al., 1966]. Therefore, another quantitative theory that can better describe the kinetics of coagulation for a ceramic composite colloidal system is needed.

1.4 Hogg, Healy and Fuerstenau (HHF) Theory

1.4.1 Development of HHF Theory

1.4.1.1 Colloidal Particle Interactions

Hogg et al. [1966] derived a relationship to describe the potential energy of interaction between the dissimilar electrical double layers associated with the particles in a multicomponent colloidal system. As in DLVO theory, the total potential energy of interaction is generally given by equation (8), and when the surface potentials of the two interacting particles are large and have the same sign, then V_R is positive and the total energy V_T passes through a maximum (Fig. 7).

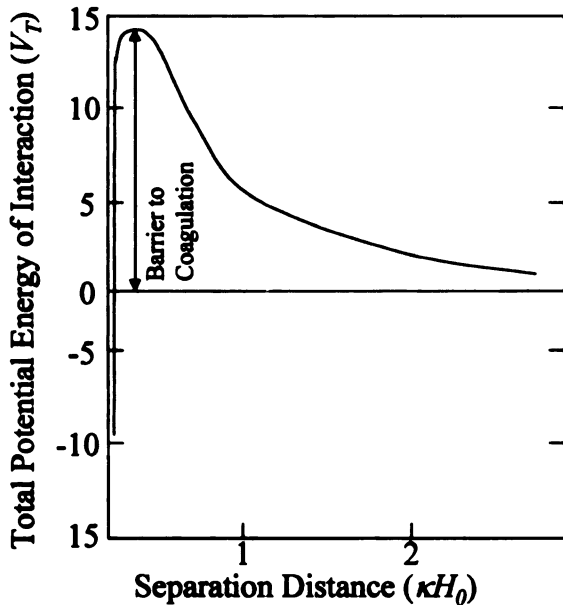


Figure 7: Total potential energy of interaction (V_T) between two particles as function of their separation, after Hogg et al. [1966].

The potential energy of the attractive forces (V_A) is as in equation (1). Hogg et al. [1966] expanded the expression for the potential energy of the repulsive forces (V_R), however, by treating the interaction between small electrical double layers on spherical particles after Derjaguin [1934, as cited in Hogg et al., 1966]. The interaction is then as infinitesimally small parallel rings, each of which can be considered as a flat plate (Fig. 8) so that:

$$V_R = \frac{\varepsilon a_1 a_2 (\psi_{0_1}^2 + \psi_{0_2}^2)}{4(a_1 + a_2)} \left[\frac{2\psi_{0_1} \psi_{0_2}}{(\psi_{0_1}^2 + \psi_{0_2}^2)} \ln \left(\frac{1 + \exp(-\kappa H_0)}{1 - \exp(-\kappa H_0)} \right) + \ln(1 - \exp(-2\kappa H_0)) \right] \quad (9)$$

where ε is the dielectric constant, a_1 and a_2 are the particle radii, ψ is the particle surface potential, κ is the Debye-Hückel parameter, and H_0 is the particle separation distance [Hogg et al., 1966].

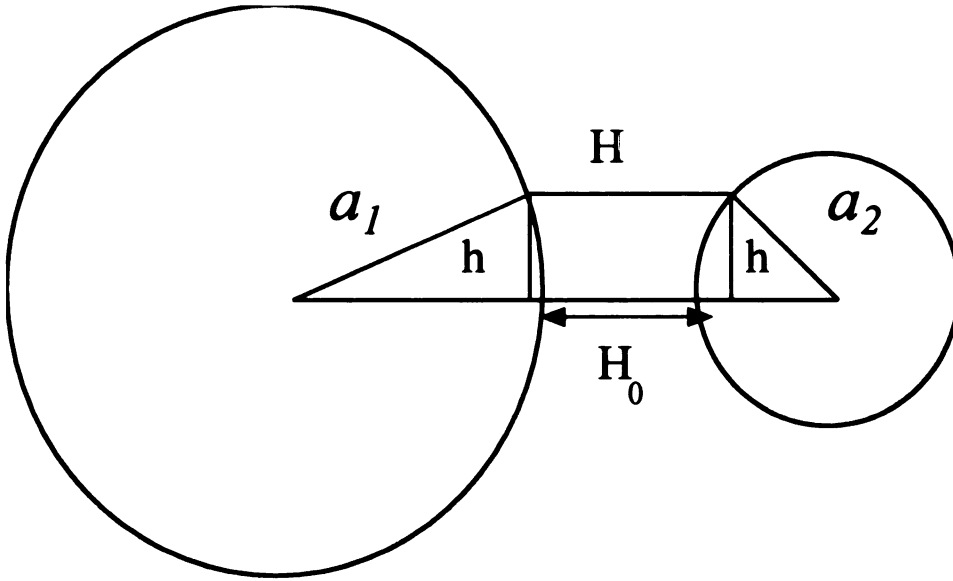


Figure 8: Geometrical representation of the interaction between two dissimilar spherical particles of radii a_1 and a_2 as two infinitesimally small, flat plates where $h \ll a_1$ and $h \ll a_2$, after Hogg et al [1966].

However, the variation in V_T , that is, the height of the barrier to coagulation (Fig. 7), affects the rate of coagulation [Hogg et al., 1966]. When the energy of interaction between the particles is zero, except for an infinite attraction when the particles are in contact, the sol is under rapid coagulation conditions [Smoluchowski (1916, 1917), as cited in Hogg et al., 1966]. When V_T is not zero, the frequency and types (between like or unlike) of collisions between particles will describe the overall rate of coagulation.

1.4.1.2 Coagulation Kinetics

When two particles collide, they stick together and fall out of suspension (coagulate); the frequency of collisions between particles determines (J), the rate of coagulation [Smoluchowski (1916, 1917), as cited in Hogg et al., 1966] so that:

$$J = \frac{-dv_0}{dt} = 8\pi D v_0^2 R_0 \quad (10)$$

where v_0 is the number of particles, D is the diffusion coefficient and R_0 is the minimum separation of particles. Where there are energy barriers between the particles, the rate of coagulation is reduced by a factor W [Fuchs (1934), as cited in Hogg et al., 1966] so that:

$$J = \frac{8\pi D v_0^2 R_0}{W} \quad (11)$$

But W is given by:

$$W = R_0 \int_{R_0}^{\infty} \exp\left(\frac{V_T}{kT}\right) \frac{dR}{R^2} \quad (12)$$

Specifically, W denotes the ratio of rapid to slow coagulation [Hogg et al., 1966].

Under conditions where the energy of interaction between the particles is not zero, the probability that particles of types i and j collide is reduced by a factor W_{ij} [Hogg et al., 1966]:

$$W_{ij} = 2 \int_0^\infty \exp\left(\frac{V_T^{ij}}{kT}\right) \frac{dS}{S^2} \quad (13)$$

Where $S \equiv R/\bar{\sigma}$ and $\bar{\sigma} = (a_i + a_j)$. The overall stability ratio (W_o) for a suspension containing two kinds of particles (1 and 2), however, is dependent upon their probabilities of interaction [Hogg et al. 1966]. Probabilities of interaction for particles 1 and 2 between like (P_{11} , P_{22}) and unlike (P_{12}) particles are as follows:

$$P_{11}=n^2 \quad P_{22}=(1-n)^2 \quad P_{12}=2n(1-n) \quad (14)$$

Three separate stability ratios, W_{11} , W_{22} , and W_{12} have to be calculated using equation (13) to define W_o . The probability that a given collision between two particles leads to adhesion is [Hogg et al., 1966]:

$$1/W_o = n^2/W_{11} + (1-n)^2/W_{22} + 2n(1-n)/W_{12} \quad (15)$$

1.4.2 Modeling HHF Theory

Wilson and Crimp [1993] base their model, *Suspension Stability*^o, on HHF theory since it is the only model which incorporates the kinetic aspect of colloidal system stability into quantitative expressions for the coagulation behavior of a system of nonidentical particles, and is therefore adaptable to ceramic composites. HHF theory was adapted to better predict the stability of ceramic composite suspensions by:

- employing zeta potential, ζ , versus pH data to replace surface potential ψ_o , where only particle size and density are necessary parameters for measurements rather than

details of ions groups present and their behavior with the medium, enabling predictions for novel ceramic composites,

- calculating an effective Hamaker constant after Shaw [1992, as cited in Wilson and Crimp, 1993] from the Hamaker constants determined in a vacuum because particle interactions in a medium are less than in a vacuum due to the presence of molecules of the medium between the two interacting particles,
- relying on a simplified Lifshitz method after Bleier [1983] to calculate Hamaker constants since a method for the calculation was not addressed by HHF theory,
- expanding the expression for the energy (V_A) of interaction of the particles themselves due to van der Waals forces to allow for other than $H/a \ll 1$, that is, small particle separations,
- deriving a relationship between the relative volume fraction of particles of the two particles and their radii to the overall proportion n used in the overall stability ratio (W_T) to permit input of the relative volume fraction of components.

The ranges of stability are indicated by pH where $\log W$ values are greater than 40 because at large separations of the particles, the errors resulting from the approximations of the potential are small [Hogg et al., 1966]. Neither 10% variations in the Hamaker constant, nor a $\pm 5^\circ \text{C}$ change in temperature from room temperature, affect the predictive abilities of the program [Wilson and Crimp, 1993].

2 Experimental Procedure

The preparations and procedures used to investigate the colloidal behavior, green and sintered densities, and resulting microstructure of SHS composite {TiB₂/Al₂O₃}, and composites of SHS TiB₂ combined with each of Sumitomo AKP-50 and Alcoa Superground A-1000 Al₂O₃ are described in this section. The starting composite materials and all laboratory chemicals and polishing compounds were obtained from commercial sources.

The equipment necessary for this investigation included scales accurate to 0.001 gram, a Matec Electrokinetic Sonic Amplitude (ESA) 8000, a Fisher Scientific pH meter, a cold isostatic press, a CM Rapid Temperature 6" Furnace, a Hewlett Packard E2378A Multimeter, a Thermal Technology, Inc. resistance-heated, graphite furnace, an 1810 Amray scanning electron microscope (SEM) equipped with an Oxford Detector for Energy Dispersive Spectroscopy (EDS), a JEOL JXA-840 SEM for backscatter imaging, and Nalgene® storage containers, graduated cylinders, and beakers.

2.1 Starting Powders

2.1.1 Self-propagating-high-temperature-synthesis (SHS) TiB₂

TiB₂ is covalently bonded in a hexagonal crystal structure typified by that of AlB₂ in which layers of titanium and boron atoms alternate in hexagonal coordination [Mroz, 1995]. To form TiB₂, the SHS process combines readily available, high purity titanium

dioxide (TiO_2), boron oxide (B_2O_3) and magnesium (Mg) powders according to the following equation [Logan Ph.D. Thesis, 1992]:



The composite TiB_2/MgO product is then leached using a nitric acid solution to produce sub-micron TiB_2 particles [Logan Ph.D. Thesis, 1992]. The sub-micron particle size and the particle-size distribution of SHS powders are appropriate for optimal green body formation [Kingery, 1976, p. 9]. Advanced Engineered Materials (AEM), LLC (Woodstock, GA), reports that Advanced TiB_2 Powder is a crystalline, non-pyrophoric, homogeneous powder produced by a proprietary continuous process [AEM, LLC, 1995]. The physical properties reported by AEM, LLC for SHS TiB_2 are summarized in Table 1.

Table 1: Physical properties reported by the manufacturer for SHS powders, TiB_2 and Composite $\{\text{TiB}_2/\text{Al}_2\text{O}_3\}$

Physical Properties	SHS TiB_2	SHS $\{\text{TiB}_2/\text{Al}_2\text{O}_3\}$
Melting Point, $^{\circ}\text{C}/^{\circ}\text{F}$	3000/5430	2100/3812
Specific area (m^2/g), minimum	25	Not reported
Bulk density (g/cc)	0.94	1.3
Theoretical density (hot press) (g/cc)	4.51	4.12
Particle size range (mm)	0.1 to 3	0.5 to 20
Median particle size (mm)	0.5	2

2.1.2 Alumina (Al_2O_3) Powders

$\alpha\text{-Al}_2\text{O}_3$ is the important form of alumina in the fabrication of ceramics [Logan Ph.D. Thesis, 1992; EMHSC, 1986; Jacobs and Kotomin, 1994]. The $\alpha\text{-Al}_2\text{O}_3$ (corundum) structure can be viewed as hexagonal close packing of oxygen atoms with aluminum atoms occupying two-thirds of the octahedral interstices. The unit cell (ten

atoms) contains two molecular units: each with three oxygen atoms (O^{2-}) forming a triangle having two aluminum atoms (Al^{3+}) on the z axis that lie symmetrically above and below the oxygen-triangle [Jacobs and Kotomin, 1994].

2.1.2.1 Sumitomo AKP-50 Al_2O_3

Sumitomo Chemical America, Inc., High Purity Alumina, AKP-50 was selected for its high surface area relative to particle size, which promotes sintering in $\alpha-Al_2O_3$ powders [Occhionero et al., 1988]. The chemical and impurity analyses and the physical properties reported by Sumitomo Chemical America, Inc. for AKP-50 are summarized in Table 2. Single crystals, abrasives, high strength alumina ceramics, and filler and blending agents are applications of AKP-50 reported by the manufacturer [Sumitomo, 2001.]

Table 2: The chemical and impurity analysis and physical properties for AKP-50 Al_2O_3 reported by the manufacturer

Al_2O_3	99.995%↑
Si	<10 ppm
Na	<10 ppm
Mg	<10 ppm
Cu	<10 ppm
Fe	<10 ppm
Particle size (μm) (Laser: Microtruck)	0.1 - 0.3
B.E.T. Special surface area (m^2/g)	9 – 15

2.1.2.2 Alcoa Superground A-1000 Al_2O_3

Alcoa Industrial Chemicals, Calcined Alumina, Realox Reactive Grade A-1000 was chosen for its origin and similarity in particle size to that used by Logan [1997]. The

chemical analysis by weight and the physical properties for Alcoa-SG reported by Alcoa Industrial Chemicals are summarized in Table 3. The ceramic properties reported by the Alcoa Industrial Chemicals for 10.5g pellets pressed in a one-inch diameter die at 34.5 MPa are summarized in Table 4.

Table 3: The chemical and impurity analysis and physical properties for Alcoa-SG Al_2O_3 reported by the manufacturer

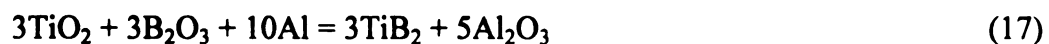
Al_2O_3	99.8 wt %
Na_2O	0.07
SiO_2	0.02
Fe_2O_3	0.02
CaO	0.02
B_2O_3	0.003
MgO	0.04
Median particle size (μm) (Sedigraph 5100)	0.4
Percent through 44 μm sieve	100
Surface area (m^2/g)	8.8

Table 4: Ceramic properties for Alcoa-SG Al_2O_3 reported by the manufacturer

Green density (g/cc)	2.18
Fired Density (g/cc)	3.89
Shrinkage (%)	17.4
Fired one hour at ($^\circ\text{C}$)	1540

2.1.3 SHS Composite $\{\text{TiB}_2/\text{Al}_2\text{O}_3\}$

To form composite $\text{TiB}_2/\text{Al}_2\text{O}_3$, the SHS process combines readily available, high purity titanium dioxide (TiO_2), boron oxide (B_2O_3) and aluminum (Al) powders according to the following equation [Logan Ph.D. Thesis, 1992]:



The composite $\text{TiB}_2/\text{Al}_2\text{O}_3$ is ball milled to reduce the particle size of the as-reacted powder and homogenize the distribution of TiB_2 and Al_2O_3 . Although it can be formulated in any ratio, the nominal composition of the $\text{TiB}_2/\text{Al}_2\text{O}_3$ for armor tile fabrication is 71 wt % Al_2O_3 and 29 wt % TiB_2 . Advanced Engineered Materials (AEM), LLC, reports that Premier Composite $\text{TiB}_2/\text{Al}_2\text{O}_3$ powder is a crystalline, non-pyrophoric, homogeneous powder produced by a proprietary continuous process [AEM LLC, 1995]. The physical properties reported by AEM, LLC for SHS $\{\text{TiB}_2/\text{Al}_2\text{O}_3\}$ are summarized in Table 1.

2.2 *Electrokinetic Sonic Amplitude (ESA) Measurement*

The ESA 8000 from Matec Applied Sciences (Northboro, MA) was used to perform zeta (ζ) potential measurements as a function of pH for each starting powder at a volume fraction of 0.005 suspended in an indifferent, liquid electrolyte, potassium nitrate (KNO_3) at a concentration of 1×10^{-3} M. The Matec ESA 8000 is equipped with a probe based electroacoustic sensor, as well as sensors for pH, conductivity, and temperature, and a stirrer. The system is linked to a double-piston, digital titration unit for performing automated potentiometric titrations and for generic volumetric additions with simultaneous measurement of the electroacoustic signal for determination of the sample zeta (ζ) potential. The titrations were performed using 1 M nitric acid (HNO_3) and 1 M potassium hydroxide (KOH).

2.3 Stability Predictions

2.3.1 Hamaker Constant Calculation

The Hamaker constant in a vacuum was calculated [Bleier, 1983] for each starting powder for entry into the computer program, *Suspension Stability*®. Dielectric constants (permittivity, ϵ_i) were from the CRC Handbook of Chemistry & Physics, 79th Edition [1998]; however, a dielectric constant was not available for TiB₂. After checking unsuccessfully with three manufacturers and other investigators for unpublished data, the permittivity for TiO₂ was used to approximate TiB₂ permittivity as both are divalent, covalently bonded species that oxidize. The calculations of the Hamaker constant in a vacuum are summarized in Table 5.

Table 5: The calculation of the Hamaker constant (A_i) in a vacuum [Bleier, 1983] where $A_i(kT) \sim 113.7 \{(\epsilon_i - 1)^2 / [(\epsilon_i + 1)^{3/2} (\epsilon_i + 2)^{1/2}]\}$

Colloidal System Component	T (° K)	A_i^* (joules)
Al ₂ O ₃	298	3.00E-19
KNO ₃	293	1.66E-19
H ₂ O	293.2	4.35E-19
TiB ₂ (TiO ₂)	300	4.51E-19

*The Hamaker constants for Al₂O₃ and TiB₂ (TiO₂) are averages since permittivity (ϵ_i) varies for each direction in the single crystal; the Hamaker constant was computed for each permittivity provided and then averaged.

2.3.2 Computer Model

Material and system data including Hamaker constants in a vacuum, particle radii, relative volume fraction of components, monatomic electrolyte concentration, and zeta (ζ) potential versus pH measurements were entered into the computer program,

Suspension Stability[®]. The stability ratio versus pH data was transferred into ASCII files and plotted using *Microsoft Excel 97-SR2* software.

2.4 Slip Preparation and Casting

2.4.1 Electrolyte

J. T. Baker, Inc., Baker Analyzed Reagent, Potassium Nitrate (KNO_3) (F.W. 101.11) was used to prepare the indifferent, liquid electrolyte in deionized water for suspension preparation.

2.4.2 Slip Suspensions

Slip suspensions for casting were prepared at 50 wt % solids and at the pH chosen for processing conditions predicted by *Suspension Stability*[®] for dispersion, coagulation and heterocoagulation. Each suspension was stirred. The stirred suspension was brought to the processing pH by the drop-wise addition of 1 M HNO_3 or 1 M KOH as measured by a pH meter (Fisher Scientific, fishersci.com). Composite $\text{TiB}_2/\text{Al}_2\text{O}_3$ slips were prepared from the SHS TiB_2 and Al_2O_3 powders in the ratio 30/70 wt% similar to the SHS composite $\{\text{TiB}_2/\text{Al}_2\text{O}_3\}$. The manufacturer reports SHS $\{\text{TiB}_2/\text{Al}_2\text{O}_3\}$ as nominally 29/71 wt% TiB_2 to Al_2O_3 .

2.4.3 Ultrasonication

All suspensions were ultrasonicated (using the Branson Sonifier 250, Danbury, CT, consisting of a power supply, a converter, and a horn). Sonication was performed to eliminate any previous particle agglomeration. The ultrasonication time for zeta (ζ)

potential measurements ranged between seven and twelve minutes; beyond twelve minutes the temperature of the beaker was hot to the touch, introducing uncontrolled temperature variation. Slip suspensions for casting were ultrasonicated for the optimum time of 20 minutes to break agglomerates [Yeh, 1996], but the optimum time was divided into two consecutive ten minute periods to replenish the ice bath used to keep the suspension at a constant temperature. Sonicator output readings were maintained at 60 kHz through occasional adjustments. The frequency drifted during ultrasonication when viscosity increased.

2.4.4 Plaster Mold Preparation

Plaster of Paris (100% Gypsum) was added to deionized water in the ratio 250g plaster/165 ml water to form absorbing molds. A detailed description of mold preparation can be found in Slipcasting [1997], pp. 14-17. Twenty-five negative molds were cast to ensure a minimum of five samples were available for each of the three composite recipes: SHS composite $\{\text{TiB}_2/\text{Al}_2\text{O}_3\}$, SHS $\text{TiB}_2/\text{AKP-50 Al}_2\text{O}_3$ and SHS $\text{TiB}_2/\text{Alcoa Superground A-1000 Al}_2\text{O}_3$. The negative molds were formed five at a time using a bar fitted with five machined lucite forms so that the impression in the plaster in each weighing dish was approximately 6.2 cm (*l*) x 0.8 cm (*w*) x 0.6 cm (*h*) for a minimum 3.0 cc sample. After drying in air for one week, each mold was sawed in two and rubber banded back together for ease of sample release after slip casting.

2.4.5 Casting

Overfilling of each mold to allow for leakage and settling was required. The weight of solids prepared for each batch was based on a mold height of 0.8 cm or 4.0 cc

per sample. The weight of material required for at least six samples of 4.0 cc volume for $\text{TiB}_2/\text{Al}_2\text{O}_3$ at 4.12 g/cc was 98 g. The 50 wt % slips were poured into molds in groups of six (or seven given slip volume increased during processing) by pouring layer upon layer of slip until each mold was filled. A non-reactive, stainless steel spatula was used as a guide to pour the slip into the mold. The high viscosity of 50 wt% slip prevented pouring from beakers directly. Pouring the slip into the molds could take as much as 1.25 hours. Samples were air-dried four to seven days prior to unmolding.

2.5 Traditional Binder

Union Carbide Chemicals and Plastics Co., Inc., CARBOWAX (Polyethylene Glycol (PEG)) Compound 20M, designated PEG20M, flaked) was used as a binder for each of the composite systems. Optimum green and sintered densities had been obtained for Al_2O_3 at 2 wt% PEG20M [Walker et al., 1992]. The AKP-50 and Alcoa Superground A-1000 composites were pressed into disk shaped, green bodies at 2 wt% PEG20M binder. A Carver press and three gram die were used to form the disks. The larger surface area of the SHS Composite particles required 6 wt % PEG20M to form green bodies.

Under a fume hood, PEG20M flake was placed in a glass beaker on a hot plate; ethanol was added and the mixture was stirred until the flakes dissolved. The composite powders were added and ultrasonicated (Branson Sonifier 250, Danbury, CT) for five minutes at 60 kHz output then returned to the hot plate and stirred with a non-reactive, stainless steel spatula until the ethanol evaporated.

2.6 Cold Isostatic Pressing (CIPing)

All samples except for the SHS $\{\text{TiB}_2/\text{Al}_2\text{O}_3\}$ were double bagged in latex; each was tied with soft string and placed in the cold isostatic press (Iso-Spectrum, Inc.) for two minutes at a specified pressure before sintering. Although the desired specified pressure for all samples was higher, the specified pressure ranged from 105 to 300 MPa due to the variability of the press operation. The SHS $\{\text{TiB}_2/\text{Al}_2\text{O}_3\}$ samples were not pressed. Even at low pressures <100 MPa, the SHS $\{\text{TiB}_2/\text{Al}_2\text{O}_3\}$ particles penetrated the bags. Whether latex, polyurethane or polyethylene, the bags leaked when pressing SHS $\{\text{TiB}_2/\text{Al}_2\text{O}_3\}$. Green densities were plotted as a function of pressure applied by the CIP.

2.7 Green Bodies

2.7.1 Density Measurement

The samples were trimmed and sanded with 600-grit paper to near rectangular shapes. A digital slide caliper was used to measure the length, width and height of each sample and then the sample was placed on a balance to measure weight (Appendix C, Tables 26-28).

2.7.2 Binder Burnout and Thermogravimetric Analysis (TGA)

For the PEG processed samples, gentle heating in crucibles in a furnace (CM Rapid Temperature 6" Furnace, Bloomfield, NJ) according to one of two schedules (Table 6) was accomplished to remove the PEG binder prior to density measurements or pressureless sintering.

Table 6: Binder burnout schedules for PEG processed samples

Schedule 1	Schedule 2
<ul style="list-style-type: none">• Ramp up temperature from 100 to 450 °C in six hours,• hold for three hours,• ramp up temperature further from 450 to 550 °C in three hours,• hold for one hour, and• then ramp down temperature from 550 to 100 °C in three hours	<ul style="list-style-type: none">• Ramp up temperature from 100 to 250 °C in one hour,• hold for one hour,• ramp down temperature from 250 to 100 °C in one hour

Walker et al. [1992] suggested thermogravimetric analysis (TGA) of PEG processed samples. TGA was performed at a heating rate of 10 °C/minute in air. SHS {TiB₂/Al₂O₃} samples were heated through a range of 35 to 500 °C, and AKP50 and Alcoa-SG samples were heated through a range of 35 to 350 °C to determine if all binder was removed prior to density measurements and pressureless sintering.

2.7.3 Conductivity Measurement

The Hewlett Packard E2378A Multimeter was used to test for conductivity in a yes-no manner indicated by a beep for yes on all green bodies.

2.8 Pressureless Sintering

The samples were sintered in an Argon (Ar) atmosphere in a resistance-heated, graphite furnace (Thermal Technology, Inc., Santa Rosa, CA). The samples were sintered in a three-layer tower constructed of graphite crucibles with a sheet of Grafoil® flexible graphite as a platform for each layer and graphite tape (grade GTA) sealing the tower. Pressureless sintering was accomplished according to one of two schedules (Table 7)

[Logan Ph.D. Thesis, 1992]. The samples were grouped: one of each processing condition, four samples per layer, that is, 12 samples per sintering run.

Table 7: Pressureless sintering schedules for all samples

Schedule 1	Schedule 2
<ul style="list-style-type: none"> • Set furnace at 35 % power to 800 °C, • continue heating at the rate of 25 °C per minute to 1000 °C, then 10 °C per minute to 1700 °C, and • hold for four hours at 1700 °C 	<ul style="list-style-type: none"> • Set furnace at 35 % power to 800 °C, • continue heating at the rate of 25 °C per minute to 1000 °C, then 10 °C per minute to 1800 °C, and • hold for four hours at 1800 °C

2.9 Sintered Samples

2.9.1 Density Measurement

Density measurements of sintered samples were performed using a balance placed above a deep bowl (approximate capacity 3 liters) of deionized water supported by two stationary slabs of TiB₂. The dry weight of the sample was taken by placing the sample on the top of the scale, and the weight of the sample submerged in the water was taken by suspending a wire basket from under the scale. The method for computing the density (ρ_a (g/cc)) of the sintered sample follows the Archimedes method described in Jones and Berard [1972]:

$$\rho_a = \frac{W_D}{V_a} = \frac{W_D \rho_L}{W_D - W_{SS}} \quad (16)$$

where W_D is the dry weight of the sample in grams (g), V_a is the apparent volume of the sample in cc, ρ_L is the density of the liquid in g/cc, and W_{SS} is the weight of the saturated sample when submerged in the liquid.

2.9.2 Conductivity Measurement

The Hewlett Packard E2378A Multimeter was used to test for conductivity in a yes-no manner indicated by a beep for yes on all sintered samples.

2.9.3 Mounting and Polishing

Samples were placed in a bakelite form so the vertical cross section of the slip cast specimen could be viewed and pressed at a pressure of about 27 MPa. The mounted specimen was hand polished through a sequence of ever finer sand papers before automatic polishing for microhardness measurements and scanning electron microscope (SEM) viewing.

For each sample, the excess bakelite was ground off with a 180 μm grade paper (coarse red) on a belt sander and then hand polished with increasingly finer papers (Table 8).

Table 8: Hand polishing papers for sample preparation in the order used

Micron Grade	Brand Name	Manufacturer
50 μm	Tufbak Durite T421, 240-A 133	Norton, USA
40 μm	413Q Wetodry Tri-M-ite Paper A, weight W2, 320 CO42	3M
30 μm	Tufbak Durite T421, 400-A	Norton, USA
15 μm	Wetodry Tri-M-ite Paper A, weight 600	3M

Further grinding and polishing for microhardness measurements [Mullins, 1999] began with two days of grinding for 15 minutes every hour with 15 μm diamond paste in kerosene on load plates followed by continuous polishing for 8 hours twice over two days, with 0.05 μm silica.

For porous and pitted samples that could not be polished, cleaning for SEM viewing was accomplished by sonicating (Cole-Parmer Instrument Company #8853 ultrasonicator, Vernon Hills, IL) for 10 to 15 minutes in an acetone bath.

2.10 Scanning Electron Microscopy (SEM) Observations

2.10.1 Powders

A SEM mount was prepared for each of the starting powders by dusting two-sided carbon tape affixed to the graphite mount. The powders were observed with an 1810 Amray SEM at 20.0 kV equipped with an Oxford Detector for Energy Dispersive Spectroscopy (EDS).

2.10.2 Polished Specimens

The JEOL JXA-840 SEM was used in the backscatter mode at 20.0 kV to view the microstructure of each polished specimen.

2.11 Microhardness Measurement

The microhardness measurements were performed in accordance with the American Society for Testing and Materials (ASTM) Designation: C 1327 – 96a, Standard Test Method for Vickers Indentation Hardness of Advanced Ceramics. The 500 g rather than 1000 g load was used when the material crushed easily with the 1000 g load.

3 Results And Discussions

Ceramic composites were prepared for three different composite systems from the four different starting powders: SHS $\text{TiB}_2/\text{AKP-50 Al}_2\text{O}_3$, SHS $\text{TiB}_2/\text{Alcoa SG A-1000 Al}_2\text{O}_3$, and SHS Composite $\{\text{TiB}_2/\text{Al}_2\text{O}_3\}$. The three different composites were formed into samples by either mixing and pressing with a traditional binder (PEG20M), or slip casting at the chosen processing pH (Table 11), and then pressureless sintered in an Argon (Ar) atmosphere. The data collected from the investigations described in the previous section include the calculated Hamaker constant (Table 5), temperature ($^{\circ}\text{C}$), density, volume fraction, particle size, zeta potential (ζ), stability ratio data (W), green densities (g/cc), thermogravimetric analysis (TGA), sintered densities (g/cc), microhardness measurements, and scanning electron micrographs. These data were used to:

- compare each colloidally-processed composite to that prepared with the traditional binder PEG20M as to the effectiveness of *Suspension Stability*[®] in predicting optimum suspension conditions for colloidal processing of $\text{TiB}_2/\text{Al}_2\text{O}_3$ ceramic composites, and
- compare the microstructures of the colloidally-processed, pressureless-sintered $\text{TiB}_2/\text{Al}_2\text{O}_3$ ceramic composites with the dry-mixed, hot-pressed $\text{TiB}_2/\text{Al}_2\text{O}_3$ ceramic composites prepared by Logan [1997], which are associated with penetration resistance in ceramic armor.

3.1 Properties of $\text{TiB}_2/\text{Al}_2\text{O}_3$ Suspensions

3.1.1 Electrokinetic Sonic Amplitude (ESA) Measurement

Low concentration suspensions (0.5 vol.%) of each starting powder were prepared and the Matec ESA 8000 measured the pressure amplitude per unit of applied electric field ($\text{ESA} (\omega)$), temperature ($^{\circ}\text{C}$), volume of acid and/or base added, and the pH during each titration. It also computed the dynamic mobility ($\mu_d (\omega)$) and zeta potential (ζ), and reported these as a function of the measured quantities. Suspensions were prepared for each of the Al_2O_3 powders and the SHS TiB_2 powder at three different electrolyte concentrations (Figures 9, 10, and 11) to determine if, and at what electrolyte concentration, optimal zeta potentials (ζ) were present for processing.

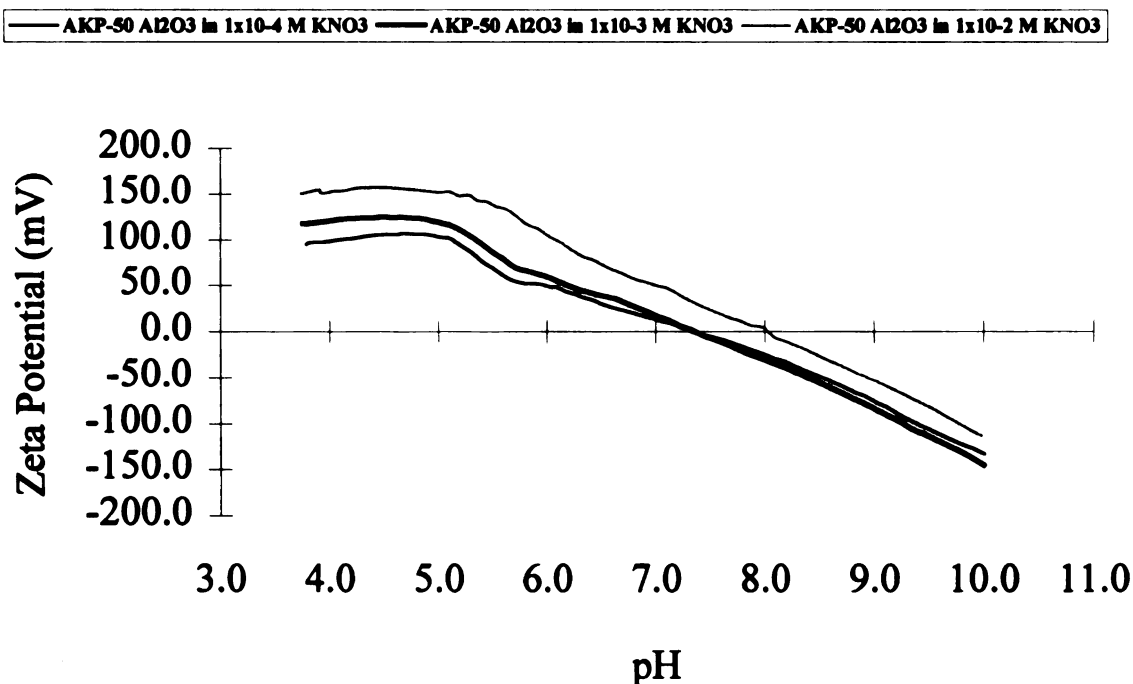


Figure 9: Zeta potentials determined from ESA data collected using the Matec ESA 8000 for AKP-50 Al_2O_3 suspended in three different concentrations of electrolyte.

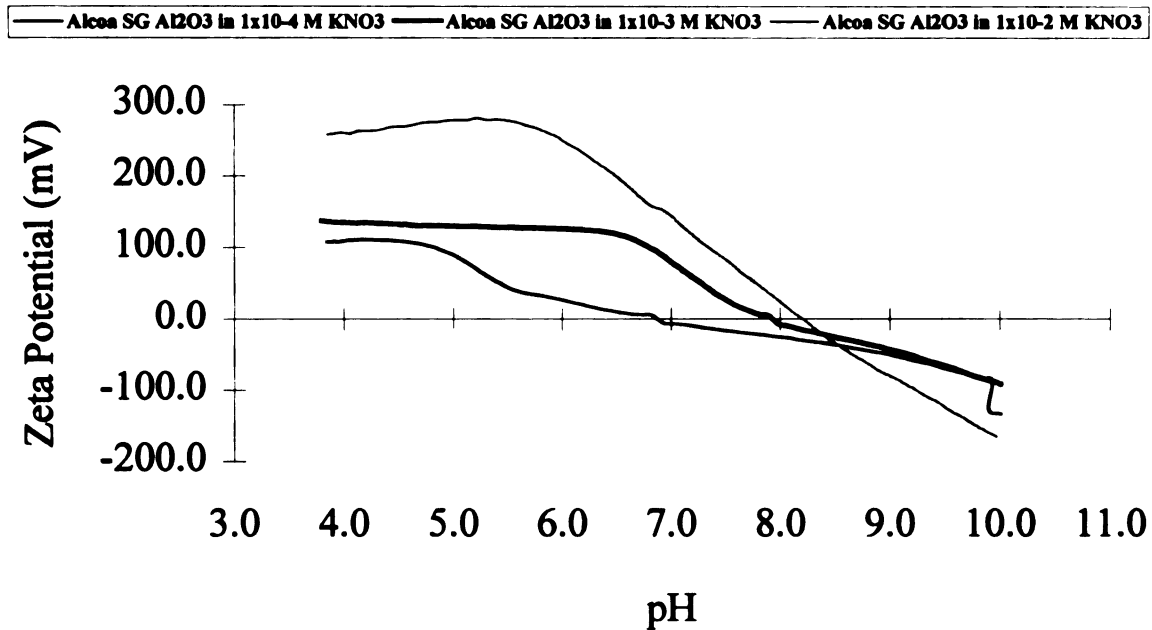


Figure 10: Zeta potentials determined from ESA data collected using the Matec ESA 8000 for Alcoa SG A-1000 Al₂O₃ suspended in three different concentrations of electrolyte.

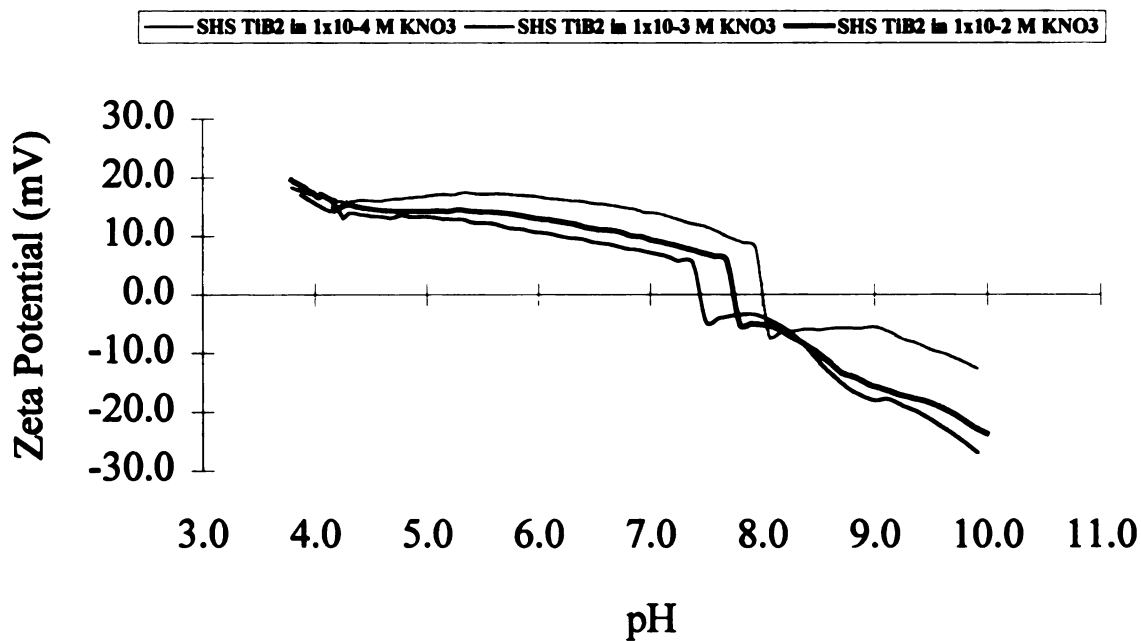


Figure 11: Zeta potentials determined from ESA data collected using the Matec ESA 8000 for SHS TiB₂ suspended in three different concentrations of electrolyte.

The electrolyte concentration of 1×10^{-3} M KNO_3 was optimal for zeta potentials (ζ) for each Al_2O_3 powder. The SHS $\{\text{TiB}_2/\text{Al}_2\text{O}_3\}$ powder was suspended in 1×10^{-3} M KNO_3 , and the zeta potential (mV) versus the pH was plotted for each powder using *Microsoft Excel 97 SR-2* (Figure 12).

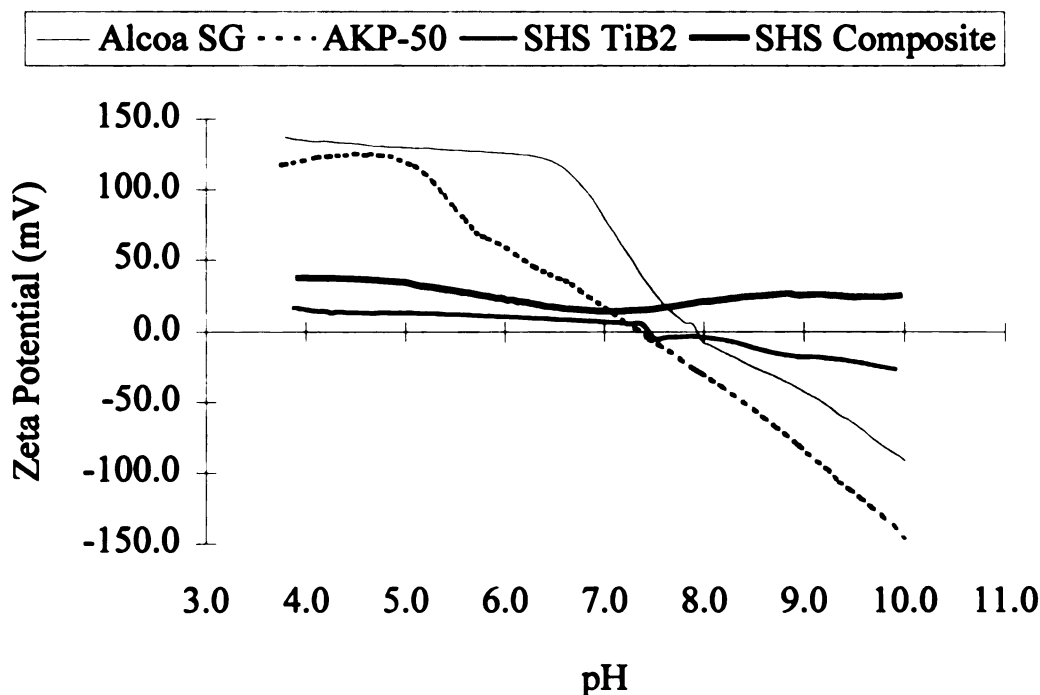


Figure 12: Zeta potentials for each starting powder suspended in 1×10^{-3} M electrolyte from ESA data collected using the Matec ESA 8000.

The estimate for the minimum potential for stability is ± 25 to 50 mV [Hunter, 1993, p. 422]. Therefore, the SHS TiB_2 and SHS composite $\{\text{TiB}_2/\text{Al}_2\text{O}_3\}$ appeared to be unstable at all pH; AKP50 was stable between about pH 4 and 6, and pH 8.5 and 10; and Alcoa-SG was stable between about pH 4 and 5.5, and pH 9 and 10. Except for the SHS composite $\{\text{TiB}_2/\text{Al}_2\text{O}_3\}$, the ζ -potential crossed the axis of zero potential for all the starting powders between pH 7 and 8; the point of zero ζ -potential was also the isoelectric point (iep) [Heimenz, 1997, p. 566].

There is no reported iep for TiB_2 as determined by a search of the joint Computerized Engineering Index and EI Engineering Meetings database (Ei COMPENDEX). However, an iep for titania powders is reported as pH 7.5 when the surface chemistry is affected by an inorganic such as Al_2O_3 and as low pH 6.1 when the surface chemistry is affected by an organic material [Greenwood and Kendall, 1999]. The iep for SHS TiB_2 at the optimum electrolyte concentration (1×10^{-3} M KNO_3) for $\text{TiB}_2/\text{Al}_2\text{O}_3$ composite processing was between pH 7.38 and 7.50.

The iep for Al_2O_3 five different $\alpha\text{-Al}_2\text{O}_3$ powders from the same manufacturer is reported as pH 9 [Franks and Lange, 1999]. The iep for the AKP 50 Al_2O_3 (Figure 9) was not in agreement with the reported iep at pH 9, but at lower electrolyte concentrations the iep was consistent, ranging between pH 7.3 and 7.5. The iep for the Alcoa SG Al_2O_3 (Figure 10) was also not in agreement with the reported iep at pH 9, but at lower electrolyte concentrations was not as consistent, ranging between 6.8 and 7.3 at the lower electrolyte concentrations. The different (manufacturing/processing) origins of the $\alpha\text{-Al}_2\text{O}_3$ powders as well as the different impurities present (Tables 2 and 3) produced differences in surface chemistry that affected colloidal properties [Everett, 1988, p. 8; Čerović et al., 1995]. These differences in surface chemistry may then account for the variations between the iep reported here and in the literature for the $\alpha\text{-Al}_2\text{O}_3$ powders. The increased electrolyte concentration was expected to shrink the diffuse double layer around the particle [Hunter, 1993, pp. 90-92] and increase the ζ -potential, but the iep was expected to remain consistent for a pure material. Variations in the molecular activity of the impurities and hence the surface chemistry may account for the inconsistency in

either the AKP 50 or the Alcoa SG Al_2O_3 iep at all electrolyte concentrations (Tables 2 and 3).

The iep is the point at which electrophoretic mobility is zero; therefore the potential energy of repulsion between particles is minimal and the optimum condition for coagulation of a particular powder is present [Heimenz, 1997, p. 567]. Generally, if two powders of different ζ -potentials are compared – all other factors being equal – the one with the higher absolute value of the ζ -potential is expected to be more stable with respect to coagulation, and the one with the lower absolute value of the potential, less stable [Heimenz, 1997, p. 567]. However, if the suspension consists of a composite of different particles – where all other factors are not equal – stability cannot be easily generalized. Rather, DLVO and HHF theories applied to ζ -potential measurements provide a more precise estimate of stability of multiple, differing components in suspension [Hogg, 1966; Wilson and Crimp, 1993]. By modeling DLVO and HHF theories, the other unequal factors, including density, particle size, the interaction of dissimilar electrical double layers, and coagulation kinetics, can be taken into account to predict the stability of a composite suspension.

The ζ -potential results for the SHS $\{\text{TiB}_2/\text{Al}_2\text{O}_3\}$ were not conclusive, and possibly unstable at every pH. Therefore, three suspension processing conditions were chosen to reflect the range of pH: pH 4 (acidic), pH 7 (neutral) and pH 9 (basic). Further calculations using DLVO and HHF theories to predict stability of the SHS composite powder were not possible because of the instability of the powder at every pH.

3.1.2 Stability Ratio (W)

For the composite systems SHS TiB_2 /AKP 50 Al_2O_3 and SHS TiB_2 /Alcoa SG A-1000 Al_2O_3 , the Stability Ratio (W) was computed (Figures 13 and 14) to predict the stability, and conversely the coagulation kinetics, of the composite suspensions. For each powder, the calculated Hamaker constant in a vacuum (Table 5), temperature ($^\circ\text{C}$), volume fraction, concentration of the electrolyte (M), particle radii (μm), ζ -potential (mV) vs. pH data, and the pH of the start and finishing points were entered into the computer program *Suspension Stability*[®]. The program bases calculation of the $\log_{10} W$ versus pH data on DLVO and HHF theories, and takes into account the factors of the different components in suspension. The $\log_{10} W$ versus pH data were plotted using *Microsoft Excel 97 SR-2* (Figures 13 and 14).

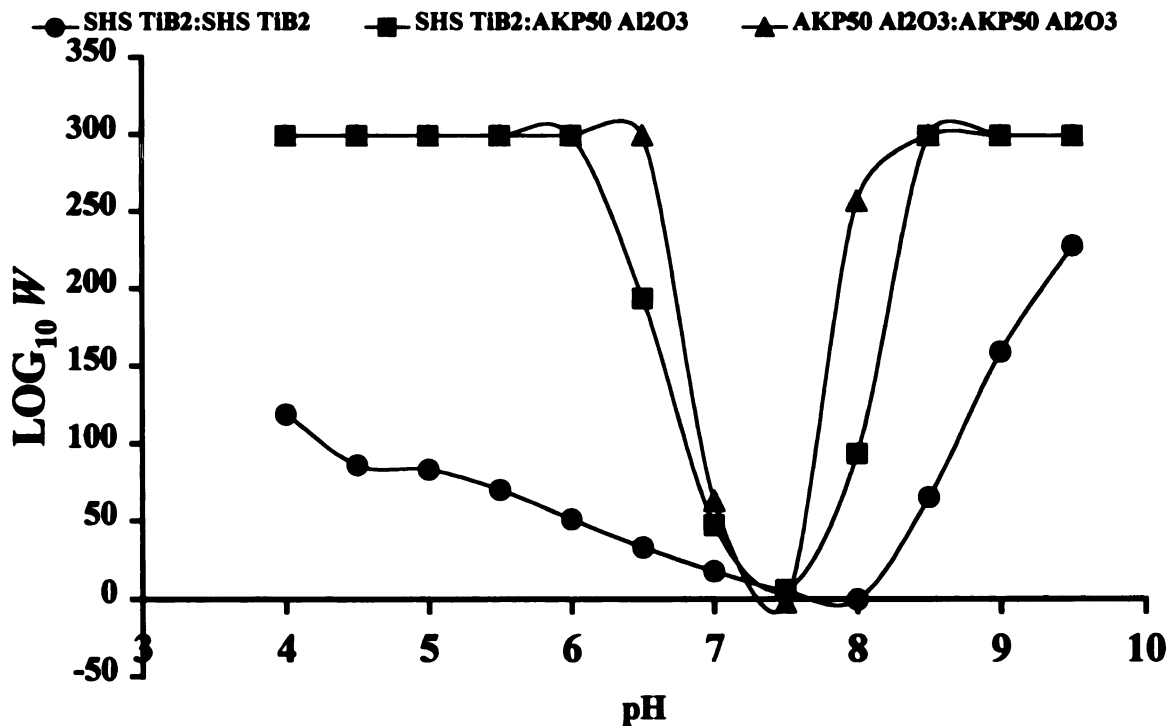


Figure 13: Stability ratio data prepared from the computer program, *Suspension Stability*[®], for SHS TiB_2 and AKP 50 Al_2O_3 .

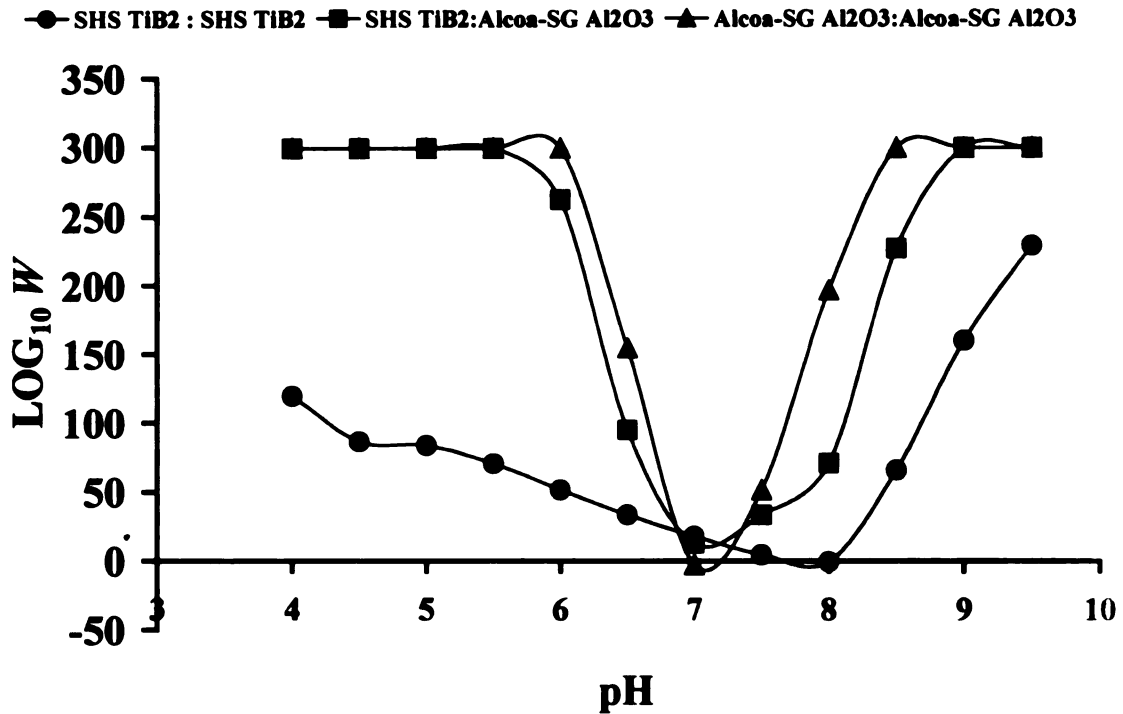


Figure 14: Stability ratio data prepared from the computer program, *Suspension Stability*[©], for SHS TiB₂ and Alcoa-SG A-1000 Al₂O₃.

The program can predict ranges of stability by pH where $\log_{10} W > 40$ [Wilson and Crimp, 1993]. Tables 9 and 10 summarize the relative stability between components, that is, where $\log_{10} W > 40$ as predicted from the stability plots in Figures 13 and 14, respectively.

Table 9: Relative stability between SHS TiB₂ and AKP50 Al₂O₃ predicted by *Suspension Stability*[©]

Stability Ratio W	SHS TiB ₂ /SHS TiB ₂ Interactions	SHS TiB ₂ /AKP50 Al ₂ O ₃ Interactions	AKP50 Al ₂ O ₃ /AKP50 Al ₂ O ₃ Interactions
Range of Predicted Stability	pH 4-6 and pH 8.5-9.5	pH 4-6 and pH 8.5-9.5	pH 4-7 and pH 8.0-9.5

Table 10: Relative stability between SHS TiB₂ and Alcoa-SG Al₂O₃ predicted by *Suspension Stability*^o

Stability Ratio <i>W</i>	SHS TiB ₂ /SHS TiB ₂ Interactions	SHS TiB ₂ /Alcoa-SG Al ₂ O ₃ Interactions	Alcoa-SG Al ₂ O ₃ /Alcoa-SG Al ₂ O ₃ Interactions
Range of Predicted Stability	pH 4-6 and pH 8.5-9.5	pH 4-6 and pH 8.5-9.5	pH 4-6.5 and pH 7.5-9.5

Suspension processing conditions were chosen to reflect three variations in stability of the components: dispersed - where both components were stable, particle double-layers were large and like-charged, repulsive forces dominant, and thoroughly mixed in suspension; coagulated - where both components were unstable, particle double-layers were small and zero-charged, attractive forces dominant, and thoroughly agglomerated in suspension; and heterocoagulated - where one component was stable and the other unstable, particle double-layer sizes and charges were dissimilar, and partially agglomerated in suspension. Heterocoagulation in the SHS TiB₂ plus Al₂O₃ composites occurred with the SHS TiB₂ unstable with respect to the Al₂O₃. Table 11 summarizes the processing conditions chosen for the three composite systems investigated.

Table 11: Summary of processing conditions chosen for the three composite systems investigated

Processing Conditions	SHS Composite TiB ₂ /Al ₂ O ₃	SHS TiB ₂ /AKP50 Al ₂ O ₃	SHS TiB ₂ /Alcoa-SG Al ₂ O ₃
Traditional Binder	PEG	PEG	PEG
Dispersed	pH 4	pH 4	pH 4
Coagulated	pH 7	pH 7.5	pH 7
Heterocoagulated	pH 9	pH 8	pH 8

3.2 Effect of pH on Green Body Density

3.2.1 Material Loss and Sample Attrition

With all liquid evaporated during slip casting and drying, each batch of each composite recipe prepared by a particular processing should yield approximately 98 grams of sample material. However, material loss was significant (Table 12). All of the material was cast into samples, but the processing steps of removing the samples from molds and cold isostatic pressing caused sample disintegration. Cold isostatic pressing completely destroyed the first set of SHS composite samples. Another batch of the SHS composite was slip cast and consequently not cold isostatically pressed prior to green density measurements to preserve sample integrity.

Table 12: Material loss during green body forming for each composite recipe and processing pH

Composite Recipe	Processing pH	Material Loss during Green Body Forming
SHS TiB ₂ -AKP 50 Al ₂ O ₃	4	74%
SHS TiB ₂ -AKP 50 Al ₂ O ₃	7.5	94%
SHS TiB ₂ -AKP 50 Al ₂ O ₃	8	98%
SHS TiB ₂ -Alcoa SG Al ₂ O ₃	4	65%
SHS TiB ₂ -Alcoa SG Al ₂ O ₃	7	84%
SHS TiB ₂ -Alcoa SG Al ₂ O ₃	8	82%
SHS CompositeTiB ₂ -Al ₂ O ₃	4	78%
SHS CompositeTiB ₂ -Al ₂ O ₃	7	71%
SHS CompositeTiB ₂ -Al ₂ O ₃	9	49%

The material loss was greatest in the SHS $\text{TiB}_2/\text{AKP 50 Al}_2\text{O}_3$ system processed at pH 8 with less than 2% of the starting material remaining. The SHS composite system processed at pH 9 had the least material loss with over 50% of the starting material remaining after processing. These findings may be consistent with Al_2O_3 being soluble under basic conditions and TiB_2 being soluble in a mixture of H_2O_2 and HNO_3 [Wilson, 2001]. Wilson [2001] also reports that the SHS composite powder is not a mixture of the two components as observed in the SEM image of the SHS composite powder (Figure 22) where the large (charging) particles were thought to be the non-conducting Al_2O_3 and the smaller (non-charging) particles the conducting TiB_2 . Rather both components constitute each particle creating a new type of surface chemistry. These composite particles may account for the material loss in the SHS composite not following the same trend as the other SHS TiB_2 plus Al_2O_3 systems (Table 12).

In addition to the problem of material loss, the number and size of samples available also varied by starting material and processing condition (Table 13). A greater number of smaller size samples were present after squeezing in the cold isostatic press (CIP) due to the original samples breaking into smaller ones.

Table 13: Sample attrition during green body forming for each composite recipe and processing pH

Composite Recipe	Processing pH	Number of Samples Intact After Casting (100%= 7)	Number of Samples Available after CIP	Average Weight of Sample Available for Green Density Measurements (g)
SHS TiB ₂ -AKP 50 Al ₂ O ₃	4	7	10	2.6
SHS TiB ₂ -AKP 50 Al ₂ O ₃	7.5	6	8	0.74
SHS TiB ₂ -AKP 50 Al ₂ O ₃	8	3	4	0.45
SHS TiB ₂ -Alcoa SG Al ₂ O ₃	4	6	9	3.84
SHS TiB ₂ -Alcoa SG Al ₂ O ₃	7	5	11	1.46
SHS TiB ₂ -Alcoa SG Al ₂ O ₃	8	6	11	1.59
SHS CompositeTiB ₂ -Al ₂ O ₃	4	5	7*	3.14
SHS CompositeTiB ₂ -Al ₂ O ₃	7	7	9*	3.15
SHS CompositeTiB ₂ -Al ₂ O ₃	9	7	9*	5.59

*SHS Composite not CIP'd

For the SHS composite system, the samples processed at pH 9 experienced the least attrition compared to the other processing conditions and the sample size averaged 5.59 g. For both of the other composite powders, the samples processed for dispersion (pH 4) showed the least attrition and the “dispersed” sample size within each system averaged more than twice the average size of the samples processed for heterocoagulation and coagulation. The number and size of samples were significantly lower for the SHS TiB₂/AKP 50 system processed at pH 8.

Each composite system began with a total of 294 g (98 g of starting material for each of three processing conditions). In the SHS TiB₂/AKP 50 system, only about 11% of the starting material remained after processing, and in the SHS TiB₂/Alcoa-SG and SHS composite systems, only about 23% and 34% remained, respectively. A large part

of the starting material was lost through overflow and adhesion to the molds during slip casting as well as trimming of the samples for dimension and density measurements.

3.2.2 Green Body Density Measurements

Green densities were measured as a function of composite recipe and pH (Figure 15). Green density measurements generally ranged from 1.34 g/cc to 2.77 g/cc, or 32.5% to 67.5% of the theoretical value (4.12 g/cc). The SHS composite system processed at pH 9 had the narrowest range of variation in densities measured for any one particular starting material or processing condition. The highest densities for both the SHS TiB_2 /AKP 50 and SHS TiB_2 /Alcoa-SG green bodies were measured in those samples processed for dispersion at pH 4 (Figure 15). Green body densities measured for SHS composites processed at pH 4 were lowest. The lowest green body densities found for any composite were for the SHS TiB_2 /AKP 50 processed at pH 7.5 and pH 8.0.

● AKP50 Comp □ Alcoa-SG Comp △ SHS COMPOSITE

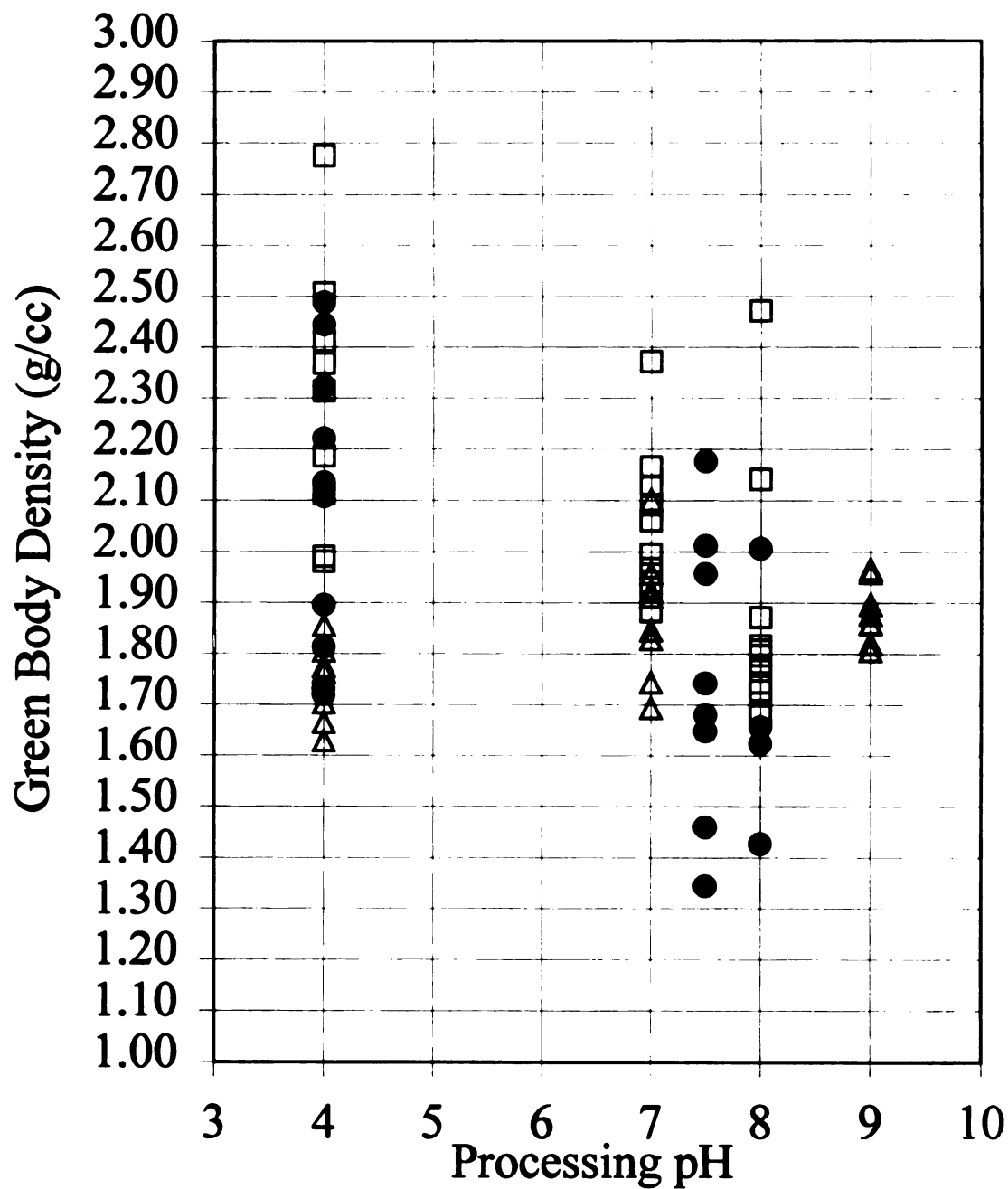


Figure 15: Green density vs. processing pH for each composite recipe

3.2.3 Green Density vs. Cold Isostatic Pressure

Neither a decrease in the range of variation in green density nor an improvement in overall green densities was achieved with cold isostatic pressing (Figure 16). The lack of any significant improvement combined with a significant risk of damage to samples during cold isostatic pressing rendered this technique very disadvantageous in improving green density.

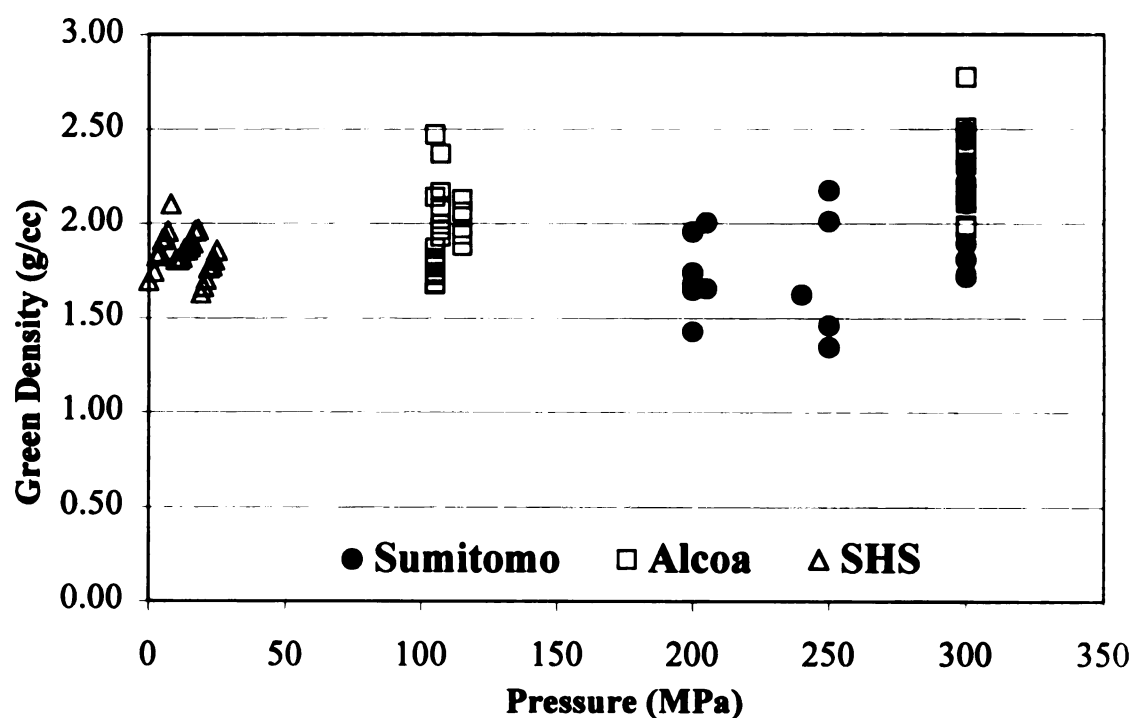


Figure 16: Green density vs. pressure applied to composite samples during cold isostatic pressing

3.2.4 Green Body Conductivity

All green bodies were non-conductive across the length, width, and height of each sample. Placing the two electrodes on the any face of the sample also indicated non-conductance.

3.3 Sintered Density

3.3.1 Binder Burnout and Thermogravimetric Analysis (TGA)

The binder burnout schedules were successful in removing the polyethylene glycol (PEG) binder from all samples prepared without colloidal processing (Figures 17, 18, 19). Although calibration errors moved starting points from the 100% point, the change in TGA curves showed that binder burnout before sintering removed 6 wt% PEG from the SHS $\{\text{TiB}_2/\text{Al}_2\text{O}_3\}$, and 2 wt% PEG, from each of the SHS $\text{TiB}_2/\text{AKP 50}$ and SHS $\text{TiB}_2/\text{Alcoa SG}$ composite samples.

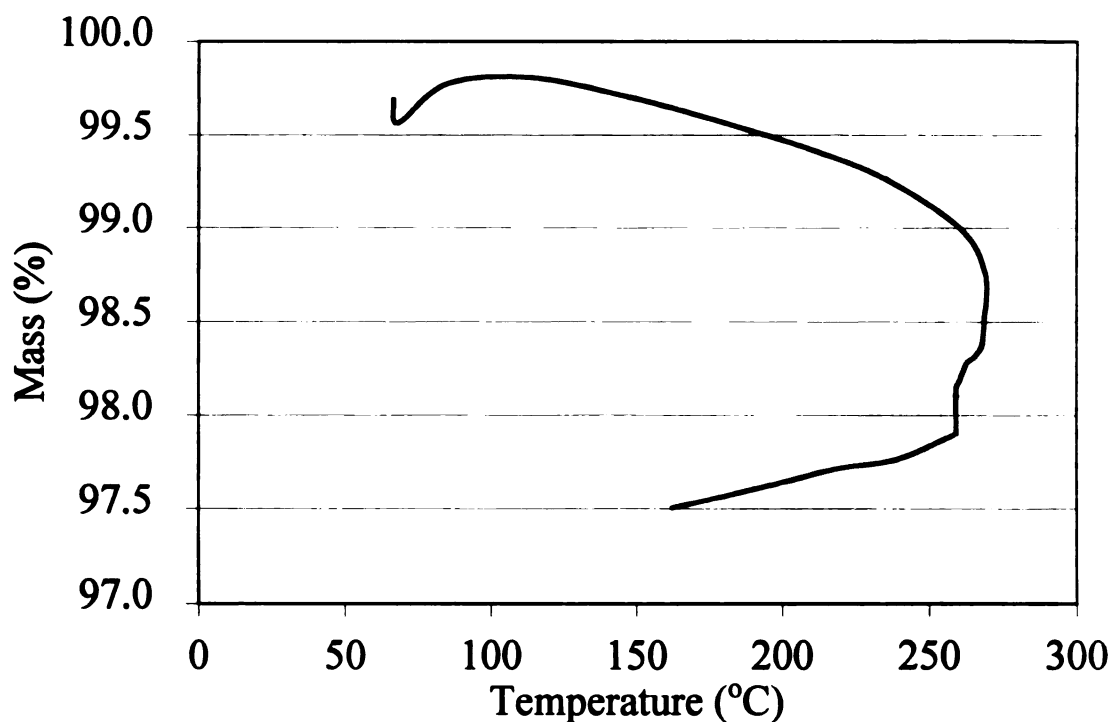


Figure 17: Thermogravimetric analysis (TGA) for the SHS TiB_2 – AKP 50 Al_2O_3 composite green samples prepared with a traditional binder; the 2 wt% polyethylene glycol (PEG) binder was removed by binder burnout before sintering.

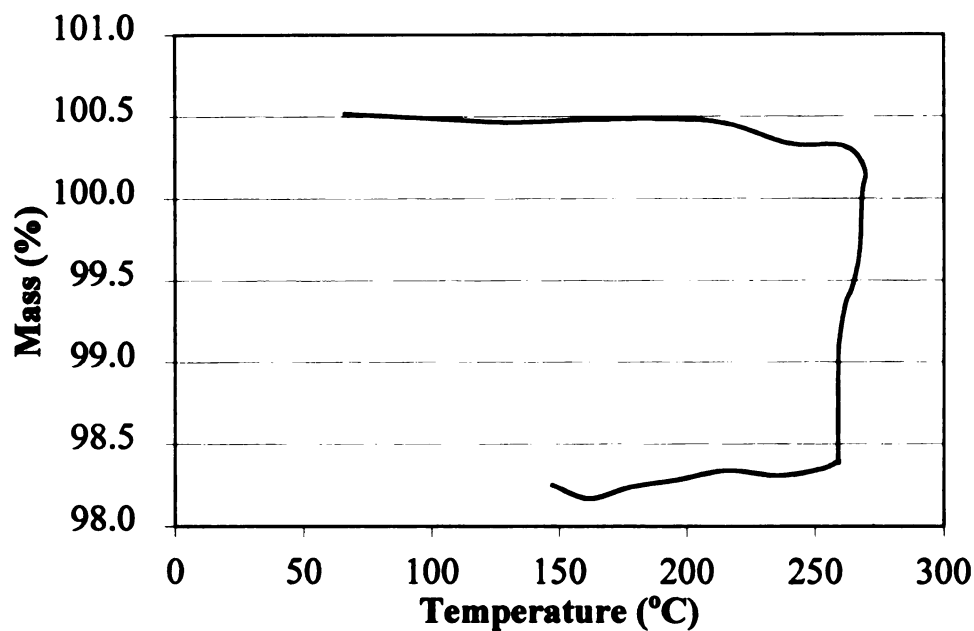


Figure 18: Thermogravimetric analysis (TGA) for the SHS TiB_2 – Alcoa SG Al_2O_3 composite green samples prepared with a traditional binder; the 2 wt% polyethylene glycol (PEG) binder was removed by binder burnout before sintering.

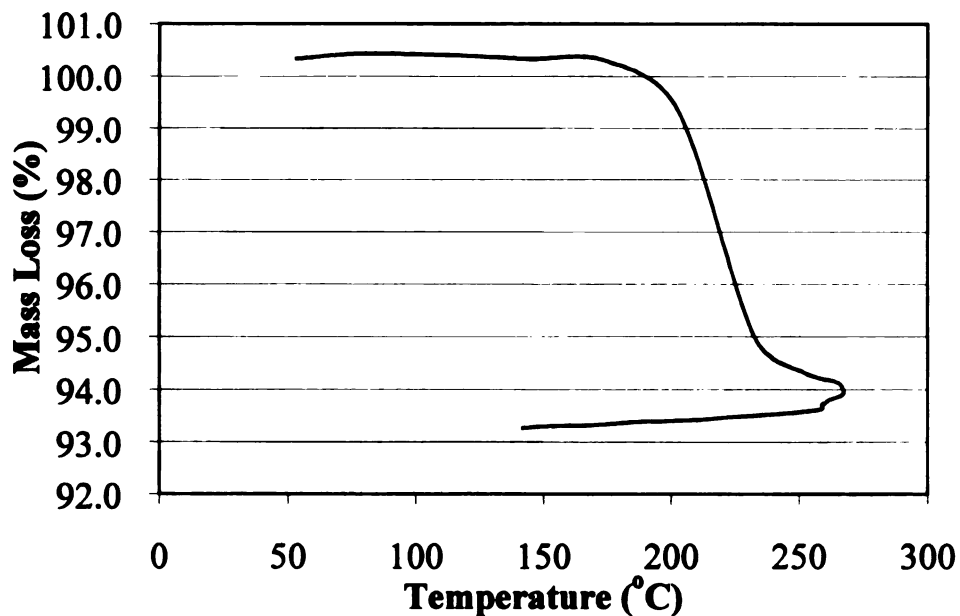


Figure 19: Thermogravimetric analysis (TGA) for the SHS $\{\text{TiB}_2/\text{Al}_2\text{O}_3\}$ composite green samples prepared with a traditional binder; the 6 wt% polyethylene glycol (PEG) binder was removed by binder burnout before sintering.

3.3.2 Material Loss and Sample Attrition

As was the case for the green samples, attrition was most severe in the SHS TiB_2/AKP 50 system processed at pH 8, and only one sample was available for sintering.

3.3.3 Sintered Density Measurements

Sintered densities were measured as a function of composite recipes and pH (Figures 20(a) and 20(b)). Although the SHS composite green densities were among the lowest at pH 4, the SHS composite sintered densities at pH 4 were among the highest. The sintered densities of the SHS composite were greater than any other composite system under any processing condition; in addition, unprocessed SHS (PEG binder) yielded the greatest sintered density.

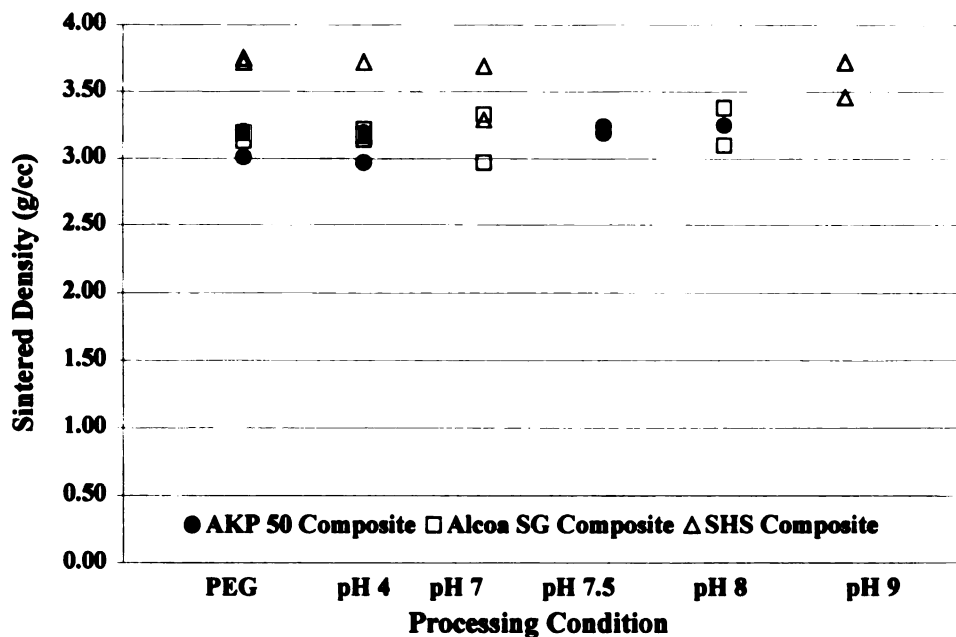


Figure 20(a): Sintered density (g/cc) vs. processing condition for each composite recipe

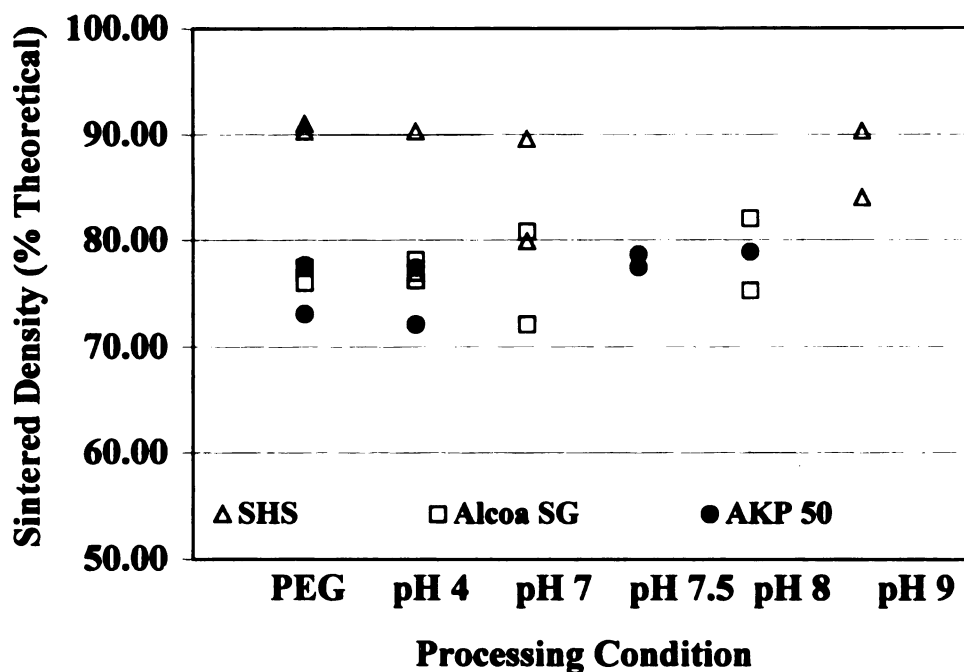


Figure 20(b): Sintered density (% Theoretical) vs. processing condition for each composite recipe

3.3.4 Consistency of Sintered Microstructure with *Suspension Stability*® Predictions

Using the samples with PEG binder as a baseline for comparison, the microstructures of the sintered samples in each of the three composite systems (Figure 21) were evaluated for consistency with the dispersion, coagulation, and heterocoagulation behavior of the TiB_2 and Al_2O_3 as predicted by *Suspension Stability*®. The results are summarized in Table 14 and pictured in Figures 21 and 21(a-l). Predicted and observed dispersion behaviors of TiB_2 in Al_2O_3 for the two component systems were in agreement. Acidic, neutral or basic processing conditions did not affect the hoped for dispersion, coagulation nor heterocoagulation behavior of the SHS composite system. The SHS powders were insensitive to colloidal processing.

In the two component systems, that is, SHS TiB₂/AKP 50 Al₂O₃ and SHS TiB₂/Alcoa SG Al₂O₃ composite systems, the microstructures differed between those processed for dispersion, coagulation and heterocoagulation. The SEM micrographs showed porosity was present in all three processing conditions to varying degrees. The microstructure at pH 4 (Figure 21(j)) showed fine TiB₂ phases uniformly distributed in an Al₂O₃ matrix with very little porosity. In the coagulated microstructures (Figures 21(g) and 21(k)), grains of Al₂O₃ and TiB₂ are distinguishable with much porosity. In the samples processed for heterocoagulation (Figures 21(h) and 21(l)), coarse TiB₂ grains are visible in the Al₂O₃ matrix, and the degree of porosity is much lower. The dispersed processing condition resulted in the most uniform and finest distribution of TiB₂ in Al₂O₃ with low porosity. Both SHS TiB₂ plus Al₂O₃ two-component-systems were sensitive to colloidal processing, and the microstructures reflected that *Suspension Stability*[®] effectively predicted the coagulation behavior of the SHS TiB₂ plus Al₂O₃ two-component-systems.

Table 14: Evaluation of sintered microstructure for consistency with processing behaviors

Processing Condition	SHS {TiB ₂ /Al ₂ O ₃ }	SHS TiB ₂ /AKP-50	SHS TiB ₂ /Alcoa-SG
PEG	Baseline	Baseline	Baseline
Dispersion	No affect	Dispersion	Dispersion
Coagulation	No affect	Coagulation	Coagulation
Heterocoagulation	No affect	Heterocoagulation	Heterocoagulation

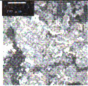
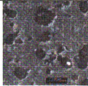

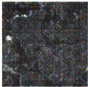
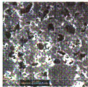


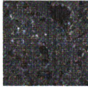




	SHS $\text{TiB}_2/\text{Al}_2\text{O}_3$	SHS $\text{TiB}_2/\text{AKP-50}$	SHS $\text{TiB}_2/\text{Alcoa SG}$
PEG			
Dispersion			
Coagulation			
Heterocoagulation			

Figure 21: Backscatter scanning electron micrographs (20.0 kV) of the microstructures of each of the three composite systems at the four processing conditions; markers are 100 μm in every micrograph; white areas are the TiB_2 , gray areas are the Al_2O_3 , and black areas are pores.

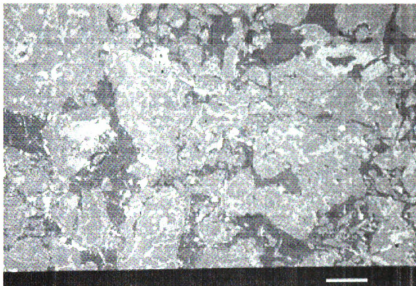


Figure 21(a): Backscatter scanning electron micrograph (20 kV) of SHS composite { $\text{TiB}_2/\text{Al}_2\text{O}_3$ } processed with PEG20M binder; marker (white line at bottom of micrograph) is 100 μm ; white areas are the TiB_2 , gray areas are the Al_2O_3 , and black areas are pores.

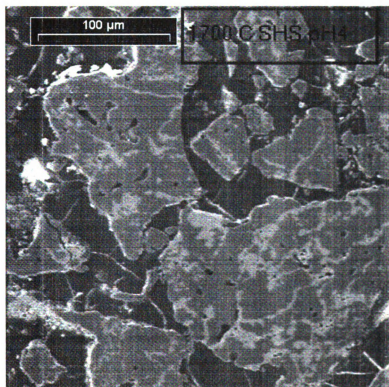


Figure 21(b): Backscatter scanning electron micrograph (20 kV) of SHS composite { $\text{TiB}_2/\text{Al}_2\text{O}_3$ } processed at pH 4; white areas are the TiB_2 , gray areas are the Al_2O_3 , and black areas are pores.

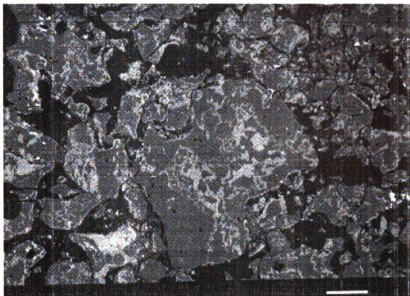


Figure 21(c): Backscatter scanning electron micrograph (20 kV) of SHS composite {TiB₂/Al₂O₃} processed at pH 7; marker (white line at bottom of micrograph) is 100 μ m; white areas are the TiB₂, gray areas are the Al₂O₃, and black areas are pores.

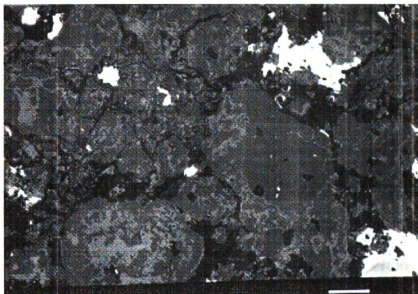


Figure 21(d): Backscatter scanning electron micrograph (20 kV) of SHS composite {TiB₂/Al₂O₃} processed at pH 9; marker (white line at bottom of micrograph) is 100 μ m; white areas are the TiB₂, gray areas are the Al₂O₃, and black areas are pores.

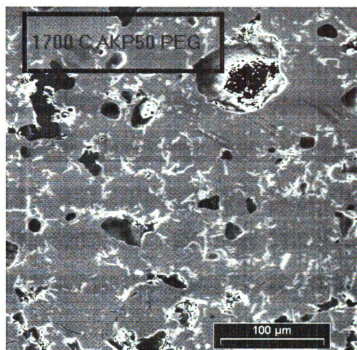


Figure 21(e): Backscatter scanning electron micrograph (20 kV) of SHS TiB_2 /AKP 50 Al_2O_3 processed with PEG20M binder; white areas are the TiB_2 , gray areas are the Al_2O_3 , and black areas are pores.

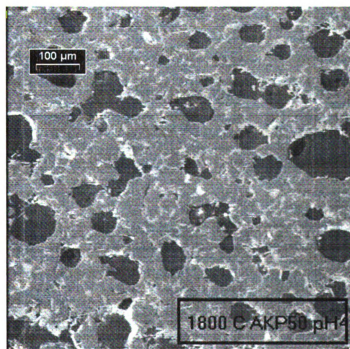


Figure 21(f): Backscatter scanning electron micrograph (20 kV) of SHS TiB_2 /AKP 50 Al_2O_3 processed pH 4; white areas are the TiB_2 , gray areas are the Al_2O_3 , and black areas are pores.

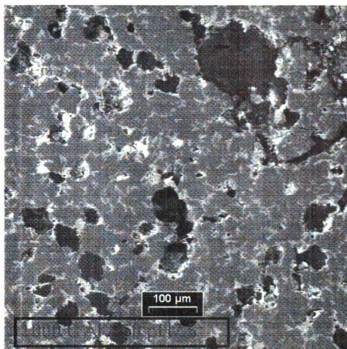


Figure 21(g): Backscatter scanning electron micrograph (20 kV) of SHS TiB_2 /AKP 50 Al_2O_3 processed pH 7.5; white areas are the TiB_2 , gray areas are the Al_2O_3 , and black areas are pores.

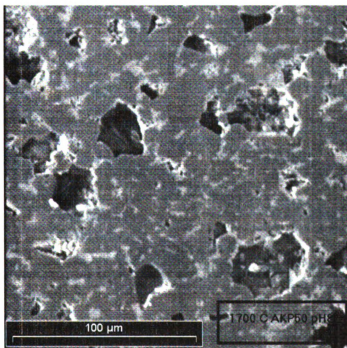


Figure 21(h): Backscatter scanning electron micrograph (20 kV) of SHS TiB_2 /AKP 50 Al_2O_3 processed pH 8; white areas are the TiB_2 , gray areas are the Al_2O_3 , and black areas are pores.

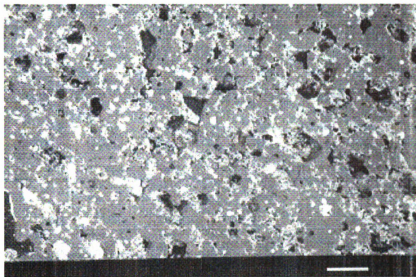


Figure 21(i): Backscatter scanning electron micrograph (20 kV) of SHS TiB_2 /Alcoa SG Al_2O_3 processed with PEG20M binder; marker (white line at bottom of micrograph) is 100 μm ; white areas are the TiB_2 , gray areas are the Al_2O_3 , and black areas are pores.

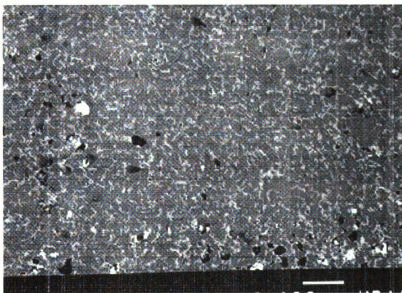


Figure 21(j): Backscatter scanning electron micrograph (20 kV) of SHS TiB_2 /Alcoa SG Al_2O_3 processed at pH 4; marker (white line at bottom of micrograph) is 100 μm ; white areas are the TiB_2 , gray areas are the Al_2O_3 , and black areas are pores.

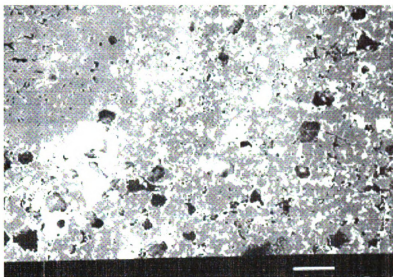


Figure 21(k): Backscatter scanning electron micrograph (20 kV) of SHS TiB_2 /Alcoa SG Al_2O_3 processed at pH 7; marker (white line at bottom of micrograph) is 100 μm ; white areas are the TiB_2 , gray areas are the Al_2O_3 , and black areas are pores.

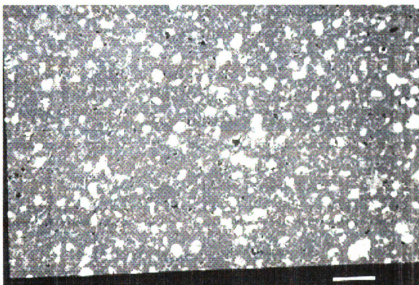


Figure 21(l): Backscatter scanning electron micrograph (20 kV) of SHS TiB_2 /Alcoa SG Al_2O_3 processed at pH 8; marker (white line at bottom of micrograph) is 100 μm ; white areas are the TiB_2 , gray areas are the Al_2O_3 , and black areas are pores.

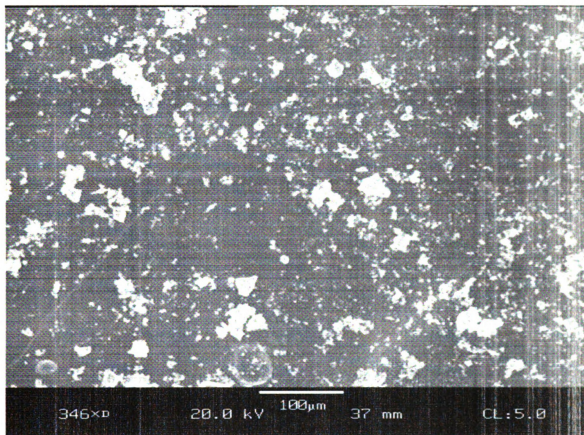


Figure 22: Scanning Electron Microscope (SEM) image of SHS $\{\text{TiB}_2/\text{Al}_2\text{O}_3\}$ composite powder dusted onto carbon tape; the large charging particles were thought to be the non-conducting Al_2O_3 and the small particles were thought to be the conducting TiB_2 ; recent investigations [Wilson, 2001] indicate most particles are a mixture of both the TiB_2 and the Al_2O_3 .

3.3.5 Sintered Sample Conductivity

All sintered samples were conductive across their length, width, and height. Placing the two electrodes on any face of all the samples also indicated conductance.

3.4 *Microstructure*

3.4.1 SHS Composites

Among the microstructures made from SHS composite starting powder, there were no significant differences. In the SHS composite samples, the TiB_2 surrounded the Al_2O_3 in an interconnecting network, which was visible from the SEM micrographs (Figures 21 and 21(a-d)) and supported by the conductivity measurements. Thus, the free-sintered SHS composite powders, no matter the processing conditions, produced the microstructure most similar to the “continuous” microstructure (Figure 1) defined by Logan [1997].

3.4.2 SHS TiB_2 / Al_2O_3 Composites

In the other SHS TiB_2 plus Al_2O_3 two-component-systems, the “continuous” microstructure was not evident in the SEM micrographs (Figures 21 (e-j, l)), except in some areas of the micrograph of the SHS TiB_2 /Alcoa SG Al_2O_3 composite processed for coagulation at pH 7 (Figure 21(k)). All the microstructures (Figures 21(e-j, l)), but the SHS TiB_2 /Alcoa SG Al_2O_3 composite processed for coagulation at pH 7 (Figure 21(k)), were similar to the “discontinuous” microstructure (Figure 2) defined by Logan [1997].

Although there were large agglomerations of TiB_2 (Figure 21(k)) in the SHS TiB_2 / Alcoa SG Al_2O_3 processed at pH 7, there were also distinct areas of the TiB_2 surrounding grains of the Al_2O_3 . The TiB_2 was interconnected even in the discontinuous microstructures (Figures 21(e-j, l)), as the measurements for conductivity were positive across all dimensions of the sintered sample where there was no conductivity in the green bodies.

3.5 Microhardness Measurement

Even at a reduced load of 500 g rather than 1000 g for the indentation test, the samples crushed easily, and the microhardness data was inconclusive.

4 Conclusions

The computer model *Suspension Stability*^o was effective in predicting optimum suspension conditions for colloidal processing of two-component ceramic composites. For SHS TiB₂ (30 wt%) plus Al₂O₃ (70 wt%) composite systems, the predicted pH value of 4 was suitable for slip casting and reduced the extent of agglomeration such that the SHS TiB₂/AKP 50 Al₂O₃ and SHS TiB₂/Alcoa SG A-1000 Al₂O₃ composite systems processed at these conditions achieved the highest green body densities. However, the process of slip casting created samples highly vulnerable to physical damage and material loss.

In both the SHS TiB₂/AKP 50 Al₂O₃ and SHS TiB₂/Alcoa SG Al₂O₃ composites prepared in other than acidic conditions, material loss was high, which was consistent with the solubility of Al₂O₃ under basic conditions. It was expected that composite systems with the highest green body densities would yield sintered composites with the highest densities. The data for both the SHS TiB₂/AKP 50 Al₂O₃ and SHS TiB₂/Alcoa SG Al₂O₃ composite systems processed at pH 4 yielded sintered densities lower than those processed at pH 7 and above. This trend was consistent with Al₂O₃ going into solution under basic conditions [Wilson, 2001], thereby leaving material with a greater percentage of the denser TiB₂. Also, the result of fewer and/or significantly smaller (less than half the average weight) samples in those processed at pH 7 was likely to create more error in these measurements, which may also have accounted for this discrepancy in the data where the highest green body densities did not produce the highest sintered densities.

That the computer model *Suspension Stability*[©] was also effective in predicting coagulating behavior of the SHS TiB₂ plus Al₂O₃ composites was evident in the backscatter micrographs of the colloiddally-processed samples compared to the traditional binder PEG20M samples. The SHS TiB₂ behavior was sensitive to colloidal processing and dispersed, coagulated or heterocoagulated with respect to both the AKP 50 and Alcoa SG A-1000 Al₂O₃.

Suspension Stability[©] was not effective in predicting optimum suspension conditions for colloidal processing of SHS composite {TiB₂/Al₂O₃}. Green body densities of the SHS composite {TiB₂/Al₂O₃} were slightly higher for those processed at pH 7, but sintered densities were similar (within 0.5%) no matter the processing condition. The sintered densities of the traditional binder samples, which were not colloiddally-processed, were less variable and slightly higher than those colloiddally-processed. Although processing at pH 4 caused some material loss in the SHS composite {TiB₂/Al₂O₃} system and slightly lower green body densities as would be expected if TiB₂ was removed after going into solution, the green body densities, the sintered densities, and the invariant microstructures in the sintered samples, indicated the SHS composite {TiB₂/Al₂O₃} system was insensitive to colloidal processing.

When the microstructures of the traditional binder PEG20M and colloiddally-processed, pressureless-sintered SHS TiB₂ plus Al₂O₃ composite systems were compared to the SHS (or non-SHS-but-dry-mixed), hot-pressed TiB₂/Al₂O₃ ceramic composites, only the SHS TiB₂/Alcoa SG Al₂O₃ processed at pH 7 was of further interest for ceramic armor applications. The coagulated behavior of the SHS TiB₂/Alcoa SG Al₂O₃ processed at pH 7 was able to produce some of the “continuous” microstructure associated with

ballistic penetration resistance with a final density comparable to the high densities achieved with the SHS composite $\{\text{TiB}_2/\text{Al}_2\text{O}_3\}$ starting powders. With more control over coagulation behavior, the desired microstructure could dominate the SHS $\text{TiB}_2/\text{Alcoa SG Al}_2\text{O}_3$ ceramic composite system.

When the microstructures of the traditional binder PEG20M and colloiddally-processed, pressureless-sintered SHS composite $\{\text{TiB}_2/\text{Al}_2\text{O}_3\}$ composite system were compared to the SHS (or non-SHS-but-dry-mixed), hot-pressed $\text{TiB}_2/\text{Al}_2\text{O}_3$ ceramic composites, all were consistent with the “continuous” microstructure associated with ballistic penetration resistance. The SHS composite $\{\text{TiB}_2/\text{Al}_2\text{O}_3\}$ starting powders continue to be of interest for armor applications as the factors necessary for the “continuous” microstructure appeared to be inherent in the powder itself and not dependent on any colloidal processing of the starting powders.

5 Future Work

In this research effort, the colloidal processing of $\text{TiB}_2/\text{Al}_2\text{O}_3$ was explored.

Further research is recommended to better understand the following:

- electrolyte options to reduce the apparent solution and loss of the TiB_2 and Al_2O_3 [Wilson, 2001] and to increase opportunities for adjusting the pH during processing so as to oppositely charge the components and agglomerate the TiB_2 around the Al_2O_3 particles as suggested by Hogg et al. [1966] and Franks et al. [1995]
- advantages of freeze drying then pressing to form samples rather than slip casting of colloidal suspensions, which experienced high material loss and sample attrition
- differences in zeta potential and stability between carbothermic TiB_2 and SHS TiB_2 ; Logan [1997] used carbothermic TiB_2 for some of the penetration resistant ceramic armor targets

REFERENCES

References

G. Abfalter, N.S. Brar, and D. Jurick, "Determination of the Dynamic Unload/Reload Characteristics of Ceramics," *Contract No.: DAAL03-88-K-0203, U.S. Army Research Office*, University of Dayton Research Institute, Dayton, Ohio, 1992

P. Becher, *Dictionary of Colloid and Surface Science*; Marcel Dekker, Inc.: New York, 1990, p. 95

A. Bleier, "Fundamentals of Preparing Suspensions of Silicon and Related Ceramic Powders," *Communications of the Am. Ceram. Soc.*, C79-81, May 1983

W. D. Callister, Jr., *Materials Science and Engineering, An Introduction*; John Wiley & Sons: New York, 2000, p. 441

L.S. Çeroviç, S.K. Milonjiç and L. Kostić-Gvozdenović, "Intrinsic Equilibrium Constants of b-Silicon Carbide Obtained from Surface Charge Data," *J. Am.Ceram.Soc.*, 78 [11] 3093-96 (1995)

M. Colic, G.V. Franks, M.L. Fisher and F.F. Lange, "Effect of Counterion Size on Short Range Repulsive Forces at High Ionic Strengths," *Langmuir* 1997, 13, 3129-3135

CRC Handbook of Chemistry & Physics, 79th Edition, David R. Lide, Ph.D., *Editor-in-Chief*, 1998, pp. 12-48

Derjaguin (1954) and Devereux and de Bruyn (1963) as cited in R. Hogg, T.W. Healy and D.W. Fuerstenau, "Mutual Coagulation of Colloidal Dispersions," *Trans. Faraday Soc.* 1966, 62, 1638-1651

Derjaguin (1934) as cited in R. Hogg, T.W. Healy and D.W. Fuerstenau, "Mutual Coagulation of Colloidal Dispersions," *Trans. Faraday Soc.* 1966, 62, 1638-1651

Encyclopedia of Materials Science and Engineering, Michael B. Bever, *Editor-in-Chief*, MIT Press: Cambridge, MA, 1986, Volume 5, O-Q, p. 3832

Engineered Materials Handbook, Vol. 4, Ceramics and Glasses; ASM International: U.S.A., 1991, pp. 48

Engineered Materials Handbook, Vol. 4, Ceramics and Glasses; ASM International: U.S.A., 1991, pp. 50

D.H. Everett, *Basic Principles of Colloid Science*; Royal Society of Chemistry: London, 1988, p. 8

D.H. Everett, *Basic Principles of Colloid Science*; Royal Society of Chemistry: London, 1988, p. 42

D.H. Everett, *Basic Principles of Colloid Science*; Royal Society of Chemistry: London, 1988, p. 90

G.V. Franks and F.F. Lange, "Mechanical Behavior of Saturated, Consolidated, Alumina Powder Compacts: Effect of Particle Size and Morphology on the Plastic-to-Brittle Transition," *Colloids and Surfaces A: Physicochem And Engr Aspects*, 146 [1-3] pp. 5-17 (15 January 1999)

G.V. Franks, B.V. Velamakanni and F.F. Lange, "Vibraforming and In Situ Flocculation of Consolidated, Coagulated, Alumina Slurries," *J. Am.Ceram.Soc.*, 78 [5] 1324-28 (1995)

Fuchs (1934) as cited in R. Hogg, T.W. Healy and D.W. Fuerstenau, "Mutual Coagulation of Colloidal Dispersions," *Trans. Faraday Soc.* 1966, 62, 1638-1651

R. Greenwood and K. Kendall, "Selection of Suitable Dispersants for Aqueous Suspensions of Zirconia and Titania Powders Using Acoustophoresis," *J. Eur. Ceram. Soc.*, 19 [4] 479-88 (1999)

Hamaker (1937) as cited in D. J. Shaw, *Introduction to Colloid and Surface Chemistry, Fourth Edition*; Butterworth-Heinemann: Oxford, 1992, p. 216

W. Blair Haworth, Jr., *The Bradley and How It Got That Way*; Greenwood Press: Westport, CT, 1999, pp. 28, 95

P.C. Heimenz and R. Rajagopaian, *Principles of Colloid and Surface Chemistry, Third Edition Revised and Expanded*; Marcel Dekker, Inc.: New York, 1997, p. 499

P.C. Heimenz and R. Rajagopaian, *Principles of Colloid and Surface Chemistry, Third Edition Revised and Expanded*; Marcel Dekker, Inc.: New York, 1997, p. 529

P.C. Heimenz and R. Rajagopaian, *Principles of Colloid and Surface Chemistry, Third Edition Revised and Expanded*; Marcel Dekker, Inc.: New York, 1997, p. 534

P.C. Heimenz and R. Rajagopaian, *Principles of Colloid and Surface Chemistry, Third Edition Revised and Expanded*; Marcel Dekker, Inc.: New York, 1997, p. 541

P.C. Heimenz and R. Rajagopaian, *Principles of Colloid and Surface Chemistry, Third Edition Revised and Expanded*; Marcel Dekker, Inc.: New York, 1997, p. 566

P.C. Heimenz and R. Rajagopaian, *Principles of Colloid and Surface Chemistry, Third Edition Revised and Expanded*; Marcel Dekker, Inc.: New York, 1997, p. 567

J.G. Hetherington, "Two-Component Composite Armours," *Lightweight Armour Systems Symposium*, Royal Military College of Science, Shrivenham, Swindon, UK 28-30 June 1995

R. Hogg, T.W. Healy and D.W. Fuerstenau, "Mutual Coagulation of Colloidal Dispersions," *Trans. Faraday Soc.* 1966, 62, 1638-1651

V. Hohler, A.J. Stilp, K. Weber, "Ranking Methods of Ceramics and Experimental Optimization of a Laminated Target with Ceramics," *Lightweight Armour Systems Symposium*, Royal Military College of Science, Shrivenham, Swindon, UK 28-30 June 1995

D.A. Hoke and M. A. Meyers, "Consolidation of Combustion-Synthesized Titanium Diboride-Based Materials," *J.Am.Ceram.Soc.*, 78 [2] 275-84 (1995)

R. J. Hunter, *Foundations of Colloid Science*; Clarendon Press: Oxford, 1993; Vol. 1., p. 2

R. J. Hunter, *Foundations of Colloid Science*; Clarendon Press: Oxford, 1993; Vol. 1., p. 7

R. J. Hunter, *Foundations of Colloid Science*; Clarendon Press: Oxford, 1993; Vol. 1., p. 90-92

R. J. Hunter, *Foundations of Colloid Science*; Clarendon Press: Oxford, 1993; Vol. 1., p. 98

R. J. Hunter, *Foundations of Colloid Science*; Clarendon Press: Oxford, 1993; Vol. 1., p. 382

R. J. Hunter, *Foundations of Colloid Science*; Clarendon Press: Oxford, 1993; Vol. 1., p. 422

P.W.M. Jacobs and E.A. Kotomin, "Modeling of Point Defects in Corundum Crystals," *J. Am.Ceram.Soc.*, 77 [10] 2505-508 (1994)

J.T. Jones and M.F. Berard, *Ceramics: Industrial Processing and Testing*; The Iowa State University Press: Ames, IA, 1972

L.J. Kecskes, A. Niiler, T. Kottke, K.V. Logan, and G.R. Villalobos, "Dynamic Consolidation of Combustion-synthesized Alumina-Titanium Diboride Composite Ceramics," *J.Am.Ceram.Soc.*, 79 [10] 2687-95 (1996)

W.D. Kingery, H.K. Bowen, and D.R. Uhlmann, *Introduction to Ceramics, Second Edition*; John Wiley & Sons: New York, 1976, p. 9

F.F. Lange, "Powder Processing Science and Technology for Increased Reliability," *J. Am. Ceram. Soc.*, 72 [1] 3-15 (1989)

F.F. Lange, B.V. Velamakanni, J.C. Chang and D.S. Pearson, "Colloidal Powder Processing for Structural Reliability: Role of Interparticle Potential on Particle Consolidation," *Structural Ceramics Processing, Microstructure and Properties Proc. of the Riso International Symposium on Metallurgy and Mater. Sci.*, Riso Natl Lab, Riso Library, Roskilde, Den. 1990, p. 57-78.

J. Liu and P.D. Ownby, "Enhanced Mechanical Properties of Alumina by Dispersed Titanium Diboride Particulate Inclusions," *J. Am. Ceram. Soc.*, 74 [1] 241-243 (1991)

K.V. Logan, "Elastic-Plastic Behavior of Hot Pressed Composite Titanium Diboride/Alumina Powders Produced Using Self-Propagating High Temperature Synthesis," Georgia Institute of Technology, Ph.D. Thesis, September 1992

Communication from K.V. Logan, Ph.D., Principal Investigator, School of Material Science and Engineering, Georgia Institute of Technology to T. Furmaniak, Project Engineer, *Contract No. DAAE07-95-C-R040, U.S. Army Tank Automotive Research Development and Engineering Center (TARDEC)*, February 28, 1997

London (1930) as cited in D. J. Shaw, *Introduction to Colloid and Surface Chemistry, Fourth Edition*; Butterworth-Heinemann: Oxford, 1992, p. 215

Matec Applied Sciences. The ESA-9800. [Online] Available <http://www.matec.com/esa9800.htm>, January 20, 2001

A.G. Merzhanov, "Self-Propagating High-Temperature Synthesis: Twenty Years of Search and Findings," *Keynote Address, The Institute of Structural Macrokinetics*, USSR Academy of Sciences, Chernogolovka, Moscow, USSR, *Combustion and Plasma Synthesis of High-Temperature Materials*, Z.A. Munir and J.B. Holt Editors, VCH, New York, 1990, pp. 1-3

C. Mroz, "Titanium Diboride," *Am. Ceram. Soc. Bulletin.*, 76 [6] 158-9 (1995)

Communication from J. Mullins, Laboratory Technician, *Weapons Material Research Directorate, Army Research Laboratory*, Aberdeen Proving Ground, Maryland, August 1999

O'Brien (1986, 1990) as cited in B.A. Wilson and M.J. Crimp, "Prediction of Composite Colloidal Suspension Stability Based upon the Hogg, Healy, and Fuerstenau Interpretation," *Langmuir* 1993, 9, 2836-2843

M.A. Occhionero, S.L. Marallo, A.E. Karas and B.E. Novich, "Influence of Surface Area and Particle Size Distribution on Sintering and Microstructure Development," *Symposium on Sintering of Advanced Ceramics*, American Ceramic Society, Cincinnati, OH, 2-5 May 1988

R.M. Ogorkiewicz, "Development of Lightweight Armour Systems," *Keynote Lecture, Lightweight Armour Systems Symposium*, Royal Military College of Science, Shrivenham, Swindon, UK 28-30 June 1995

D. J. Shaw, *Introduction to Colloid and Surface Chemistry, Fourth Edition*; Butterworth-Heinemann: Oxford, 1992, p. 174

D. J. Shaw, *Introduction to Colloid and Surface Chemistry, Fourth Edition*; Butterworth-Heinemann: Oxford, 1992, p. 178

D. J. Shaw, *Introduction to Colloid and Surface Chemistry, Fourth Edition*; Butterworth-Heinemann: Oxford, 1992, p.190

D. J. Shaw, *Introduction to Colloid and Surface Chemistry, Fourth Edition*; Butterworth-Heinemann: Oxford, 1992, p. 216

D. J. Shaw, *Introduction to Colloid and Surface Chemistry, Fourth Edition*; Butterworth-Heinemann: Oxford, 1992, p. 217

D. J. Shaw, *Introduction to Colloid and Surface Chemistry, Fourth Edition*; Butterworth-Heinemann: Oxford, 1992, p. 218

Shaw (1992) as cited in B.A. Wilson and M.J. Crimp, "Prediction of Composite Colloidal Suspension Stability Based upon the Hogg, Healy, and Fuerstenau Interpretation," *Langmuir* 1993, 9, 2836-2843

Smoluchowski (1916, 1917) as cited in R. Hogg, T.W. Healy and D.W. Fuerstenau, "Mutual Coagulation of Colloidal Dispersions," *Trans. Faraday Soc.* 1966, 62, 1638-1651

Stern (1924) as cited in D. J. Shaw, *Introduction to Colloid and Surface Chemistry, Fourth Edition*; Butterworth-Heinemann: Oxford, 1992, p. 182, and P.C. Heimenz and R. Rajagopalan, *Principles of Colloid and Surface Chemistry, Third Edition Revised and Expanded*; Marcel Dekker, Inc.: New York, 1997, p.527

E. Strassburger, H. Senf, H. Rothenhäusler, "Comparison of Failure Behaviour During Impact and Ballistic Performance of Different Al₂O₃ Ceramics," *Lightweight Armour Systems Symposium*, Royal Military College of Science, Shrivenham, Swindon, UK 28-30 June 1995

Sumitomo Chemical. Alumina products. [Online] Available http://sumitomo-chem.co.jp/kiso_e/alumina/index.html, March 9, 2001.

M. Takeo, *Disperse Systems*; Wiley-VCH: New York, 1999, p. 1

M. Takeo, *Disperse Systems*; Wiley-VCH: New York, 1999, p. 5

J. Texter, *Particle Characterization*; Strider Research Corporation: Rochester, NY, 2000

W.J. Walker, Jr., J.S. Reed and S.K. Verma, "Polyethylene Glycol Binders for Advanced Ceramics," *Paper 52-EP-92, 94th Annual Meeting of the Am. Ceram. Soc.*, Minneapolis, MN, April 12-16, 1992

S. Warden, *Slip Casting*; A&C Black: London, 1997, pp. 14-17

B.A. Wilson and M.J. Crimp, "Prediction of Composite Colloidal Suspension Stability Based upon the Hogg, Healy, and Fuerstenau Interpretation," *Langmuir* 1993, 9, 2836-2843

Communication from O.C. Wilson, Jr., "Characterization of Aluminum Oxide/Titanium Diboride Composite Powders Formed by SHS Reactions," *Paper SI-013-01, 25th Annual International Conference on Advanced Ceramics & Composites*, American Ceramic Society, Cocoa Beach, FL, 21-26 January 2001

P. Woolsey, D. Kokidko and S. Mariano, "An alternative Test Methodology for Ballistic Performance Ranking of Armor Ceramic," *MTL TR 89-43, U.S. Army Materials Technology Laboratory*, Watertown, MA, 1989

Z. Yeh, "Colloidal Processing of SiC(w)/Si₃N₄ Ceramic Composites by Slip Casting." Michigan State University, Masters Thesis, February 1996

APPENDICES

APPENDIX A

Equations for Evaluating Armor Efficiencies

Tests of depths of penetration (DOP) are conducted to characterize the ballistic performance of a specific armor material. DOP test data can be used to calculate the mass efficiency (e_m), as well as space efficiency (e_s) and the armor quality factor (q^2), which is a quality of particular interest to armor designers. The armor quality factor (q^2) relates both mass and space efficiencies and provides a quantity to compare between different armor materials. The weight and space claim of an armor material is necessary for armor designers to evaluate ballistic performance for protection of military ground vehicles.

The following equations [Woolsey et al., 1989] were used to calculate space efficiency (e_s) mass efficiency (e_m), and the armor quality factor (q^2):

$$e_s = \frac{P_{WITN} - P_R}{T_{CER}} \quad (17)$$

$$e_m = \frac{(P_{WITN} - P_R) * \rho_{WITN}}{T_{CER} * \rho_{CER}} = e_s * \frac{\rho_{WITN}}{\rho_{CER}} \quad (18)$$

$$q^2 = e_m * e_s \quad (19)$$

P_{WITN} is the depth of penetration of the projectile into the semi-infinite witness plate without the ceramic facing, P_R is the penetration of the projectile into the semi-infinite witness plate with the ceramic mounted to the front face, T_{CER} is the thickness of the ceramic applied to the face of the witness plate, and ρ is the density of the respective material. Each of these quantities is dimensionless.

The e_m compares the areal density (AD), that is, (density * thickness) of a material to the areal density of the witness plate also called the backing material, which is usually RHA steel. Aluminum is usually employed for DOP tests when the projectile velocity or mass is too low to penetrate the reference material. When aluminum is used as the

witness plate, e_m is then called the ballistic efficiency (n). The e_m and e_s of the witness plate, that is, the reference material, is by definition equal to 1.0; results greater than 1.0 indicate better ballistic performance as compared to the reference material.

APPENDIX B

Electrokinetic Sonic Amplitude (ESA) Measurements

Table 15: Potentiometric Titration (POTN729.esa), 0.5 vol. % TiB₂, 1x10⁻⁴ M KNO₃

Net (meq/l)	ESA (mPa·M/V)	Dyn Mob (m ² /V·s)	Zeta (mV)	Phase (deg)	pH (units)	Cond. (uS/cm)	Temp (deg C)	Acid (ml)	Base (ml)	Total (ml)
-0.430	0.409	1.585	18.307	-18.000	3.790	1689.000	35.700	0.086	0.000	200.086
-0.330	0.394	1.505	17.583	-10.900	3.900	1665.000	35.700	0.086	0.000	200.066
-0.235	0.380	1.452	16.961	-6.700	4.020	1645.000	35.700	0.047	0.000	200.047
-0.130	0.369	1.409	16.450	-1.300	4.150	1620.000	35.800	0.026	0.000	200.026
0.000	0.363	1.389	16.271	-0.600	4.180	1675.000	35.600	0.086	0.086	200.172
0.010	0.357	1.366	16.002	0.300	4.190	1677.000	35.600	0.086	0.086	200.174
0.060	0.358	1.369	16.050	2.400	4.230	1678.000	35.600	0.086	0.098	200.184
-0.030	0.352	1.344	15.678	3.600	4.270	1604.000	35.800	0.006	0.000	200.006
0.000	0.358	1.368	15.955	4.800	4.280	1599.000	35.800	0.000	0.000	200.000
-0.010	0.349	1.335	15.566	4.600	4.290	1597.000	35.800	0.002	0.000	200.002
0.180	0.356	1.363	15.976	7.600	4.320	1680.000	35.600	0.086	0.122	200.208
0.320	0.362	1.384	16.233	11.100	4.420	1677.000	35.600	0.086	0.150	200.236
0.454	0.359	1.374	16.128	15.200	4.510	1680.000	35.600	0.086	0.177	200.263
0.594	0.358	1.372	16.109	18.500	4.600	1683.000	35.500	0.086	0.205	200.291
0.749	0.365	1.397	16.409	22.500	4.690	1683.000	35.500	0.086	0.236	200.322
0.914	0.366	1.400	16.447	25.600	4.790	1688.000	35.500	0.086	0.269	200.355
1.063	0.370	1.418	16.668	28.000	4.880	1691.000	35.500	0.086	0.303	200.389
1.268	0.374	1.431	16.823	31.300	4.970	1697.000	35.500	0.086	0.340	200.426
1.473	0.379	1.453	17.089	32.800	5.060	1698.000	35.500	0.086	0.381	200.467
1.697	0.382	1.463	17.218	35.200	5.150	1707.000	35.400	0.086	0.426	200.512
1.936	0.380	1.455	17.122	37.300	5.240	1715.000	35.500	0.086	0.474	200.560
2.195	0.388	1.467	17.515	39.100	5.330	1716.000	35.400	0.086	0.526	200.612
2.475	0.383	1.469	17.308	40.100	5.430	1729.000	35.400	0.086	0.582	200.668
2.749	0.382	1.463	17.244	41.500	5.540	1740.000	35.400	0.086	0.637	200.723
2.998	0.383	1.469	17.318	41.900	5.640	1750.000	35.400	0.086	0.687	200.773
3.237	0.378	1.452	17.124	43.500	5.750	1758.000	35.400	0.086	0.735	200.821
3.456	0.376	1.443	17.026	43.400	5.860	1758.000	35.300	0.086	0.779	200.865
3.650	0.372	1.429	16.866	44.500	5.980	1763.000	35.300	0.086	0.818	200.904
3.819	0.365	1.401	16.545	45.700	6.080	1766.000	35.300	0.086	0.852	200.938
3.973	0.362	1.389	16.404	45.800	6.180	1773.000	35.300	0.086	0.883	200.969
4.123	0.356	1.367	16.151	46.400	6.280	1779.000	35.300	0.086	0.913	200.999
4.277	0.353	1.357	16.043	46.600	6.380	1786.000	35.300	0.086	0.944	201.030
4.431	0.345	1.326	15.683	47.700	6.480	1787.000	35.300	0.086	0.975	201.061
4.585	0.343	1.318	15.590	47.500	6.570	1789.000	35.300	0.086	1.006	201.092
4.744	0.336	1.293	15.298	48.600	6.670	1792.000	35.200	0.086	1.038	201.124
4.908	0.330	1.267	14.993	50.100	6.760	1800.000	35.200	0.086	1.071	201.157
5.082	0.322	1.237	14.648	50.700	6.870	1801.000	35.200	0.086	1.106	201.192
5.231	0.310	1.191	14.116	51.300	6.950	1808.000	35.200	0.086	1.136	201.222
5.425	0.307	1.182	14.006	52.300	7.040	1816.000	35.200	0.086	1.175	201.261
5.654	0.297	1.142	13.537	52.500	7.140	1822.000	35.200	0.086	1.221	201.307
5.937	0.282	1.085	12.873	54.200	7.250	1834.000	35.100	0.086	1.278	201.364
6.239	0.266	1.023	12.150	56.000	7.370	1847.000	35.100	0.086	1.339	201.425
6.557	0.258	0.992	11.773	57.700	7.480	1860.000	35.100	0.086	1.403	201.489
6.914	0.236	0.909	10.801	62.500	7.600	1882.000	35.100	0.086	1.475	201.561
7.296	0.212	0.817	9.720	68.700	7.710	1902.000	35.000	0.086	1.552	201.638
7.732	0.193	0.744	8.838	76.000	7.830	1925.000	35.100	0.086	1.640	201.726
8.193	0.174	0.672	7.984	85.900	7.940	1955.000	35.100	0.086	1.733	201.819
8.718	-0.156	-0.601	-7.148	101.400	8.060	1992.000	35.000	0.086	1.839	201.925
9.273	-0.142	-0.547	-6.500	114.000	8.170	2022.000	35.000	0.086	1.951	202.037
9.906	-0.136	-0.527	-6.268	132.200	8.290	2068.000	35.000	0.086	2.079	202.165
10.573	-0.130	-0.502	-5.977	142.300	8.400	2111.000	35.000	0.086	2.214	202.300
11.334	-0.132	-0.512	-6.093	153.300	8.520	2170.000	35.000	0.086	2.368	202.454
12.138	-0.126	-0.486	-5.788	162.100	8.630	2230.000	35.000	0.086	2.531	202.617
12.981	-0.125	-0.485	-5.781	173.500	8.760	2286.000	35.000	0.086	2.702	202.788
13.829	-0.126	-0.489	-5.834	-175.100	8.870	2345.000	34.900	0.086	2.874	202.960
14.779	-0.121	-0.468	-5.584	-159.600	9.000	2413.000	34.900	0.086	3.067	203.153
15.718	-0.139	-0.538	-6.424	-149.400	9.130	2474.000	34.900	0.086	3.258	203.344
16.647	-0.165	-0.642	-7.658	-141.700	9.250	2534.000	34.900	0.086	3.447	203.533
17.565	-0.180	-0.702	-8.385	-137.900	9.380	2598.000	34.900	0.086	3.634	203.720
18.472	-0.207	-0.805	-9.629	-136.900	9.520	2663.000	34.800	0.086	3.819	203.905
19.310	-0.221	-0.862	-10.306	-135.400	9.640	2710.000	34.800	0.086	3.990	204.076
20.137	-0.247	-0.963	-11.529	-137.800	9.790	2775.000	34.800	0.086	4.159	204.245
20.861	-0.271	-1.060	-12.681	-140.900	9.910	2835.000	34.800	0.086	4.307	204.393

Table 16: Potentiometric Titration (POTN733.esa), 0.5 vol. % TiB₂, 1x10⁻³ M KNO₃

Net (meq/l)	ESA (mPa·M/V)	Dyn Mob (m ² /V·s)	Zeta (mV)	Phase (deg)	pH (units)	Cond. (uS/cm)	Temp (deg C)	Acid (ml)	Base (ml)	Total (ml)
-0.330	0.357	1.363	17.052	-1.600	3.880	1735.000	33.000	0.066	0.000	200.066
-0.235	0.328	1.254	15.671	-0.100	4.000	1712.000	33.000	0.047	0.000	200.047
-0.130	0.301	1.149	14.357	3.400	4.130	1693.000	33.000	0.026	0.000	200.026
0.000	0.303	1.157	14.478	7.200	4.160	1724.000	33.000	0.066	0.066	200.132
0.010	0.300	1.149	14.376	8.800	4.170	1726.000	32.900	0.066	0.066	200.134
0.060	0.301	1.150	14.385	9.200	4.210	1723.000	33.000	0.066	0.078	200.144
-0.030	0.278	1.056	13.184	8.300	4.250	1671.000	33.000	0.006	0.000	200.006
0.000	0.278	1.061	13.263	9.500	4.260	1672.000	33.000	0.000	0.000	200.000
-0.010	0.260	1.069	13.345	9.200	4.270	1668.000	33.000	0.002	0.000	200.002
0.195	0.292	1.116	13.960	15.000	4.310	1731.000	32.900	0.066	0.105	200.171
0.330	0.287	1.099	13.758	19.600	4.400	1723.000	32.900	0.066	0.132	200.198
0.470	0.282	1.077	13.484	23.600	4.500	1726.000	32.900	0.066	0.160	200.226
0.609	0.279	1.068	13.374	27.700	4.590	1722.000	32.900	0.066	0.186	200.254
0.754	0.274	1.048	13.117	30.500	4.680	1734.000	32.900	0.066	0.217	200.283
0.924	0.284	1.085	13.596	35.200	4.770	1733.000	32.900	0.066	0.251	200.317
1.109	0.277	1.059	13.278	39.600	4.870	1742.000	32.900	0.066	0.288	200.354
1.298	0.276	1.063	13.336	42.000	4.950	1741.000	32.800	0.066	0.326	200.392
1.513	0.277	1.061	13.290	45.800	5.050	1749.000	32.900	0.066	0.369	200.435
1.742	0.270	1.036	12.982	47.500	5.140	1759.000	32.900	0.066	0.415	200.481
1.987	0.269	1.032	12.930	50.300	5.230	1758.000	32.900	0.066	0.464	200.530
2.266	0.268	1.026	12.883	52.300	5.320	1766.000	32.900	0.066	0.520	200.586
2.565	0.257	0.985	12.359	54.500	5.420	1780.000	32.900	0.066	0.580	200.646
2.869	0.256	0.982	12.317	57.700	5.520	1788.000	32.900	0.066	0.641	200.707
3.163	0.250	0.958	12.017	58.800	5.630	1796.000	32.800	0.066	0.700	200.766
3.431	0.237	0.910	11.420	59.400	5.740	1802.000	32.800	0.066	0.754	200.820
3.675	0.234	0.896	11.253	61.300	5.850	1813.000	32.800	0.066	0.803	200.869
3.889	0.223	0.854	10.739	61.900	5.960	1815.000	32.800	0.066	0.846	200.912
4.074	0.219	0.840	10.554	62.700	6.080	1823.000	32.800	0.066	0.883	200.949
4.233	0.209	0.801	10.061	65.200	6.190	1832.000	32.800	0.066	0.915	200.981
4.372	0.200	0.789	9.662	65.600	6.290	1830.000	32.800	0.066	0.943	201.009
4.506	0.197	0.755	9.483	66.200	6.390	1838.000	32.800	0.066	0.970	201.036
4.636	0.185	0.711	8.926	66.600	6.490	1835.000	32.800	0.066	0.996	201.062
4.775	0.181	0.694	8.721	68.700	6.580	1841.000	32.800	0.066	1.024	201.090
4.914	0.173	0.666	8.377	71.100	6.680	1844.000	32.800	0.066	1.052	201.118
5.058	0.161	0.619	7.779	73.100	6.800	1851.000	32.800	0.066	1.081	201.147
5.178	0.159	0.610	7.671	72.400	6.870	1859.000	32.800	0.066	1.105	201.171
5.332	0.152	0.583	7.330	73.500	6.950	1858.000	32.700	0.066	1.136	201.202
5.530	0.144	0.553	6.965	76.400	7.040	1866.000	32.700	0.066	1.176	201.242
5.744	0.136	0.523	6.578	79.000	7.140	1878.000	32.700	0.066	1.219	201.285
6.002	0.119	0.457	5.746	81.500	7.250	1890.000	32.700	0.066	1.271	201.337
6.290	0.112	0.429	5.400	84.700	7.380	1895.000	32.700	0.066	1.329	201.395
6.573	-0.099	-0.380	-4.767	90.400	7.500	1902.000	32.700	0.066	1.386	201.452
6.871	-0.086	-0.329	-4.145	96.100	7.610	1923.000	32.700	0.066	1.446	201.512
7.208	-0.078	-0.300	-3.778	110.500	7.720	1937.000	32.700	0.066	1.514	201.580
7.600	-0.072	-0.276	-3.479	127.800	7.830	1963.000	32.700	0.066	1.593	201.659
8.031	-0.073	-0.280	-3.529	145.600	7.940	1986.000	32.700	0.066	1.680	201.746
8.517	-0.092	-0.353	-4.451	166.200	8.060	2020.000	32.700	0.066	1.778	201.844
9.027	-0.112	-0.434	-5.471	179.500	8.170	2046.000	32.600	0.066	1.881	201.947
9.606	-0.146	-0.564	-7.108	-169.800	8.290	2087.000	32.700	0.066	1.998	202.064
10.254	-0.182	-0.742	-9.348	-162.100	8.410	2124.000	32.700	0.066	2.129	202.195
10.936	-0.243	-0.941	-11.852	-158.600	8.520	2169.000	32.700	0.066	2.267	202.333
11.667	-0.284	-1.097	-13.823	-154.100	8.630	2222.000	32.700	0.066	2.415	202.481
12.481	-0.326	-1.263	-15.912	-149.800	8.760	2280.000	32.600	0.066	2.580	202.646
13.324	-0.352	-1.366	-17.214	-146.900	8.880	2341.000	32.600	0.066	2.751	202.817
14.162	-0.368	-1.429	-18.005	-143.200	9.000	2398.000	32.600	0.066	2.921	202.987
15.043	-0.363	-1.411	-17.785	-140.500	9.120	2455.000	32.600	0.066	3.100	203.166
15.967	-0.387	-1.502	-18.943	-138.800	9.250	2512.000	32.600	0.066	3.288	203.354
16.876	-0.407	-1.583	-19.966	-136.200	9.380	2576.000	32.600	0.066	3.473	203.539
17.770	-0.437	-1.700	-21.446	-134.500	9.510	2638.000	32.600	0.066	3.655	203.721
18.603	-0.467	-1.818	-22.983	-134.000	9.640	2687.000	32.500	0.066	3.825	203.891
19.407	-0.503	-1.960	-24.741	-133.400	9.770	2736.000	32.600	0.066	3.989	204.055
20.215	-0.544	-2.123	-26.826	-134.300	9.910	2787.000	32.500	0.066	4.154	204.220

Table 17: Potentiometric Titration (POTN731.esa), 0.5 vol. % TiB₂, 1x10⁻² M KNO₃

Net (meq/l)	ESA (mPa·M/V)	Dyn Mob (m ² /V·s)	Zeta (mV)	Phase (deg)	pH (units)	Cond. (uS/cm)	Temp (deg C)	Acid (ml)	Base (ml)	Total (ml)
-0.365	0.441	1.688	19.578	-17.500	3.790	3383.000	36.000	0.073	0.000	200.073
-0.260	0.413	1.579	18.318	-16.000	3.910	3358.000	36.000	0.052	0.000	200.052
0.000	0.403	1.541	17.920	-16.300	3.930	3371.000	35.900	0.073	0.073	200.146
0.020	0.397	1.518	17.686	-15.100	3.950	3364.000	35.800	0.073	0.077	200.150
0.120	0.391	1.497	17.436	-14.100	3.980	3356.000	35.900	0.073	0.097	200.170
-0.160	0.377	1.439	16.699	-14.100	4.030	3332.000	36.000	0.032	0.000	200.032
0.435	0.385	1.474	17.168	-11.900	4.050	3353.000	35.900	0.073	0.160	200.233
0.849	0.359	1.372	15.991	-7.600	4.160	3352.000	35.800	0.073	0.243	200.316
-0.045	0.341	1.304	15.125	-9.000	4.170	3313.000	36.000	0.009	0.000	200.009
0.000	0.339	1.295	15.004	-8.100	4.200	3303.000	36.100	0.000	0.000	200.000
-0.015	0.335	1.281	14.843	-8.600	4.210	3308.000	36.000	0.003	0.000	200.003
1.218	0.346	1.326	15.466	-2.100	4.290	3353.000	35.800	0.073	0.317	200.390
1.517	0.338	1.293	15.079	3.400	4.390	3348.000	35.800	0.073	0.377	200.450
1.792	0.331	1.267	14.780	7.900	4.490	3350.000	35.800	0.073	0.432	200.505
2.081	0.325	1.244	14.521	14.500	4.600	3342.000	35.800	0.073	0.486	200.559
2.305	0.321	1.231	14.378	18.300	4.700	3346.000	35.800	0.073	0.535	200.608
2.545	0.322	1.236	14.439	23.300	4.800	3349.000	35.700	0.073	0.583	200.656
2.784	0.321	1.231	14.375	27.400	4.900	3353.000	35.800	0.073	0.631	200.704
3.023	0.320	1.226	14.326	31.300	5.000	3357.000	35.700	0.073	0.679	200.752
3.267	0.322	1.236	14.450	34.500	5.090	3365.000	35.700	0.073	0.728	200.801
3.526	0.320	1.228	14.366	37.700	5.190	3357.000	35.700	0.073	0.780	200.853
3.785	0.326	1.252	14.649	40.900	5.290	3366.000	35.700	0.073	0.832	200.905
4.063	0.320	1.229	14.391	43.400	5.380	3370.000	35.700	0.073	0.888	200.961
4.342	0.317	1.216	14.243	45.600	5.480	3378.000	35.600	0.073	0.944	201.017
4.620	0.315	1.211	14.185	48.900	5.590	3386.000	35.600	0.073	1.000	201.073
4.894	0.311	1.196	14.017	49.300	5.690	3396.000	35.600	0.073	1.055	201.128
5.147	0.302	1.161	13.612	51.600	5.830	3400.000	35.600	0.073	1.106	201.179
5.326	0.293	1.128	13.227	51.900	5.930	3403.000	35.600	0.073	1.142	201.215
5.510	0.288	1.107	12.996	53.400	6.030	3412.000	35.600	0.073	1.179	201.252
5.699	0.283	1.087	12.763	54.600	6.130	3415.000	35.500	0.073	1.217	201.290
5.883	0.274	1.055	12.384	56.100	6.230	3419.000	35.500	0.073	1.254	201.327
6.061	0.267	1.029	12.087	56.000	6.330	3418.000	35.500	0.073	1.290	201.363
6.230	0.254	0.979	11.508	57.400	6.430	3429.000	35.500	0.073	1.324	201.397
6.389	0.248	0.953	11.214	58.500	6.530	3428.000	35.400	0.073	1.356	201.429
6.543	0.245	0.943	11.102	60.200	6.630	3431.000	35.400	0.073	1.387	201.460
6.692	0.237	0.913	10.732	60.700	6.730	3440.000	35.500	0.073	1.417	201.490
6.846	0.223	0.858	10.093	61.400	6.830	3445.000	35.500	0.073	1.448	201.521
7.004	0.218	0.841	9.897	62.200	6.920	3445.000	35.400	0.073	1.480	201.553
7.173	0.207	0.796	9.378	65.100	7.000	3456.000	35.400	0.073	1.514	201.587
7.366	0.198	0.762	8.969	65.300	7.100	3456.000	35.400	0.073	1.553	201.626
7.609	0.187	0.720	8.486	67.600	7.210	3465.000	35.400	0.073	1.602	201.675
7.887	0.172	0.664	7.821	69.600	7.330	3472.000	35.400	0.073	1.658	201.731
8.179	0.158	0.607	7.165	73.500	7.450	3493.000	35.400	0.073	1.717	201.790
8.482	0.144	0.554	6.537	77.500	7.570	3502.000	35.400	0.073	1.778	201.851
8.809	0.129	0.497	5.865	82.200	7.680	3517.000	35.400	0.073	1.844	201.917
9.180	-0.115	-0.443	-5.228	94.600	7.800	3538.000	35.300	0.073	1.919	201.992
9.576	-0.111	-0.429	-5.070	110.200	7.900	3557.000	35.300	0.073	1.999	202.072
10.046	-0.115	-0.444	-5.242	134.100	8.020	3576.000	35.300	0.073	2.094	202.167
10.520	-0.128	-0.494	-5.835	149.300	8.130	3603.000	35.300	0.073	2.190	202.263
11.108	-0.155	-0.599	-7.076	164.300	8.240	3640.000	35.300	0.073	2.309	202.382
11.730	-0.181	-0.699	-8.267	174.900	8.360	3686.000	35.300	0.073	2.435	202.508
12.397	-0.211	-0.819	-9.682	-174.900	8.470	3723.000	35.200	0.073	2.570	202.643
13.151	-0.249	-0.965	-11.416	-166.000	8.590	3769.000	35.200	0.073	2.723	202.796
13.949	-0.292	-1.132	-13.405	-158.700	8.710	3832.000	35.200	0.073	2.885	202.958
14.791	-0.309	-1.198	-14.191	-152.000	8.830	3884.000	35.200	0.073	3.056	203.129
15.691	-0.334	-1.297	-15.366	-147.300	8.950	3935.000	35.200	0.073	3.239	203.312
16.644	-0.348	-1.354	-16.047	-143.800	9.070	3997.000	35.200	0.073	3.433	203.506
17.587	-0.365	-1.422	-16.851	-140.300	9.190	4062.000	35.200	0.073	3.625	203.698
18.573	-0.381	-1.483	-17.586	-138.400	9.330	4120.000	35.100	0.073	3.826	203.899
19.499	-0.392	-1.530	-18.163	-136.300	9.450	4173.000	35.100	0.073	4.015	204.088
20.414	-0.413	-1.611	-19.127	-136.000	9.580	4221.000	35.100	0.073	4.202	204.275
21.295	-0.443	-1.729	-20.536	-136.600	9.720	4280.000	35.100	0.073	4.382	204.455
22.121	-0.481	-1.880	-22.329	-136.800	9.860	4339.000	35.100	0.073	4.551	204.624
22.868	-0.508	-1.986	-23.599	-137.800	9.990	4385.000	35.100	0.073	4.704	204.777

Table 18: Potentiometric Titration (POTN717.esa), 0.5 vol. % AKP-50 Al₂O₃, 1x10⁻⁴ M KNO₃

Net (meq/l)	ESA (mPa·M/V)	Dyn Mob (m ² /V·s)	Zeta (mV)	Phase (deg)	pH (units)	Cond. (uS/cm)	Temp (deg C)	Acid (ml)	Base (ml)	Total (ml)
0.000	1.789	8.148	94.595	-13.000	3.780	121.000	31.400	0.000	0.000	200.000
0.030	1.837	8.324	96.680	-13.500	3.810	121.000	31.300	0.000	0.006	200.006
0.130	1.854	8.401	97.603	-13.300	3.960	123.000	31.300	0.000	0.026	200.026
0.195	1.898	8.598	99.927	-12.200	4.090	125.000	31.300	0.000	0.039	200.039
0.240	1.926	8.728	101.491	-10.900	4.220	127.000	31.300	0.000	0.048	200.048
0.270	1.968	8.917	103.599	-10.500	4.320	129.000	31.300	0.000	0.054	200.054
0.295	1.998	9.044	105.108	-10.800	4.410	130.000	31.300	0.000	0.059	200.059
0.325	2.011	9.114	106.012	-10.100	4.510	132.000	31.300	0.000	0.065	200.065
0.350	2.005	9.088	105.736	-9.200	4.610	133.000	31.300	0.000	0.070	200.070
0.375	2.032	9.210	107.121	-8.500	4.690	136.000	31.300	0.000	0.075	200.075
0.405	2.015	9.130	106.228	-7.500	4.780	138.000	31.300	0.000	0.081	200.081
0.435	2.007	9.098	106.040	-8.500	4.870	140.000	31.200	0.000	0.087	200.087
0.465	1.982	8.983	104.647	-8.200	4.950	143.000	31.200	0.000	0.093	200.093
0.500	1.941	8.796	102.463	-5.200	5.040	146.000	31.200	0.000	0.100	200.100
0.535	1.920	8.701	101.457	-4.200	5.110	149.000	31.200	0.000	0.107	200.107
0.585	1.782	8.076	94.093	-3.100	5.200	154.000	31.200	0.000	0.117	200.117
0.635	1.633	7.404	86.288	-1.600	5.300	158.000	31.200	0.000	0.127	200.127
0.680	1.430	6.482	75.539	-1.700	5.410	163.000	31.200	0.000	0.136	200.136
0.720	1.272	5.766	67.197	-1.000	5.520	167.000	31.200	0.000	0.144	200.144
0.755	1.089	4.935	57.549	-0.100	5.640	170.000	31.200	0.000	0.151	200.151
0.780	0.993	4.502	52.492	-0.100	5.770	172.000	31.200	0.000	0.156	200.156
0.795	0.982	4.450	51.905	0.400	5.870	173.000	31.200	0.000	0.159	200.159
0.805	0.957	4.337	50.590	0.200	5.960	173.000	31.200	0.000	0.161	200.161
0.815	0.910	4.126	48.152	0.900	6.030	174.000	31.100	0.000	0.163	200.163
0.825	0.905	4.102	47.883	0.000	6.090	175.000	31.100	0.000	0.165	200.165
0.840	0.823	3.731	43.571	1.700	6.170	176.000	31.100	0.000	0.168	200.168
0.855	0.786	3.474	40.580	0.900	6.250	177.000	31.100	0.000	0.171	200.171
0.870	0.686	3.110	36.326	0.800	6.340	178.000	31.100	0.000	0.174	200.174
0.885	0.626	2.838	33.150	0.600	6.430	179.000	31.100	0.000	0.177	200.177
0.900	0.551	2.499	29.197	0.500	6.510	180.000	31.100	0.000	0.180	200.180
0.915	0.488	2.213	25.854	-0.100	6.600	181.000	31.100	0.000	0.183	200.183
0.930	0.431	1.952	22.821	0.000	6.700	183.000	31.100	0.000	0.186	200.186
0.945	0.368	1.669	19.519	-0.200	6.790	184.000	31.100	0.000	0.189	200.189
0.960	0.310	1.407	16.450	-0.900	6.880	185.000	31.100	0.000	0.192	200.192
0.975	0.251	1.138	13.336	-2.500	6.980	187.000	31.000	0.000	0.195	200.195
0.989	0.201	0.912	10.675	-4.700	7.080	187.000	31.000	0.000	0.198	200.198
1.004	0.153	0.693	8.114	-6.300	7.150	189.000	31.000	0.000	0.201	200.201
1.024	0.071	0.324	3.787	-21.600	7.250	191.000	31.000	0.000	0.205	200.205
1.044	-0.034	-0.154	-1.800	-94.000	7.360	193.000	31.000	0.000	0.209	200.209
1.064	-0.085	-0.385	-4.505	-147.800	7.460	195.000	31.000	0.000	0.213	200.213
1.084	-0.141	-0.638	-7.489	-160.000	7.560	197.000	31.000	0.000	0.217	200.217
1.104	-0.199	-0.903	-10.571	-162.700	7.650	198.000	31.000	0.000	0.221	200.221
1.129	-0.287	-1.302	-15.252	-167.500	7.760	201.000	31.000	0.000	0.226	200.226
1.154	-0.363	-1.646	-19.293	-168.600	7.860	204.000	30.900	0.000	0.231	200.231
1.184	-0.449	-2.035	-23.851	-169.600	7.970	207.000	31.000	0.000	0.237	200.237
1.214	-0.549	-2.492	-29.204	-169.700	8.080	211.000	31.000	0.000	0.243	200.243
1.244	-0.619	-2.810	-32.930	-171.300	8.180	215.000	30.900	0.000	0.249	200.249
1.279	-0.722	-3.274	-38.389	-171.700	8.280	219.000	30.900	0.000	0.256	200.256
1.319	-0.824	-3.740	-43.864	-173.200	8.390	226.000	30.900	0.000	0.264	200.264
1.364	-0.909	-4.125	-48.397	-173.300	8.490	232.000	30.900	0.000	0.273	200.273
1.419	-1.028	-4.664	-54.721	-174.100	8.610	241.000	30.900	0.000	0.284	200.284
1.474	-1.129	-5.120	-60.062	-174.200	8.710	250.000	30.900	0.000	0.295	200.295
1.539	-1.242	-5.634	-66.120	-174.300	8.820	261.000	30.900	0.000	0.308	200.308
1.609	-1.327	-6.021	-70.702	-175.200	8.920	274.000	30.900	0.000	0.322	200.322
1.694	-1.459	-6.620	-77.767	-175.500	9.030	291.000	30.900	0.000	0.339	200.339
1.793	-1.563	-7.094	-83.258	-175.300	9.130	310.000	30.900	0.000	0.359	200.359
1.913	-1.701	-7.722	-90.721	-175.500	9.230	335.000	30.800	0.000	0.383	200.383
2.058	-1.829	-8.304	-97.532	-176.100	9.340	367.000	30.900	0.000	0.412	200.412
2.227	-1.966	-8.928	-104.902	-175.800	9.470	406.000	30.800	0.000	0.446	200.446
2.392	-2.078	-9.438	-110.877	-175.600	9.580	445.000	30.800	0.000	0.479	200.479
2.577	-2.178	-9.894	-116.288	-175.800	9.680	489.000	30.800	0.000	0.516	200.516
2.801	-2.290	-10.405	-122.290	-175.800	9.790	544.000	30.800	0.000	0.561	200.561
3.055	-2.388	-10.850	-127.573	-175.500	9.900	606.000	30.800	0.000	0.612	200.612
3.354	-2.500	-11.363	-133.601	-175.600	10.010	681.000	30.800	0.000	0.672	200.672

Table 19: Potentiometric Titration (POTN719.esa), 0.5 vol. % AKP-50 Al₂O₃, 1x10⁻³ M KNO₃

Net (meq/l)	ESA (mPa·M/V)	Dyn Mob (m ² /V·s)	Zeta (mV)	Phase (deg)	pH (units)	Cond. (uS/cm)	Temp (deg C)	Acid (ml)	Base (ml)	Total (ml)
0.000	2.292	10.385	117.702	5.500	3.750	288.000	32.400	0.000	0.000	200.000
0.035	2.298	10.400	117.911	5.400	3.790	289.000	32.400	0.000	0.007	200.007
0.135	2.338	10.592	120.188	5.900	3.960	272.000	32.400	0.000	0.027	200.027
0.190	2.382	10.795	122.754	6.200	4.110	274.000	32.300	0.000	0.038	200.038
0.225	2.400	10.875	123.422	6.500	4.230	276.000	32.300	0.000	0.045	200.045
0.250	2.410	10.918	123.948	6.400	4.310	277.000	32.300	0.000	0.050	200.050
0.275	2.415	10.944	124.275	7.000	4.390	278.000	32.300	0.000	0.055	200.055
0.305	2.435	11.033	125.300	7.500	4.490	281.000	32.300	0.000	0.061	200.061
0.330	2.415	10.945	124.308	8.000	4.600	283.000	32.300	0.000	0.066	200.066
0.350	2.431	11.015	125.156	8.200	4.650	284.000	32.300	0.000	0.070	200.070
0.380	2.408	10.914	124.075	8.500	4.750	287.000	32.300	0.000	0.076	200.076
0.410	2.398	10.869	123.545	8.800	4.840	288.000	32.300	0.000	0.082	200.082
0.440	2.355	10.872	121.311	9.800	4.930	292.000	32.300	0.000	0.088	200.088
0.470	2.296	10.407	118.348	9.600	5.030	293.000	32.300	0.000	0.094	200.094
0.500	2.280	10.245	116.436	10.300	5.100	296.000	32.300	0.000	0.100	200.100
0.535	2.182	9.798	111.463	10.800	5.190	299.000	32.200	0.000	0.107	200.107
0.570	2.042	9.258	105.349	11.200	5.280	302.000	32.200	0.000	0.114	200.114
0.610	1.862	8.439	98.077	11.700	5.390	305.000	32.200	0.000	0.122	200.122
0.645	1.688	7.651	87.124	12.500	5.490	308.000	32.200	0.000	0.129	200.129
0.675	1.524	6.910	78.724	12.400	5.600	311.000	32.200	0.000	0.135	200.135
0.700	1.348	6.101	69.453	12.600	5.710	314.000	32.200	0.000	0.140	200.140
0.720	1.270	5.756	65.554	13.000	5.820	315.000	32.200	0.000	0.144	200.144
0.735	1.206	5.466	62.313	13.500	5.920	316.000	32.100	0.000	0.147	200.147
0.750	1.139	5.165	58.874	14.100	6.010	317.000	32.200	0.000	0.150	200.150
0.765	1.051	4.767	54.333	13.900	6.100	319.000	32.200	0.000	0.153	200.153
0.780	0.972	4.407	50.233	14.000	6.190	319.000	32.200	0.000	0.156	200.156
0.795	0.873	3.957	45.142	14.200	6.300	321.000	32.100	0.000	0.159	200.159
0.805	0.822	3.729	42.543	14.200	6.380	322.000	32.100	0.000	0.161	200.161
0.815	0.778	3.527	40.260	14.000	6.450	321.000	32.100	0.000	0.163	200.163
0.825	0.731	3.316	37.835	13.400	6.530	323.000	32.100	0.000	0.165	200.165
0.835	0.693	3.142	35.859	14.400	6.610	323.000	32.100	0.000	0.167	200.167
0.845	0.647	2.932	33.486	13.700	6.670	323.000	32.100	0.000	0.169	200.169
0.860	0.564	2.555	29.204	13.400	6.750	325.000	32.000	0.000	0.172	200.172
0.875	0.482	2.184	24.955	13.200	6.840	327.000	32.000	0.000	0.175	200.175
0.890	0.402	1.823	20.823	12.500	6.930	327.000	32.100	0.000	0.178	200.178
0.905	0.319	1.448	16.532	11.500	7.010	328.000	32.000	0.000	0.181	200.181
0.920	0.245	1.112	12.710	9.100	7.100	329.000	32.000	0.000	0.184	200.184
0.940	0.116	0.527	6.025	2.400	7.220	332.000	32.000	0.000	0.188	200.188
0.960	0.032	0.144	1.645	-68.100	7.330	334.000	32.000	0.000	0.192	200.192
0.980	-0.102	-0.460	-5.266	-141.000	7.450	336.000	32.000	0.000	0.196	200.196
0.999	-0.185	-0.838	-9.588	-152.600	7.550	338.000	32.000	0.000	0.200	200.200
1.019	-0.266	-1.208	-13.825	-155.100	7.650	341.000	32.000	0.000	0.204	200.204
1.044	-0.377	-1.707	-19.541	-157.900	7.760	344.000	32.000	0.000	0.209	200.209
1.069	-0.485	-2.201	-25.195	-158.400	7.870	347.000	32.000	0.000	0.214	200.214
1.094	-0.578	-2.623	-30.032	-159.600	7.980	350.000	32.000	0.000	0.219	200.219
1.119	-0.662	-3.000	-34.370	-159.900	8.070	353.000	31.900	0.000	0.224	200.224
1.149	-0.757	-3.432	-39.313	-160.900	8.180	356.000	31.900	0.000	0.230	200.230
1.184	-0.856	-3.880	-44.466	-160.800	8.280	361.000	31.900	0.000	0.237	200.237
1.224	-0.960	-4.356	-49.933	-161.500	8.390	366.000	31.900	0.000	0.245	200.245
1.269	-1.071	-4.858	-55.680	-162.100	8.500	374.000	31.900	0.000	0.254	200.254
1.319	-1.183	-5.365	-61.500	-162.100	8.600	383.000	31.900	0.000	0.264	200.264
1.379	-1.305	-5.920	-67.890	-162.600	8.720	393.000	31.900	0.000	0.276	200.276
1.444	-1.402	-6.358	-72.965	-163.000	8.810	405.000	31.900	0.000	0.289	200.289
1.524	-1.530	-6.943	-79.624	-163.300	8.930	420.000	31.900	0.000	0.305	200.305
1.609	-1.648	-7.479	-85.829	-163.100	9.030	437.000	31.900	0.000	0.322	200.322
1.709	-1.761	-7.989	-91.677	-163.200	9.130	457.000	31.900	0.000	0.342	200.342
1.828	-1.880	-8.534	-98.024	-163.600	9.240	484.000	31.800	0.000	0.366	200.366
1.973	-2.038	-9.250	-106.280	-163.400	9.350	516.000	31.800	0.000	0.390	200.395
2.133	-2.145	-9.739	-111.828	-163.400	9.480	552.000	31.800	0.000	0.427	200.427
2.302	-2.264	-10.280	-118.116	-163.400	9.570	594.000	31.800	0.000	0.461	200.461
2.502	-2.377	-10.793	-124.033	-163.200	9.670	642.000	31.800	0.000	0.501	200.501
2.746	-2.496	-11.337	-130.301	-163.500	9.780	705.000	31.800	0.000	0.550	200.550
3.020	-2.632	-11.961	-137.496	-163.400	9.890	771.000	31.800	0.000	0.605	200.605
3.329	-2.781	-12.642	-145.404	-163.600	10.000	851.000	31.800	0.000	0.667	200.667

Table 20: Potentiometric Titration (POTN723.esa), 0.5 vol. % AKP-50 Al₂O₃, 1x10⁻² M KNO₃

Net (meq/l)	ESA (mPa*W/V)	Dyn Mob (m ² /V*s)	Zeta (mV)	Phase (deg)	pH (units)	Cond. (uS/cm)	Temp (deg C)	Acid (ml)	Base (ml)	Total (ml)
0.700	3.131	14.184	150.288	38.900	3.740	1093.000	35.200	0.019	0.000	200.019
0.725	3.210	14.546	154.428	37.700	3.890	1092.000	35.100	0.019	0.019	200.038
0.750	3.211	14.549	154.509	37.700	3.910	1093.000	35.100	0.019	0.024	200.043
0.775	3.153	14.286	151.321	37.300	3.920	1077.000	35.200	0.005	0.000	200.005
0.805	3.155	14.293	151.395	37.200	3.970	1074.000	35.200	0.000	0.000	200.000
0.834	3.187	14.444	153.484	37.400	4.040	1091.000	35.100	0.019	0.049	200.068
0.864	3.190	14.458	153.779	37.500	4.140	1092.000	35.000	0.019	0.067	200.086
0.894	3.247	14.719	156.409	37.200	4.240	1095.000	35.100	0.019	0.084	200.103
0.919	3.262	14.788	157.265	37.400	4.360	1097.000	35.000	0.019	0.100	200.119
0.939	3.267	14.811	157.509	37.900	4.510	1101.000	35.000	0.019	0.113	200.132
0.959	3.238	14.680	156.256	38.800	4.620	1103.000	35.000	0.019	0.121	200.140
0.979	3.218	14.589	155.242	39.000	4.740	1107.000	35.000	0.019	0.128	200.147
0.994	3.195	14.484	154.226	38.000	4.830	1108.000	35.000	0.019	0.133	200.152
1.009	3.171	14.376	153.214	38.000	4.910	1109.000	34.900	0.019	0.138	200.157
1.024	3.143	14.252	151.957	39.800	5.010	1111.000	34.900	0.019	0.144	200.163
1.039	3.161	14.330	152.819	39.300	5.100	1113.000	34.900	0.019	0.149	200.168
1.054	3.066	13.902	148.336	39.600	5.190	1115.000	34.900	0.019	0.154	200.173
1.064	3.078	13.958	148.872	40.200	5.280	1118.000	34.900	0.019	0.159	200.178
1.074	2.961	13.425	143.292	40.200	5.360	1118.000	34.900	0.019	0.164	200.183
1.084	2.925	13.264	141.682	39.300	5.450	1123.000	34.900	0.019	0.169	200.188
1.094	2.820	12.788	138.556	41.100	5.530	1124.000	34.900	0.019	0.174	200.193
1.109	2.755	12.492	133.495	41.800	5.620	1130.000	34.800	0.019	0.180	200.199
1.129	2.600	11.792	126.057	42.000	5.720	1127.000	34.800	0.019	0.186	200.205
1.149	2.422	10.985	117.416	42.000	5.810	1134.000	34.800	0.019	0.192	200.211
1.169	2.310	10.474	111.988	42.900	5.920	1135.000	34.800	0.019	0.198	200.217
1.189	2.136	9.687	103.597	42.300	6.020	1137.000	34.800	0.019	0.203	200.222
1.204	2.008	9.106	97.451	42.600	6.120	1139.000	34.800	0.019	0.207	200.226
1.224	1.843	8.357	89.429	43.300	6.220	1144.000	34.800	0.019	0.211	200.230
1.244	1.688	7.657	81.986	43.700	6.320	1143.000	34.800	0.019	0.215	200.234
1.264	1.609	7.296	78.104	43.600	6.420	1143.000	34.800	0.019	0.218	200.237
1.284	1.493	6.771	72.528	43.300	6.510	1145.000	34.700	0.019	0.221	200.240
1.309	1.380	6.259	67.081	43.800	6.600	1147.000	34.700	0.019	0.224	200.243
1.334	1.281	5.812	62.330	43.300	6.700	1148.000	34.700	0.019	0.227	200.246
1.364	1.168	5.296	56.825	44.000	6.800	1146.000	34.700	0.019	0.230	200.249
1.394	1.108	5.027	53.947	42.900	6.890	1148.000	34.700	0.019	0.232	200.251
1.429	1.046	4.743	50.911	43.100	6.970	1148.000	34.700	0.019	0.234	200.253
1.469	1.003	4.551	48.866	43.400	7.040	1149.000	34.600	0.019	0.236	200.255
1.514	0.947	4.296	46.130	43.200	7.110	1150.000	34.600	0.019	0.238	200.257
1.563	0.838	3.799	40.818	43.100	7.200	1151.000	34.600	0.019	0.241	200.260
1.623	0.680	3.085	33.154	40.800	7.310	1152.000	34.600	0.019	0.245	200.264
1.683	0.545	2.472	26.570	39.300	7.430	1153.000	34.600	0.019	0.249	200.268
1.768	0.423	1.920	20.653	35.800	7.550	1156.000	34.600	0.019	0.253	200.272
1.858	0.297	1.347	14.485	30.600	7.680	1159.000	34.600	0.019	0.257	200.276
1.968	0.238	1.078	11.595	26.800	7.760	1159.000	34.600	0.019	0.260	200.279
2.102	0.130	0.588	6.327	6.000	7.880	1163.000	34.600	0.019	0.264	200.283
2.257	0.092	0.417	4.490	-48.400	7.980	1165.000	34.500	0.019	0.268	200.287
2.441	-0.134	-0.606	-8.527	-90.400	8.090	1166.000	34.500	0.019	0.272	200.291
2.656	-0.218	-0.988	-10.637	-106.700	8.180	1167.000	34.500	0.019	0.276	200.295
	-0.326	-1.480	-15.935	-116.000	8.290	1176.000	34.500	0.019	0.281	200.300
	-0.425	-1.929	-20.797	-119.500	8.390	1174.000	34.500	0.019	0.286	200.305
	-0.554	-2.512	-27.080	-122.400	8.500	1181.000	34.500	0.019	0.292	200.311
	-0.665	-3.018	-32.542	-124.200	8.600	1182.000	34.500	0.019	0.298	200.317
	-0.778	-3.528	-38.058	-125.700	8.710	1192.000	34.500	0.019	0.305	200.324
	-0.902	-4.094	-44.199	-126.600	8.820	1196.000	34.400	0.019	0.313	200.332
	-1.018	-4.620	-49.889	-127.600	8.930	1203.000	34.400	0.019	0.322	200.341
	-1.137	-5.161	-55.748	-128.500	9.040	1214.000	34.400	0.019	0.332	200.351
	-1.262	-5.727	-61.848	-130.600	9.150	1225.000	34.400	0.019	0.344	200.363
	-1.384	-6.192	-66.924	-130.400	9.240	1236.000	34.400	0.019	0.356	200.375
	-1.502	-6.820	-73.754	-131.000	9.360	1256.000	34.400	0.019	0.373	200.392
	-1.623	-7.366	-79.777	-132.000	9.460	1273.000	34.300	0.019	0.391	200.410
	-1.747	-7.933	-85.803	-132.100	9.560	1299.000	34.300	0.019	0.413	200.432
	-1.902	-8.636	-93.407	-132.600	9.670	1329.000	34.300	0.019	0.440	200.459
	-2.033	-9.233	-99.928	-133.400	9.770	1366.000	34.300	0.019	0.471	200.490
	-2.187	-9.935	-107.556	-133.100	9.880	1415.000	34.300	0.019	0.508	200.527
	-2.308	-10.486	-113.537	-133.900	9.980	1467.000	34.300	0.019	0.551	200.570

**Table 21: Potentiometric Titration (POTN710.esa), 0.5 vol. % Alcoa SG A-1000
Al₂O₃, 1x10⁻⁴ M KNO₃**

Net (meq/l)	ESA (mPa·M/V)	Dyn Mob (m ² /V·s)	Zeta (mV)	Phase (deg)	pH (units)	Cond. (uS/cm)	Temp (deg C)	Acid (ml)	Base (ml)	Total (ml)
-0.030	1.855	8.605	107.615	-10.300	3.840	217.000	29.700	0.006	0.000	200.006
0.000	1.859	8.624	107.998	-9.900	3.890	217.000	29.700	0.006	0.006	200.012
0.025	1.873	8.693	108.857	-9.800	3.920	218.000	29.700	0.006	0.011	200.017
0.000	1.857	8.614	107.723	-10.400	3.930	211.000	29.700	0.000	0.000	200.000
0.120	1.888	8.762	109.777	-9.300	4.040	219.000	29.600	0.006	0.030	200.036
0.190	1.905	8.842	110.785	-8.300	4.170	222.000	29.600	0.006	0.044	200.050
0.240	1.900	8.818	110.457	-7.300	4.300	224.000	29.600	0.006	0.054	200.060
0.280	1.888	8.763	109.798	-7.000	4.400	226.000	29.600	0.006	0.062	200.068
0.315	1.879	8.722	109.310	-6.500	4.490	228.000	29.600	0.006	0.069	200.075
0.355	1.851	8.590	107.701	-5.700	4.580	231.000	29.600	0.006	0.077	200.083
0.395	1.818	8.439	105.822	-5.200	4.660	234.000	29.600	0.006	0.085	200.091
0.440	1.786	8.198	102.812	-5.300	4.760	237.000	29.600	0.006	0.094	200.100
0.485	1.719	7.982	100.096	-4.200	4.830	240.000	29.600	0.006	0.103	200.109
0.545	1.620	7.521	94.328	-5.100	4.920	246.000	29.600	0.006	0.115	200.121
0.610	1.534	7.120	89.331	-5.600	5.010	251.000	29.600	0.006	0.128	200.134
0.685	1.388	6.447	80.888	-5.400	5.100	257.000	29.600	0.006	0.143	200.149
0.760	1.225	5.686	71.378	-5.800	5.200	263.000	29.500	0.006	0.158	200.164
0.835	1.050	4.878	61.201	-6.200	5.300	269.000	29.600	0.006	0.173	200.179
0.905	0.889	4.035	50.641	-6.900	5.420	275.000	29.600	0.006	0.187	200.193
0.964	0.716	3.325	41.745	-9.100	5.540	280.000	29.500	0.006	0.199	200.205
1.009	0.620	2.881	36.179	-10.900	5.670	283.000	29.500	0.006	0.208	200.214
1.039	0.576	2.678	33.639	-10.900	5.780	286.000	29.500	0.006	0.214	200.220
1.064	0.539	2.506	31.481	-11.900	5.870	288.000	29.500	0.006	0.219	200.225
1.089	0.488	2.267	28.482	-12.400	5.980	289.000	29.500	0.006	0.224	200.230
1.114	0.427	1.988	24.951	-12.400	6.060	291.000	29.500	0.006	0.229	200.235
1.139	0.368	1.709	21.475	-14.000	6.150	293.000	29.500	0.006	0.234	200.240
1.164	0.309	1.434	18.017	-16.100	6.250	295.000	29.500	0.006	0.239	200.245
1.189	0.250	1.160	14.578	-18.800	6.340	296.000	29.500	0.006	0.244	200.250
1.214	0.205	0.951	11.954	-24.100	6.440	297.000	29.500	0.006	0.249	200.255
1.239	0.159	0.739	9.292	-33.800	6.530	299.000	29.500	0.006	0.254	200.260
1.264	0.122	0.567	7.132	-45.600	6.630	301.000	29.500	0.006	0.259	200.265
1.289	0.098	0.456	5.735	-63.800	6.730	302.000	29.500	0.006	0.264	200.270
1.314	0.096	0.445	5.599	-89.500	6.820	305.000	29.400	0.006	0.269	200.275
1.339	-0.103	-0.478	-6.016	-113.600	6.930	306.000	29.400	0.006	0.274	200.280
1.359	-0.116	-0.537	-6.753	-125.000	7.010	308.000	29.400	0.006	0.278	200.284
1.379	-0.137	-0.636	-8.009	-130.900	7.100	309.000	29.400	0.006	0.282	200.288
1.404	-0.158	-0.733	-9.226	-140.500	7.180	310.000	29.400	0.006	0.287	200.293
1.439	-0.206	-0.957	-12.041	-148.100	7.290	313.000	29.400	0.006	0.294	200.300
1.474	-0.246	-1.144	-14.399	-155.000	7.410	316.000	29.400	0.006	0.301	200.307
1.509	-0.282	-1.312	-16.524	-156.200	7.530	319.000	29.400	0.006	0.308	200.314
1.544	-0.321	-1.494	-18.813	-158.600	7.640	321.000	29.400	0.006	0.315	200.321
1.579	-0.351	-1.631	-20.543	-160.600	7.750	325.000	29.400	0.006	0.322	200.328
1.614	-0.386	-1.793	-22.589	-161.900	7.860	328.000	29.400	0.006	0.329	200.335
1.653	-0.422	-1.961	-24.700	-162.900	7.970	332.000	29.400	0.006	0.337	200.343
1.693	-0.455	-2.116	-26.663	-163.800	8.080	337.000	29.400	0.006	0.345	200.351
1.738	-0.500	-2.326	-29.307	-163.500	8.180	341.000	29.400	0.006	0.354	200.360
1.788	-0.543	-2.524	-31.813	-164.700	8.300	347.000	29.300	0.006	0.364	200.370
1.838	-0.573	-2.664	-33.587	-165.800	8.400	354.000	29.300	0.006	0.374	200.380
1.903	-0.625	-2.905	-36.621	-166.500	8.510	362.000	29.300	0.006	0.387	200.393
1.973	-0.676	-3.142	-39.619	-166.800	8.620	372.000	29.300	0.006	0.401	200.407
2.048	-0.731	-3.399	-42.872	-167.900	8.730	385.000	29.300	0.006	0.416	200.422
2.128	-0.783	-3.640	-45.935	-167.400	8.840	398.000	29.300	0.006	0.432	200.438
2.222	-0.835	-3.883	-48.985	-169.000	8.950	415.000	29.300	0.006	0.451	200.457
2.327	-0.897	-4.171	-52.632	-169.400	9.060	433.000	29.300	0.006	0.472	200.478
2.442	-0.968	-4.491	-56.685	-169.500	9.170	454.000	29.300	0.006	0.495	200.501
2.576	-1.031	-4.796	-60.543	-169.700	9.280	482.000	29.300	0.006	0.522	200.528
2.726	-1.089	-5.066	-63.941	-170.000	9.380	513.000	29.300	0.006	0.552	200.558
2.905	-1.176	-5.473	-69.092	-170.100	9.490	552.000	29.300	0.006	0.588	200.594
3.105	-1.250	-5.820	-73.463	-170.000	9.600	596.000	29.300	0.006	0.628	200.634
3.329	-1.346	-6.267	-79.155	-170.900	9.720	650.000	29.300	0.006	0.673	200.679
3.583	-1.428	-6.648	-83.963	-169.900	9.830	710.000	29.300	0.006	0.724	200.730
3.872	-1.481	-6.897	-87.131	-170.100	9.930	780.000	29.300	0.006	0.782	200.788

**Table 22: Potentiometric Titration (POTN713.esa), 0.5 vol. % Alcoa SG A-1000
Al₂O₃, 1x10⁻³ M KNO₃**

Net (meq/l)	ESA (mPa·M/V)	Dyn Mob (m ² /V·s)	Zeta (mV)	Phase (deg)	pH (units)	Cond. (uS/cm)	Temp (deg C)	Acid (ml)	Base (ml)	Total (ml)
2.062	2.348	10.951	137.054	17.700	3.790	880.000	29.700	0.416	0.828	201.244
2.097	2.319	10.828	135.552	17.800	3.900	872.000	29.700	0.409	0.828	201.237
2.126	2.305	10.781	134.739	17.600	4.000	865.000	29.700	0.403	0.828	201.231
2.151	2.295	10.716	134.058	17.200	4.100	859.000	29.700	0.398	0.828	201.226
2.176	2.300	10.736	134.244	17.500	4.210	856.000	29.700	0.393	0.828	201.221
2.196	2.282	10.651	133.290	17.900	4.310	852.000	29.700	0.389	0.828	201.217
2.216	2.278	10.633	133.028	17.400	4.410	848.000	29.700	0.385	0.828	201.213
2.236	2.266	10.580	132.319	17.600	4.520	845.000	29.700	0.381	0.828	201.209
2.251	2.253	10.515	131.543	17.800	4.610	841.000	29.700	0.378	0.828	201.206
2.261	2.238	10.449	130.681	17.800	4.690	842.000	29.700	0.376	0.828	201.204
2.266	2.243	10.471	130.905	17.700	4.740	841.000	29.700	0.375	0.828	201.203
2.271	2.234	10.427	130.359	17.700	4.810	840.000	29.700	0.374	0.828	201.202
2.275	2.233	10.423	130.304	17.700	4.890	839.000	29.700	0.373	0.828	201.201
2.280	2.227	10.394	129.967	17.800	4.970	837.000	29.700	0.372	0.828	201.200
2.285	2.221	10.368	129.564	18.100	5.080	837.000	29.700	0.371	0.828	201.199
2.290	2.220	10.360	129.435	17.400	5.220	838.000	29.800	0.370	0.828	201.198
2.295	2.200	10.271	128.373	17.800	5.390	835.000	29.700	0.369	0.828	201.197
2.300	2.188	10.211	127.621	17.800	5.590	833.000	29.700	0.368	0.828	201.196
2.305	2.173	10.142	126.716	17.900	5.830	834.000	29.800	0.367	0.828	201.195
2.315	2.152	10.043	125.470	18.200	6.090	834.000	29.800	0.365	0.828	201.193
2.340	2.106	9.827	122.713	17.900	6.360	835.000	29.800	0.360	0.828	201.188
2.385	1.991	9.292	116.057	18.300	6.580	827.000	29.800	0.351	0.828	201.179
2.449	1.790	8.354	104.334	19.000	6.750	824.000	29.800	0.338	0.828	201.166
2.514	1.621	7.566	94.491	18.100	6.870	821.000	29.800	0.325	0.828	201.153
2.559	1.472	6.870	85.753	18.300	6.950	818.000	29.800	0.316	0.828	201.144
2.599	1.314	6.131	76.520	17.700	7.030	815.000	29.800	0.308	0.828	201.136
2.628	1.170	5.459	68.125	18.200	7.110	813.000	29.800	0.302	0.828	201.130
2.653	1.034	4.826	60.220	17.500	7.180	814.000	29.800	0.297	0.828	201.125
2.678	0.877	4.090	51.031	16.800	7.270	808.000	29.800	0.292	0.828	201.120
2.703	0.719	3.354	41.850	15.800	7.350	810.000	29.800	0.287	0.828	201.115
2.728	0.568	2.652	33.078	14.000	7.440	805.000	29.800	0.282	0.828	201.110
2.758	0.415	1.935	24.140	11.000	7.540	802.000	29.800	0.276	0.828	201.104
2.788	0.290	1.353	16.875	6.100	7.630	801.000	29.800	0.270	0.828	201.098
2.817	0.188	0.876	10.922	-3.100	7.730	796.000	29.800	0.264	0.828	201.092
2.847	0.109	0.507	6.321	-30.600	7.810	793.000	29.900	0.258	0.828	201.086
2.872	0.092	0.428	5.341	-66.700	7.890	795.000	29.900	0.253	0.828	201.081
2.897	-0.115	-0.537	-6.692	-106.400	7.980	792.000	29.900	0.248	0.828	201.076
2.922	-0.161	-0.752	-9.372	-123.900	8.080	791.000	29.900	0.243	0.828	201.071
2.947	-0.224	-1.044	-13.004	-134.400	8.150	786.000	29.900	0.238	0.828	201.066
2.972	-0.280	-1.305	-16.258	-138.000	8.240	785.000	29.900	0.233	0.828	201.061
2.996	-0.333	-1.552	-19.338	-142.200	8.340	784.000	29.900	0.228	0.828	201.056
3.021	-0.394	-1.837	-22.891	-143.700	8.430	785.000	29.900	0.223	0.828	201.051
3.046	-0.447	-2.087	-26.001	-145.500	8.520	781.000	29.900	0.218	0.828	201.046
3.071	-0.491	-2.289	-28.509	-147.300	8.600	784.000	29.900	0.213	0.828	201.041
3.101	-0.551	-2.569	-31.989	-147.700	8.710	783.000	29.900	0.207	0.828	201.035
3.136	-0.612	-2.855	-35.545	-148.900	8.810	782.000	29.900	0.200	0.828	201.028
3.175	-0.681	-3.177	-39.539	-150.200	8.920	786.000	29.900	0.192	0.828	201.020
3.220	-0.761	-3.549	-44.224	-151.000	9.030	789.000	29.900	0.183	0.828	201.011
3.265	-0.826	-3.851	-47.922	-152.000	9.130	791.000	29.900	0.174	0.828	201.002
3.320	-0.914	-4.263	-53.072	-153.700	9.240	797.000	29.900	0.163	0.828	200.991
3.384	-1.020	-4.756	-59.174	-153.400	9.350	804.000	29.900	0.150	0.828	200.978
3.459	-1.096	-5.109	-63.558	-154.600	9.460	816.000	29.900	0.135	0.828	200.963
3.554	-1.207	-5.627	-70.022	-155.000	9.590	830.000	29.900	0.116	0.828	200.944
3.668	-1.333	-6.212	-77.270	-156.000	9.710	847.000	30.000	0.093	0.828	200.921
3.817	-1.443	-6.726	-83.645	-155.400	9.840	874.000	30.000	0.063	0.828	200.891
3.987	-1.524	-7.102	-88.325	-155.700	9.950	908.000	30.000	0.029	0.828	200.857
4.086	-1.575	-7.338	-91.261	-156.000	10.000	931.000	30.000	0.009	0.828	200.837
4.106	-1.575	-7.337	-91.246	-155.700	10.010	936.000	30.000	0.005	0.828	200.833

**Table 23: Potentiometric Titration (POTN725.esa), 0.5 vol. % Alcoa SG A-1000
Al₂O₃, 1x10⁻² M KNO₃**

Net (meq/l)	ESA (mPa·M/V)	Dyn Mob (m ² /V·s)	Zeta (mV)	Phase (deg)	pH (units)	Cond. (uS/cm)	Temp (deg C)	Acid (ml)	Base (ml)	Total (ml)
-0.145	4.925	22.854	258.584	0.200	3.850	2089.000	34.200	0.029	0.000	200.029
-0.090	4.982	23.119	261.164	0.500	3.980	2049.000	34.300	0.018	0.000	200.018
0.000	4.941	22.932	259.436	1.400	4.060	2065.000	34.200	0.029	0.029	200.057
0.015	4.959	23.017	260.554	1.300	4.070	2061.000	34.200	0.029	0.032	200.060
0.090	5.028	23.337	264.175	1.400	4.140	2061.000	34.200	0.029	0.047	200.075
-0.015	5.033	23.354	263.697	0.900	4.140	2035.000	34.300	0.003	0.000	200.003
0.000	5.042	23.394	264.033	1.000	4.160	2043.000	34.300	0.000	0.000	200.000
0.200	5.027	23.333	264.251	2.100	4.220	2064.000	34.200	0.029	0.069	200.097
0.325	5.043	23.411	265.256	3.200	4.330	2068.000	34.200	0.029	0.094	200.122
0.440	5.120	23.772	269.468	3.500	4.450	2067.000	34.100	0.029	0.117	200.145
0.535	5.144	23.886	270.713	4.300	4.590	2072.000	34.100	0.029	0.136	200.164
0.600	5.231	24.293	275.330	5.500	4.740	2072.000	34.100	0.029	0.149	200.177
0.640	5.242	24.343	275.933	6.900	4.850	2080.000	34.100	0.029	0.157	200.185
0.675	5.278	24.514	278.082	7.800	4.960	2084.000	34.100	0.029	0.164	200.192
0.705	5.288	24.560	278.645	8.300	5.060	2084.000	34.100	0.029	0.170	200.198
0.729	5.287	24.556	278.597	8.800	5.130	2084.000	34.100	0.029	0.175	200.203
0.759	5.340	24.803	281.441	9.900	5.220	2086.000	34.100	0.029	0.181	200.209
0.789	5.290	24.573	278.956	10.900	5.310	2085.000	34.100	0.029	0.187	200.215
0.824	5.294	24.592	279.421	11.800	5.400	2089.000	34.000	0.029	0.194	200.222
0.859	5.276	24.506	278.242	12.900	5.490	2101.000	34.100	0.029	0.201	200.229
0.894	5.229	24.290	275.906	13.700	5.580	2103.000	34.100	0.029	0.208	200.236
0.929	5.144	23.898	271.575	14.900	5.670	2104.000	34.000	0.029	0.215	200.243
0.964	5.076	23.582	268.108	15.700	5.760	2099.000	34.000	0.029	0.222	200.250
0.999	4.966	23.071	262.337	16.300	5.850	2104.000	34.000	0.029	0.229	200.257
1.039	4.839	22.479	255.724	18.700	5.950	2112.000	34.000	0.029	0.237	200.265
1.074	4.673	21.712	246.919	19.500	6.040	2115.000	34.000	0.029	0.244	200.272
1.109	4.491	20.867	237.597	20.500	6.150	2114.000	34.000	0.029	0.251	200.279
1.139	4.263	19.806	225.477	20.800	6.260	2118.000	34.000	0.029	0.257	200.285
1.164	4.082	18.968	215.971	21.900	6.350	2122.000	34.000	0.029	0.262	200.290
1.189	3.886	18.056	205.647	21.800	6.450	2118.000	33.900	0.029	0.267	200.295
1.214	3.626	16.849	192.044	22.600	6.560	2125.000	33.900	0.029	0.272	200.300
1.234	3.404	15.820	180.289	22.000	6.650	2127.000	33.900	0.029	0.276	200.304
1.254	3.188	14.813	168.817	22.700	6.730	2129.000	33.900	0.029	0.280	200.308
1.274	2.977	13.836	157.743	22.800	6.820	2128.000	33.900	0.029	0.284	200.312
1.294	2.886	13.411	152.922	23.600	6.920	2131.000	33.900	0.029	0.288	200.316
1.314	2.688	12.493	142.496	23.300	7.010	2128.000	33.900	0.029	0.292	200.320
1.334	2.480	11.523	131.476	24.300	7.090	2127.000	33.900	0.029	0.296	200.324
1.359	2.214	10.291	117.419	25.000	7.200	2130.000	33.900	0.029	0.301	200.329
1.389	1.954	9.080	103.631	26.200	7.310	2135.000	33.900	0.029	0.307	200.335
1.419	1.738	8.080	92.216	26.600	7.420	2131.000	33.900	0.029	0.313	200.341
1.448	1.490	6.924	79.074	27.500	7.540	2136.000	33.800	0.029	0.319	200.347
1.478	1.217	5.657	64.632	27.700	7.650	2141.000	33.800	0.029	0.325	200.353
1.508	0.992	4.610	52.659	28.900	7.760	2146.000	33.800	0.029	0.331	200.359
1.543	0.731	3.398	38.824	30.800	7.880	2147.000	33.800	0.029	0.338	200.366
1.578	0.465	2.162	24.715	32.200	8.000	2151.000	33.800	0.029	0.345	200.373
1.613	0.212	0.987	11.290	32.200	8.100	2151.000	33.800	0.029	0.352	200.380
1.653	-0.059	-0.273	-3.121	179.900	8.230	2157.000	33.700	0.029	0.360	200.388
1.693	-0.306	-1.424	-16.287	-155.000	8.340	2161.000	33.800	0.029	0.368	200.396
1.733	-0.527	-2.448	-28.041	-151.800	8.440	2167.000	33.700	0.029	0.376	200.404
1.778	-0.749	-3.484	-39.872	-151.300	8.560	2168.000	33.700	0.029	0.385	200.413
1.828	-0.960	-4.465	-51.102	-150.600	8.670	2170.000	33.700	0.029	0.395	200.423
1.878	-1.142	-5.310	-60.780	-150.000	8.780	2175.000	33.700	0.029	0.405	200.433
1.938	-1.348	-6.269	-71.785	-150.700	8.890	2183.000	33.700	0.029	0.417	200.445
1.997	-1.510	-7.023	-80.459	-150.300	9.000	2190.000	33.700	0.029	0.429	200.457
2.062	-1.668	-7.759	-88.875	-150.600	9.110	2205.000	33.700	0.029	0.442	200.470
2.137	-1.847	-8.588	-98.439	-150.500	9.220	2212.000	33.700	0.029	0.457	200.485
2.222	-2.040	-9.489	-108.794	-150.300	9.330	2225.000	33.700	0.029	0.474	200.502
2.317	-2.200	-10.234	-117.345	-150.500	9.440	2243.000	33.700	0.029	0.493	200.521
2.421	-2.396	-11.148	-127.783	-150.100	9.540	2266.000	33.700	0.029	0.514	200.542
2.546	-2.569	-11.953	-137.107	-150.200	9.650	2289.000	33.700	0.029	0.539	200.567
2.686	-2.751	-12.802	-146.911	-150.800	9.750	2314.000	33.600	0.029	0.567	200.595
2.855	-2.922	-13.598	-156.252	-150.700	9.860	2357.000	33.600	0.029	0.601	200.629
3.044	-3.101	-14.437	-165.723	-151.400	9.970	2397.000	33.600	0.029	0.639	200.667

Table 24: Potentiometric Titration (POTN702.esa), 0.5 vol. % SHS Composite {TiB₂/Al₂O₃}, 1x10⁻³ M KNO₃

Net (meq/l)	ESA (mPa·M/V)	Dyn Mob (m ² /V·s)	Zeta (mV)	Phase (deg)	pH (units)	Cond. (uS/cm)	Temp (deg C)	Acid (ml)	Base (ml)	Total (ml)
-1.978	0.380	1.838	37.438	141.200	4.270	814.000	45.300	0.396	0.000	200.396
-1.968	0.354	1.525	34.942	142.600	4.630	816.000	45.300	0.396	0.002	200.398
-1.963	0.328	1.412	32.406	142.400	4.860	822.000	45.200	0.396	0.003	200.399
-1.958	0.311	1.340	30.881	142.500	5.030	829.000	45.100	0.396	0.004	200.400
-1.953	0.296	1.273	29.330	142.600	5.180	832.000	45.100	0.396	0.005	200.401
-1.948	0.278	1.196	27.656	143.700	5.280	835.000	45.000	0.396	0.006	200.402
-1.943	0.263	1.131	26.144	142.000	5.380	837.000	45.000	0.396	0.007	200.403
-1.938	0.253	1.090	25.192	142.500	5.480	844.000	45.000	0.396	0.008	200.404
-1.933	0.243	1.046	24.202	142.400	5.570	844.000	45.000	0.396	0.009	200.405
-1.928	0.233	1.005	23.341	142.100	5.650	850.000	44.900	0.396	0.010	200.406
-1.923	0.228	0.984	22.662	142.100	5.730	850.000	44.900	0.396	0.011	200.407
-1.918	0.221	0.952	22.168	142.400	5.810	856.000	44.800	0.396	0.012	200.408
-1.913	0.210	0.905	21.077	141.300	5.870	860.000	44.800	0.396	0.013	200.409
-1.908	0.204	0.877	20.491	141.500	5.930	859.000	44.700	0.396	0.014	200.410
-1.903	0.196	0.844	19.740	141.300	5.990	862.000	44.700	0.396	0.015	200.411
-1.898	0.194	0.834	19.548	140.900	6.040	862.000	44.600	0.396	0.016	200.412
-1.888	0.186	0.801	18.781	141.300	6.100	865.000	44.600	0.396	0.018	200.414
-1.873	0.178	0.768	18.019	140.900	6.150	864.000	44.600	0.396	0.021	200.417
-1.848	0.169	0.730	17.151	139.600	6.210	869.000	44.500	0.396	0.026	200.422
-1.813	0.164	0.708	16.871	139.100	6.290	874.000	44.500	0.396	0.033	200.429
-1.768	0.153	0.659	15.516	138.300	6.370	878.000	44.500	0.396	0.042	200.438
-1.714	0.148	0.637	15.034	136.500	6.480	880.000	44.400	0.396	0.053	200.449
-1.654	0.142	0.612	14.458	136.100	6.540	885.000	44.300	0.396	0.065	200.461
-1.579	0.133	0.573	13.579	135.800	6.620	893.000	44.300	0.396	0.080	200.476
-1.489	0.127	0.547	12.978	133.500	6.700	902.000	44.200	0.396	0.098	200.494
-1.384	0.128	0.550	13.059	133.500	6.790	908.000	44.200	0.396	0.119	200.515
-1.270	0.121	0.522	12.403	132.800	6.870	920.000	44.200	0.396	0.142	200.538
-1.135	0.123	0.530	12.619	131.500	6.960	933.000	44.100	0.396	0.169	200.565
-0.970	0.120	0.519	12.382	130.400	7.050	946.000	44.100	0.396	0.202	200.598
-0.791	0.123	0.529	12.652	129.900	7.140	963.000	44.000	0.396	0.238	200.634
-0.547	0.127	0.546	13.050	131.200	7.240	990.000	44.000	0.396	0.287	200.683
-0.253	0.129	0.556	13.340	128.600	7.340	1021.000	43.900	0.396	0.348	200.742
0.106	0.137	0.590	14.137	129.400	7.460	1057.000	44.000	0.396	0.418	200.814
0.489	0.148	0.638	15.297	129.100	7.570	1100.000	43.900	0.396	0.495	200.891
0.947	0.156	0.675	16.188	127.800	7.680	1144.000	43.900	0.396	0.587	200.983
1.454	0.167	0.721	17.342	127.600	7.790	1196.000	43.800	0.396	0.689	201.085
2.025	0.181	0.781	18.778	128.400	7.910	1261.000	43.800	0.396	0.804	201.200
2.626	0.192	0.831	19.979	126.000	8.020	1320.000	43.800	0.396	0.925	201.321
3.297	0.198	0.856	20.660	127.000	8.140	1385.000	43.700	0.396	1.060	201.456
4.011	0.209	0.904	21.879	127.000	8.270	1454.000	43.600	0.396	1.204	201.600
4.695	0.222	0.961	23.301	126.500	8.390	1528.000	43.600	0.396	1.342	201.738
5.388	0.228	0.990	23.990	124.800	8.520	1598.000	43.600	0.396	1.482	201.878
6.076	0.235	1.022	24.791	124.200	8.650	1658.000	43.500	0.396	1.621	202.017
6.769	0.244	1.062	25.800	122.500	8.780	1732.000	43.500	0.396	1.761	202.157
7.436	0.250	1.085	26.434	120.700	8.920	1801.000	43.400	0.396	1.896	202.292
8.024	0.242	1.054	25.681	118.500	9.030	1861.000	43.400	0.396	2.015	202.411
8.691	0.242	1.053	25.649	115.500	9.200	1968.000	43.400	0.396	2.150	202.546
9.174	0.243	1.060	25.858	112.700	9.320	2041.000	43.400	0.396	2.248	202.644
9.682	0.239	1.042	25.447	110.700	9.450	2133.000	43.300	0.396	2.351	202.747
10.180	0.234	1.021	24.946	107.400	9.570	2240.000	43.300	0.396	2.452	202.848
10.712	0.235	1.027	25.129	105.900	9.680	2351.000	43.300	0.396	2.560	202.956
11.289	0.243	1.060	25.974	102.700	9.790	2486.000	43.200	0.396	2.677	203.073
11.928	0.249	1.086	26.679	102.200	9.910	2658.000	43.200	0.396	2.807	203.203

Table 25: Potentiometric Titration (POTN705.esa), 0.5 vol. % SHS Composite {TiB₂/Al₂O₃}, 1x10⁻³ M KNO₃

Net (meq/l)	ESA (mPa*MV)	Dyn Mob (m ² /V*s)	Zeta (mV)	Phase (deg)	pH (units)	Cond. (uS/cm)	Temp (deg C)	Acid (ml)	Base (ml)	Total (ml)
-2.168	0.422	1.816	37.900	145.900	3.920	919.000	47.900	0.434	0.000	200.434
-2.148	0.418	1.799	37.706	146.300	4.100	917.000	47.800	0.434	0.004	200.438
-2.138	0.416	1.793	37.542	147.100	4.320	915.000	47.900	0.434	0.006	200.440
-2.133	0.406	1.751	36.761	147.900	4.580	919.000	47.800	0.434	0.007	200.441
-2.128	0.392	1.690	35.537	147.900	4.810	922.000	47.700	0.434	0.008	200.442
-2.123	0.381	1.643	34.605	148.400	5.000	926.000	47.700	0.434	0.009	200.443
-2.118	0.356	1.534	32.353	149.500	5.150	928.000	47.600	0.434	0.010	200.444
-2.113	0.345	1.484	31.316	149.400	5.280	933.000	47.600	0.434	0.011	200.445
-2.108	0.328	1.413	29.889	150.100	5.390	941.000	47.600	0.434	0.012	200.446
-2.103	0.319	1.375	29.079	150.100	5.480	942.000	47.600	0.434	0.013	200.447
-2.098	0.308	1.329	28.132	149.900	5.570	945.000	47.600	0.434	0.014	200.448
-2.093	0.299	1.288	27.413	150.900	5.650	946.000	47.400	0.434	0.015	200.449
-2.088	0.287	1.238	26.385	150.700	5.720	947.000	47.400	0.434	0.016	200.450
-2.083	0.277	1.195	25.465	150.900	5.790	951.000	47.400	0.434	0.017	200.451
-2.078	0.271	1.166	24.905	150.900	5.850	954.000	47.300	0.434	0.018	200.452
-2.073	0.261	1.126	24.065	149.900	5.910	958.000	47.300	0.434	0.019	200.453
-2.068	0.256	1.104	23.606	150.500	5.970	955.000	47.300	0.434	0.020	200.454
-2.063	0.245	1.057	22.650	150.400	6.020	958.000	47.200	0.434	0.021	200.455
-2.058	0.244	1.053	22.642	151.600	6.070	963.000	47.100	0.434	0.022	200.456
-2.048	0.235	1.013	21.832	151.000	6.120	960.000	47.100	0.434	0.024	200.458
-2.028	0.228	0.982	21.291	151.100	6.180	962.000	46.900	0.434	0.028	200.462
-1.998	0.219	0.945	20.422	150.800	6.240	967.000	47.000	0.434	0.034	200.468
-1.958	0.210	0.904	19.575	149.100	6.320	969.000	46.900	0.434	0.042	200.476
-1.908	0.194	0.834	18.094	149.500	6.410	972.000	46.900	0.434	0.052	200.486
-1.853	0.189	0.813	17.651	149.600	6.490	979.000	46.900	0.434	0.063	200.497
-1.788	0.177	0.763	16.603	148.600	6.580	984.000	46.800	0.434	0.076	200.510
-1.714	0.174	0.749	16.305	146.500	6.660	982.000	46.800	0.434	0.091	200.525
-1.629	0.167	0.719	15.698	147.200	6.750	996.000	46.700	0.434	0.108	200.542
-1.529	0.163	0.703	15.408	145.600	6.830	1016.000	46.600	0.434	0.128	200.562
-1.414	0.159	0.685	14.989	143.300	6.910	1021.000	46.600	0.434	0.151	200.585
-1.275	0.156	0.671	14.728	144.500	7.000	1036.000	46.500	0.434	0.179	200.613
-1.120	0.153	0.660	14.500	144.500	7.080	1048.000	46.500	0.434	0.210	200.644
-0.886	0.155	0.670	14.762	143.500	7.190	1069.000	46.400	0.434	0.257	200.691
-0.627	0.163	0.701	15.465	142.700	7.300	1094.000	46.400	0.434	0.309	200.743
-0.328	0.164	0.706	15.619	142.500	7.410	1124.000	46.300	0.434	0.369	200.803
0.015	0.171	0.740	16.368	142.100	7.510	1157.000	46.300	0.434	0.438	200.872
0.428	0.183	0.792	17.542	141.300	7.630	1202.000	46.300	0.434	0.521	200.955
0.891	0.193	0.833	18.486	140.800	7.740	1250.000	46.200	0.434	0.614	201.048
1.418	0.206	0.888	19.729	140.800	7.850	1305.000	46.200	0.434	0.720	201.154
1.999	0.221	0.957	21.298	140.400	7.970	1362.000	46.200	0.434	0.837	201.271
2.625	0.225	0.975	21.756	140.900	8.080	1425.000	46.100	0.434	0.963	201.397
3.344	0.235	1.020	22.781	141.200	8.200	1496.000	46.000	0.434	1.108	201.542
4.073	0.247	1.071	23.991	139.700	8.320	1585.000	46.000	0.434	1.255	201.689
4.816	0.256	1.112	24.929	139.500	8.440	1637.000	45.900	0.434	1.405	201.839
5.593	0.262	1.138	25.545	138.900	8.570	1712.000	45.900	0.434	1.562	201.996
6.350	0.269	1.170	26.267	137.800	8.690	1783.000	45.900	0.434	1.715	202.149
7.116	0.276	1.202	27.091	136.500	8.840	1855.000	45.800	0.434	1.870	202.304
7.793	0.266	1.155	26.034	134.200	8.950	1928.000	45.800	0.434	2.007	202.441
8.553	0.270	1.177	26.523	131.600	9.120	2037.000	45.800	0.434	2.161	202.595
9.096	0.264	1.149	25.941	130.100	9.250	2106.000	45.700	0.434	2.271	202.705
9.633	0.257	1.119	25.316	126.200	9.380	2201.000	45.700	0.434	2.380	202.814
10.141	0.250	1.091	24.714	124.000	9.500	2286.000	45.600	0.434	2.483	202.917
10.693	0.251	1.097	24.887	121.400	9.620	2407.000	45.600	0.434	2.595	203.029
11.249	0.250	1.092	24.844	118.800	9.740	2520.000	45.500	0.434	2.708	203.142
11.839	0.252	1.100	25.010	117.400	9.850	2687.000	45.500	0.434	2.828	203.262
12.528	0.257	1.125	25.727	115.200	9.950	2844.000	45.400	0.434	2.968	203.402

APPENDIX C

Green Body Density Measurements

Table 26: Green Body Density Data and Calculations for SHS TiB ₂ / AKP 50 Al ₂ O ₃ Ceramic Composites									
Composite System	Processing pH	Plaster Mold #	CIP Pressure (MPa)	Bag Leakage during CIP	Length (mm)	Width (mm)	Height (mm)	Weight (g)	Density (g/cc)
AKP50 Comp	PEG	N/ A	160	NO				3.000-3.049	
AKP50 Comp	4	23b	300	UNK	16.10	8.71	6.42	1.548	1.72
AKP50 Comp	4	8b	300	UNK	9.75	6.12	8.80	0.909	1.73
AKP50 Comp	4	23a	300	UNK	19.90	9.85	6.29	2.236	1.81
AKP50 Comp	4	3	300	UNK	10.19	5.56	6.61	0.710	1.90
AKP50 Comp	4	9	300	UNK	11.17	6.01	7.18	1.016	2.11
AKP50 Comp	4	18c	300	UNK	20.10	8.95	5.91	2.270	2.14
AKP50 Comp	4	18b	300	UNK	19.25	5.72	8.19	2.003	2.22
AKP50 Comp	4	24	300	UNK	56.48	9.74	5.91	7.553	2.32
AKP50 Comp	4	13	300	UNK	55.70	7.54	5.86	6.016	2.44
AKP50 Comp	4	18a	300	UNK	15.90	5.75	7.50	1.706	2.49
AKP50 Comp	7.5	23	250	YES	7.30	4.11	4.14	0.167	1.34
AKP50 Comp	7.5	24a	250	NO	14.00	10.31	4.54	0.957	1.46
AKP50 Comp	7.5	18	200	NO	16.00	10.08	5.38	1.430	1.65
AKP50 Comp	7.5	13	200	YES	8.29	5.43	3.28	0.248	1.68
AKP50 Comp	7.5	8b	200	NO	12.85	8.21	5.37	0.987	1.74
AKP50 Comp	7.5	8a	200	NO	18.46	7.39	5.27	1.407	1.96
AKP50 Comp	7.5	15	250	YES	7.41	5.56	3.86	0.320	2.01
AKP50 Comp	7.5	24b	250	NO	15.17	3.37	3.37	0.375	2.18
AKP50 Comp	8	9	200	YES	17.29	5.28	8.22	1.071	1.43
AKP50 Comp	8	15	240	YES	10.28	6.87	2.80	0.321	1.62
AKP50 Comp	8	13a	205	NO	11.86	2.84	5.27	0.294	1.66
AKP50 Comp	8	13b	205	NO	7.87	3.65	2.03	0.117	2.01

Table 27: Green Body Density Data and Calculations for SHS TiB₂/ Alcoa SG A-1000 Al₂O₃ Ceramic Composites									
Composite System	Processing pH	Plaster Mold #	CIP Pressure (MPa)	Bag Leakage during CIP	Length (mm)	Width (mm)	Height (mm)	Weight (g)	Density (g/cc)
Alcoa-SG Comp	PEG	N/ A	UNK	NO				3.000-3.049	
Alcoa-SG Comp	4	25b	300	NO	22.93	6.54	7.58	2.251	1.98
Alcoa-SG Comp	4	10b	300	NO	40.43	7.09	5.76	3.286	1.99
Alcoa-SG Comp	4	10a	300	NO	10.98	6.65	6.12	0.944	2.11
Alcoa-SG Comp	4	2b	300	NO	40.06	5.71	7.32	3.660	2.19
Alcoa-SG Comp	4	25a	300	NO	20.72	5.76	8.00	2.209	2.31
Alcoa-SG Comp	4	2a	300	NO	17.85	6.12	5.86	1.516	2.37
Alcoa-SG Comp	4	17	300	NO	57.83	6.07	8.66	7.333	2.41
Alcoa-SG Comp	4	22	300	NO	57.20	6.15	7.45	6.569	2.51
Alcoa-SG Comp	4	12	300	NO	58.19	6.01	7.03	6.821	2.77
Alcoa-SG Comp	7	4b	107	NO	6.78	6.12	4.52	0.362	1.93
Alcoa-SG Comp	7	12	107	NO	18.33	6.40	8.50	1.962	1.97
Alcoa-SG Comp	7	7b	107	NO	9.55	6.03	6.97	0.801	2.00
Alcoa-SG Comp	7	4a	107	NO	24.25	7.45	5.66	2.139	2.09
Alcoa-SG Comp	7	7c	107	NO	9.67	6.13	7.58	0.973	2.17
Alcoa-SG Comp	7	7a	107	NO	21.28	7.23	6.66	2.430	2.37
Alcoa-SG Comp	7	25a	115	NO	17.62	6.92	8.53	1.958	1.88
Alcoa-SG Comp	7	2b	115	NO	10.43	5.67	7.53	0.839	1.88
Alcoa-SG Comp	7	25b	115	NO	13.55	7.72	7.41	1.505	1.94
Alcoa-SG Comp	7	2a	115	NO	16.96	6.52	7.21	1.643	2.06
Alcoa-SG Comp	7	25c	115	NO	15.13	6.75	6.87	1.493	2.13
Alcoa-SG Comp	8	22b	105	NO	13.53	5.84	8.58	1.138	1.68
Alcoa-SG Comp	8	7c	105	NO	16.31	5.39	5.90	0.873	1.66

Table 27 (contd): Green Body Density Data and Calculations for SHS TiB₂/ Alcoa SG A-1000 Al₂O₃ Ceramic Composite									
Composite System	Processing pH	Plaster Mold #	CIP Pressure (MPa)	Bag Leakage during CIP	Length (mm)	Width (mm)	Height (mm)	Weight (g)	Density (g/cc)
Alcoa-SG Comp	8	2b	105	NO	13.20	6.62	5.00	0.755	1.73
Alcoa-SG Comp	8	4	105	NO	15.82	6.55	7.74	1.398	1.74
Alcoa-SG Comp	8	7a	105	NO	8.61	6.90	6.87	0.725	1.78
Alcoa-SG Comp	8	22a	105	NO	22.72	5.65	7.93	1.829	1.80
Alcoa-SG Comp	8	2a	105	NO	20.14	7.12	7.35	1.905	1.81
Alcoa-SG Comp	8	12	105	NO	6.95	7.03	7.01	0.622	1.82
Alcoa-SG Comp	8	25a	105	NO	30.40	9.22	7.79	4.086	1.87
Alcoa-SG Comp	8	25b	105	NO	22.75	6.54	10.69	3.405	2.14
Alcoa-SG Comp	8	7b	105	NO	7.26	6.04	6.95	0.753	2.47

Table 28: Green Body Density Data and Calculations for SHS TiB ₂ / Al ₂ O ₃ Ceramic Composites									
Composite System	Processing pH	Plaster Mold #	CIP Pressure (MPa)	Bag Leakage during CIP	Length (mm)	Width (mm)	Height (mm)	Weight (g)	Density (g/cc)
SHS COMPOSIT	PEG	N/ A	N/A	N/A				9.000-9.049	
SHS COMPOSIT	4	19B	N/A	N/A	19.98	8.26	4.72	1.268	1.63
SHS COMPOSIT	4	6	N/A	N/A	62.21	7.96	6.43	5.299	1.66
SHS COMPOSIT	4	20	N/A	N/A	25.75	8.43	4.73	1.748	1.70
SHS COMPOSIT	4	1A	N/A	N/A	35.31	8.55	7.49	3.989	1.76
SHS COMPOSIT	4	1B	N/A	N/A	15.92	8.07	7.64	1.742	1.77
SHS COMPOSIT	4	19A	N/A	N/A	35.76	5.71	8.52	3.140	1.80
SHS COMPOSIT	4	16	N/A	N/A	62.35	8.17	5.05	4.773	1.86
SHS COMPOSIT	4	5	N/A	N/A	---	---	---	---	DROPPED
SHS COMPOSIT	4	11	N/A	N/A	---	---	---	3.001	IRREGULAR
SHS COMPOSIT	7	24B	N/A	N/A	32.38	8.59	8.02	3.778	1.69
SHS COMPOSIT	7	13	N/A	N/A	23.40	8.94	5.62	2.049	1.74
SHS COMPOSIT	7	23	N/A	N/A	25.84	8.11	7.11	2.724	1.83
SHS COMPOSIT	7	24A	N/A	N/A	18.87	8.59	5.52	1.651	1.85
SHS COMPOSIT	7	9	N/A	N/A	31.75	7.59	7.16	3.299	1.91
SHS COMPOSIT	7	8	N/A	N/A	47.80	7.58	6.33	4.409	1.92
SHS COMPOSIT	7	18A	N/A	N/A	34.41	8.43	5.90	3.350	1.96
SHS COMPOSIT	7	15	N/A	N/A	61.01	7.98	5.35	5.460	2.10
SHS COMPOSIT	7	18B	N/A	N/A	19.62	7.18	2.74	1.614	4.18

Table 28 (cont'd): Green Body Density Data and Calculations for SHS TiB ₂ / Al ₂ O ₃ Ceramic Composites									
Composite System	Processing pH	Plaster Mold #	CIP Pressure (MPa)	Bag Leakage during CIP	Length (mm)	Width (mm)	Height (mm)	Weight (g)	Density (g/cc)
SHS COMPOSIT	9	B	N/A	N/A	9.27	6.74	6.70	0.756	1.81
SHS COMPOSIT	9	7	N/A	N/A	63.29	8.19	9.06	8.486	1.81
SHS COMPOSIT	9	17	N/A	N/A	28.52	7.79	10.16	4.107	1.82
SHS COMPOSIT	9	12	N/A	N/A	64.56	9.18	9.53	10.497	1.86
SHS COMPOSIT	9	22	N/A	N/A	62.49	9.66	9.55	10.721	1.86
SHS COMPOSIT	9	C	N/A	N/A	8.50	5.10	6.60	0.537	1.88
SHS COMPOSIT	9	A	N/A	N/A	16.7	5.610	6.80	1.208	1.90
SHS COMPOSIT	9	25	N/A	N/A	54.62	9.30	7.50	7.463	1.96
SHS COMPOSIT	9	4	N/A	N/A	61.74	7.14	7.59	6.575	1.97

APPENDIX D

Sintered Density Measurements

Table 29: Sintered Density Measurements for the Three Composite Systems Investigated

Processing Condition/1700C Sintering Temperature		SHS Composite	Density	% Theoretical
PEG	Wd = Weight Dry	7.84	3.75	0.910
	Ww = Weight in Water	5.75		
pH 4	Wd = Weight Dry	3.72	3.72	0.903
	Ww = Weight in Water	2.72		
pH 7	Wd = Weight Dry	3.22	3.29	0.798
	Ww = Weight in Water	2.24		
pH 9	Wd = Weight Dry	10.10	3.46	0.840
	Ww = Weight in Water	7.18		
Processing Condition/1800C Sintering Temperature		SHS Composite	Density	% Theoretical
PEG	Wd = Weight Dry	6.58	3.72	0.902
	Ww = Weight in Water	4.81		
pH 4	Wd = Weight Dry	4.03	3.17	0.770
	Ww = Weight in Water	2.76		
pH 7	Wd = Weight Dry	4.24	3.69	0.895
	Ww = Weight in Water	3.09		
pH 9	Wd = Weight Dry	5.81	3.72	0.904
	Ww = Weight in Water	4.25		
Processing Condition/1700C Sintering Temperature		SHS TiB ₂ /Alcoa-SG Al ₂ O ₃	Density	% Theoretical
PEG	Wd = Weight Dry	2.81	3.19	0.775
	Ww = Weight in Water	1.93		
pH 4	Wd = Weight Dry	3.55	3.14	0.763
	Ww = Weight in Water	2.42		
pH 7	Wd = Weight Dry	0.80	3.33	0.809
	Ww = Weight in Water	0.56		
pH 8	Wd = Weight Dry	0.71	3.38	0.821
	Ww = Weight in Water	0.50		
Processing Condition/1800C Sintering Temperature		SHS TiB ₂ /Alcoa-SG Al ₂ O ₃	Density	% Theoretical
PEG	Wd = Weight Dry	2.44	3.13	0.759
	Ww = Weight in Water	1.66		
pH 4	Wd = Weight Dry	6.32	3.22	0.783
	Ww = Weight in Water	4.36		
pH 7	Wd = Weight Dry	2.02	2.97	0.721
	Ww = Weight in Water	1.34		
pH 8	Wd = Weight Dry	1.55	3.10	0.752
	Ww = Weight in Water	1.05		
Processing Condition/1700C Sintering Temperature		SHS TiB ₂ /AKP-50 Al ₂ O ₃	Density	% Theoretical
PEG	Wd = Weight Dry	2.88	3.20	0.777
	Ww = Weight in Water	1.98		
pH 4	Wd = Weight Dry	0.99	3.19	0.775
	Ww = Weight in Water	0.68		
pH 7.5	Wd = Weight Dry	0.94	3.24	0.787
	Ww = Weight in Water	0.65		
pH 8	Wd = Weight Dry	0.26	3.25	0.789
	Ww = Weight in Water	0.18		
Processing Condition/1800C Sintering Temperature		SHS TiB ₂ /AKP-50 Al ₂ O ₃	Density	% Theoretical
PEG	Wd = Weight Dry	2.77	3.01	0.731
	Ww = Weight in Water	1.85		
pH 4	Wd = Weight Dry	5.64	2.97	0.720
	Ww = Weight in Water	3.74		
pH 7.5	Wd = Weight Dry	0.83	3.19	0.775
	Ww = Weight in Water	0.57		
pH 8	Wd = Weight Dry	no sample	no sample	no sample
	Ww = Weight in Water	no sample	no sample	no sample

APPENDIX E

Conductivity Measurements

Table 30: Conductivity Measurements				
Green Body Conductivity	Direction on Sample	SHS Composite	SHS TiB₂/ Alcoa SG Al₂O₃	SHS TiB₂/ AKP-50 Al₂O₃
All Processing Conditions	All directions	No Conductivity	No Conductivity	No Conductivity
General Sintered Body Conductivity	Direction on Sample	SHS Composite	SHS TiB₂/ Alcoa SG Al₂O₃	SHS TiB₂/ AKP-50 Al₂O₃
All Processing Conditions	All directions	Conductive	Conductive	Conductive
Note: electrode to electrode conductivity 0.1 M Ω				
Specific Sintered Body Conductivities MΩ (1700 °C)	Direction on Sample	SHS Composite	SHS TiB₂/ Alcoa SG Al₂O₃	SHS TiB₂/ AKP-50 Al₂O₃
PEG	Surface	0.2	0.2	***
	Across broadest point of sample	1.3	0.2	0.2
pH 4	Surface	0.2	**	0.2-1.8
	Across broadest point of sample	0.7-42	0.3	3.0
pH 7 or 7.5	Surface	0.2	0.1-0.4	0.3-9k Ω
	Across broadest point of sample	1.1-9k Ω *	0.2	0.2-6
pH 8 or 9	Surface	0.2	0.1	no data
	Across broadest point of sample	0.4-3.5	varies 0.5-10-40	no data
		Fluctuates - multimeter will not come to rest		
		*top surface had light and dark areas; multimeter readings ranged from 0.1-0.9 but went as high as 162.47 and down to 137+		
		multimeter will not come to rest		
		**variation over top surface: matte black 0.6, grey powdery 7.4, matte black to grey 72.1; bottom 0.2		
Specific Sintered Body Conductivities MΩ (1800 °C)	Direction on Sample	SHS Composite	SHS TiB₂/ Alcoa SG Al₂O₃	SHS TiB₂/ AKP-50 Al₂O₃
PEG	Surface	0.3-1.1	0.2	None
	Across broadest point of sample	0.5-2.1*	0.4	2.2
pH 4	Surface	0.3-0.9	3.4*	3.3-4.0
	Across broadest point of sample	0.8-4.1*		5.0*
pH 7 or 7.5	Surface	0.2	2.1 (very small, irregular shaped sample)	3.4*
	Across broadest point of sample	0.6-4.1*	1.5*	2.4*
pH 8 or 9	Surface	0.5	0.2	2.9 (very small sample)
	Across broadest point of sample	0.4	0.5	1.2
		*Fluctuates-multimeter will not come to rest		

APPENDIX F

Microhardness Measurements

Table 31: Microhardness Measurements (Vickers (HV))*

		Composite System	SHS	AKP-50	ALCOA
Processing Condition	PEG	1700 C	NO DATA	5/17; AVG 1109; 270 STD DEV	0/5
		1800 C	NO DATA	3/15; 874 AVG; 90 STD DEV	NO DATA
	pH 4	1700 C	1/12; 1382 "AVG"; 0 STD DEV	0/6	0/8
		1800 C	NO DATA	5/15; 913 AVG; 222 STD DEV	5/20; 679 AVG; 368 STD DEV
	pH 7 or 7.5	1700 C	2/15; 1426 AVG; 34 STD DEV	NO DATA	3/15; 901 AVG; 126 STD DEV
		1800 C	5/20; 915 AVG; 356 STD DEV	4/19; 846 AVG; 238 STD DEV	10/20; 860 AVG; 293 STD DEV
	pH 8 or 9	1700 C	NO DATA	3/16; 633 AVG; 224 STD DEV	8/20; 747 AVG; 351 STD DEV
		1800 C	NO DATA	N/A	10/26; 974 AVG; 234 STD DEV
	None	Hot Pressed	11/24; 1892 AVG; 175.1 STD DEV	N/A	N/A

*Data: valid measurements/attempted measurements (# / #); average of valid #'s (AVG); standard deviation for valid #'s (STD DEV); Note that HV =GPa x 102

APPENDIX G

Porosity Measurements from Backscatter SEM Micrographs

Reconstruction of three-dimensional information about the pore structure was determined by a direct lineal analysis of backscatter SEM micrographs. This direct method was sufficient for estimations to compare between micrographs, but was not as detailed as would be expected by instrumental analysis. The definition of porosity was [EMSE, 1986, p. 3832]:

$$\varepsilon = \frac{L_p}{(L_p + L_s)} \quad (20)$$

where L_p and L_s are the total lengths of lines lying in pores and matrix of a series of lines across the micrograph (Figure 23).

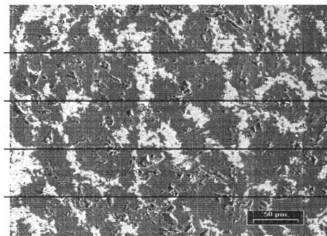


Figure 23: Backscatter SEM micrograph with lineal analysis, after EMSE [1986, p. 3832]

Although it was of no consequence whether the lines were regularly or randomly distributed, a regular pattern is typical of instrumental analysis, and was used in these direct measurements. Further, this type of analysis is independent of magnification [EMSE, 1986, p. 3832], which was convenient since micrographs of various origins were compared in this study.

Table 32: Porosity Measurements from Backscatter SEM Micrographs

Porosity (ϵ) $\epsilon = L_p / (L_p + L_s)$

Composite Recipe Processing Condition

SHS {TiB ₂ /Al ₂ O ₃ }		PEG (Figure 21(a))							
Line 1		Line 2				Line 3		Line 4	
L _p (mm)	L _s (mm)	L _p (mm)	L _s (mm)	L _p (mm)	L _s (mm)	L _p (mm)	L _s (mm)	L _p (mm)	L _s (mm)
0	55	11	17	18	18	2	48		
2	3	2	75	8	6	5	11		
10	3	4		12	18	6	2		
3	13			1	22	7	5		
4	2				6	3	20		
5	8								
24	84	17	92	39	70	23	86		
		108		109		109			109
									$\epsilon = 23.68\%$

SHS {TiB ₂ /Al ₂ O ₃ }		pH 4 (Figure 21(b))							
Line 1		Line 2				Line 3		Line 4	
L _p (mm)	L _s (mm)	L _p (mm)	L _s (mm)	L _p (mm)	L _s (mm)	L _p (mm)	L _s (mm)	L _p (mm)	L _s (mm)
30	42	5	6	11	19	16	27		
5	12	8	31	1	13		58		
	11	6	8		57				
		1	22						
		6	7						
35	65	26	74	12	89	16	85		
		100		100		101			101
									$\epsilon = 22.14\%$

SHS {TiB ₂ /Al ₂ O ₃ }		pH 7 (Figure 21(c))							
Line 1		Line 2				Line 3		Line 4	
L _p (mm)	L _s (mm)	L _p (mm)	L _s (mm)	L _p (mm)	L _s (mm)	L _p (mm)	L _s (mm)	L _p (mm)	L _s (mm)
2	25	12	7	15	2	17	47		
35	15	3	8	3	56	5	5		
7	12	7	6	1	2	15	11		
11		1	7	18	8	5	3		
		5	30	2					
		6	11						
			4						
55	52	34	73	39	68	42	66		
		107		107		107			108
									$\epsilon = 39.63\%$

SHS {TiB ₂ /Al ₂ O ₃ } pH 9 (Figure 21(d))									
Line 1		Line 2		Line 3		Line 4			
L _p (mm)	L _s (mm)	L _p (mm)	L _s (mm)	L _p (mm)	L _s (mm)	L _p (mm)	L _s (mm)		
19	10	6	5	2	16	7	44		
14	22	8	63	10	10	6	4		
10	23	11	3	5	15	7	24		
7	9	7	3	6	30	10	5		
		4	2		20	7			
		6							
50	64	42	76	23	91	37	77		
		114		118		114		114	
									$\varepsilon = 33.04\%$

SHS TiB ₂ /AKP 50 Al ₂ O ₃ PEG (Figure 21(e))									
Line 1		Line 2		Line 3		Line 4			
L _p (mm)	L _s (mm)	L _p (mm)	L _s (mm)	L _p (mm)	L _s (mm)	L _p (mm)	L _s (mm)		
7	10	5	5	4	15	5	43		
	76	10	61	2	67	10	12		
			12		5		23		
7	86	15	78	6	87	15	78		
		93		93		93		93	
									$\varepsilon = 11.56\%$

SHS TiB ₂ /AKP 50 Al ₂ O ₃ pH 4 (Figure 21(f))									
Line 1		Line 2		Line 3		Line 4			
L _p (mm)	L _s (mm)	L _p (mm)	L _s (mm)	L _p (mm)	L _s (mm)	L _p (mm)	L _s (mm)		
10	8	7	54	10	2	4	32		
9	7	10	5	5	10	5	19		
6	31	15		10	20	4	25		
7	11			5	21		2		
	2				8				
32	59	32	59	30	61	13	78		
		91		91		91		91	
									$\varepsilon = 29.40\%$

SHS TiB ₂ /AKP 50 Al ₂ O ₃ pH 7.5 (Figure 21(g))									
Line 1		Line 2		Line 3		Line 4			
L _p (mm)	L _s (mm)	L _p (mm)	L _s (mm)	L _p (mm)	L _s (mm)	L _p (mm)	L _s (mm)		
20	51	1	12	8	5	5	9		
4	9	4	20	9	28	6	7		
	7	2	30	7	30	3	41		
		11	11		4	2	6		
							12		
24	67	18	73	24	67	16	75		
		91		91		91		91	
									$\varepsilon = 22.53\%$

SHS TiB ₂ /AKP 50 Al ₂ O ₃ pH 8 (Figure 21(h))									
Line 1		Line 2		Line 3		Line 4			
L _p (mm)	L _s (mm)	L _p (mm)	L _s (mm)	L _p (mm)	L _s (mm)	L _p (mm)	L _s (mm)		
8	65	3	5	3	15	7	36		
3	15	9	19	3	70	13	20		
			55				15		
11	80	12	79	6	85	20	71		
		91		91		91		91	
								ε =	13.46%

SHS TiB ₂ /Alcoa SG Al ₂ O ₃ PEG (Figure 21(i))									
Line 1		Line 2		Line 3		Line 4			
L _p (mm)	L _s (mm)	L _p (mm)	L _s (mm)	L _p (mm)	L _s (mm)	L _p (mm)	L _s (mm)		
4	13	3	15	2	12	3	41		
4	16	1	20	7	21	5	17		
1	18	1	20	6	12	6	42		
2	10	6	18	7	15				
2	17	6	13	2	18				
2	18	1	10		10				
	7								
15	99	18	96	24	88	14	100		
		114		114		112		114	
								ε =	15.64%

SHS TiB ₂ /Alcoa SG Al ₂ O ₃ pH 4 (Figure 21(j))									
Line 1		Line 2		Line 3		Line 4			
L _p (mm)	L _s (mm)	L _p (mm)	L _s (mm)	L _p (mm)	L _s (mm)	L _p (mm)	L _s (mm)		
3	8	1	13	4	17	3	2		
1	5	1	4	1	10	1	12		
1	52		95	1	33	1	22		
2	4			5	35	1	44		
1	10				8	2	15		
4	9						11		
	13								
12	101	2	112	11	103	8	106		
		113		114		114		114	
								ε =	7.25%

SHS TiB ₂ /Alcoa SG Al ₂ O ₃ pH 7 (Figure 21(k))									
Line 1		Line 2		Line 3		Line 4			
L _p (mm)	L _s (mm)	L _p (mm)	L _s (mm)	L _p (mm)	L _s (mm)	L _p (mm)	L _s (mm)		
3	5	2	5	1	3	4	5		
2	32	2	32	1	6	1	4		
1	23	1	70	4	60	4	32		
1	36		2	1	5	2	18		
	11			5	15	5	3		
				3	2	2	4		
				1	3	1	25		
					4		3		
7	107	5	109	16	98	19	94		
		114		114		114		113	
								ε =	10.33%

SHS TiB ₂ /Alcoa SG Al ₂ O ₃ pH 8 (Figure 21(l))									
Line 1		Line 2		Line 3		Line 4			
L _p (mm)	L _s (mm)	L _p (mm)	L _s (mm)	L _p (mm)	L _s (mm)	L _p (mm)	L _s (mm)		
1	31	1	3	4	15	2	12		
2	31	1	6	2	65	4	29		
1	6	3	16		28	2	48		
1	20	2	22				17		
	21	2	35						
			23						
5	109	9	105	6	108	8	106		
		114		114		114		114	
								ε =	6.14%

Hot Pressed "Continuous" Microstructure SHS {TiB ₂ /Al ₂ O ₃ }									
Line 1		Line 2		Line 3		Line 4			
L _p (mm)	L _s (mm)	L _p (mm)	L _s (mm)	L _p (mm)	L _s (mm)	L _p (mm)	L _s (mm)		
1	16	7	5	15	52	3	20		
4	28	1	5	2	91	6	10		
6	17	4	5	14	15	4	47		
2	31	6	29		8	5	35		
6	45	3	5			6	4		
	41	4	23				56		
		2	4						
		3	2						
		4	34						
		2	10						
		17	22						
19	178	53	144	31	166	24	172		
		197		197		197		196	
								ε =	16.14%

Table 33: Summary of Lineal Analysis Data for Porosity Measurements from Backscatter SEM Micrographs

Processing Condition	SHS {TiB₂/Al₂O₃}	SHS TiB₂/AKP 50 Al₂O₃	SHS TiB₂/Alcoa SG Al₂O₃
PEG	23.7%	11.6%	15.6%
Dispersion	22.1%	29.4%	7.3%
Coagulation	39.6%	22.5%	10.3%
Heterocoagulation	33.0%	13.5%	6.1%
Hot Pressed	16.1%	N/A	N/A

MICHIGAN STATE LIBRARIES



3 1293 02318 8042